NORWEGIAN JOURNAL OF GEOLOGY
https://dx.doi.org/10.1785/njg101-1-4

GEOLOGICAL SOCIETY OF NORWAY

Morris Jesup Spur and Rise north of Greenland – exploring present seabed features, the history of sediment deposition, volcanism and tectonic deformation at a Late Cretaceous/early Cenozoic triple junction in the Arctic Ocean

Yngve Kristoffersen[1], John K. Hall[2] and Espen Harris Nilsen[3]

[1]*Department of Earth Science, University of Bergen, Bergen Norway (retired).*
[2]*Geological Survey of Israel, Jerusalem, Israel (retired).*
[3]*Lundin Energy Norway, NO–1366 Lysaker, Norway*

E-mail corresponding author (Yngve Kristoffersen): yngve.kristoffersen@uib.no

Keywords:
- *Arctic Ocean*
- *North Greenland*
- *Marginal plateau*
- *Continental sliver*
- *Deformation zone*

Received:
18. May 2020

Accepted:
17. February 20201

Published online:
20. May 2021

The narrow Morris Jesup Spur and an adjacent broader western rise extend 220 km into the Eurasia Basin from the shelf edge north of Greenland. We have used a hovercraft platform drifting with the sea ice to collect the first seismic reflection transect across an area postulated to be a former triple junction between the Greenland, Eurasian and North American plates. The narrow, flat-topped Morris Jesup Spur is a succession of west-dipping (~3°) sediments overlying a basal volcanic unit truncated at the top by an unconformity. The Morris Jesup Rise is formed by intensely deformed sediments and volcanic rocks with a deformation front to the northwest. The basin between the Morris Jesup Rise and the Lomonosov Ridge has a sediment thickness of >3 km with a large submarine channel/levee complex in the upper part and repeated volcanic units present in the deeper stratigraphy below 1.0 sec. sub-bottom. Volcanism on the Morris Jesup Spur is considered to be Late Cretaceous–early Cenozoic in age, and continued into the late Miocene on the Morris Jesup Rise and possibly into early Oligocene in the SW Amundsen Basin. The western slope of the Morris Jesup Spur represented the continental slope north of Svalbard in the Late Cretaceous. A block which included the Morris Jesup Spur and Yermak Plateau rifted off during the initial opening of the Eurasia Basin and moved as part of Greenland until about Chron 22. The architecture of the Morris Jesup Rise is a result of plate convergence possibly including a former extensional plate boundary segment which connected the Gakkel spreading centre to the Hornsund Fault between Chron 22 and Chron 13. The Morris Jesup Rise may be a northern tectonic outlier of a more extensive Eurekan tectonic domain hidden below the Lincoln Sea continental shelf. The Morris Jesup Spur remained subaerial until latest Miocene and submergence of the spur most likely intensified the East Greenland Current.

Kristoffersen, Y., Hall, J.K. & Nilsen, E. H. 2021: Morris Jesup Spur and Rise north of Greenland – exploring present seabed features, the history of sediment deposition, volcanism and tectonic deformation at a Late Cretaceous/early Cenozoic triple junction in the Arctic Ocean. *Norwegian Journal of Geology 101*, 202104. https://dx.doi.org/10.17850/njg101-1-4.

Introduction

The marginal submarine structures known as the Morris Jesup Rise north of Greenland and the Yermak Plateau north of Svalbard are symmetric with respect to the Gakkel spreading centre in the Arctic Ocean (Fig. 1). Initially, the term Morris Jesup Rise included both a 25 km-wide eastern ridge (water depth ~ 800 m) which extends 220 km northeast from the continental shelf edge and to the west a deeper (1000–1500 m) 70 km-wide parallel rise of 150 km northward extent (Figs. 1 & 2). Improved bathymetry prompted the *GEBCO Sub-Committee of Undersea Feature Names* to name the narrow eastern ridge the Morris Jesup Spur (IOC–IHO/GEBCO SCUFN–XVI/3, 2003). We use the term Morris

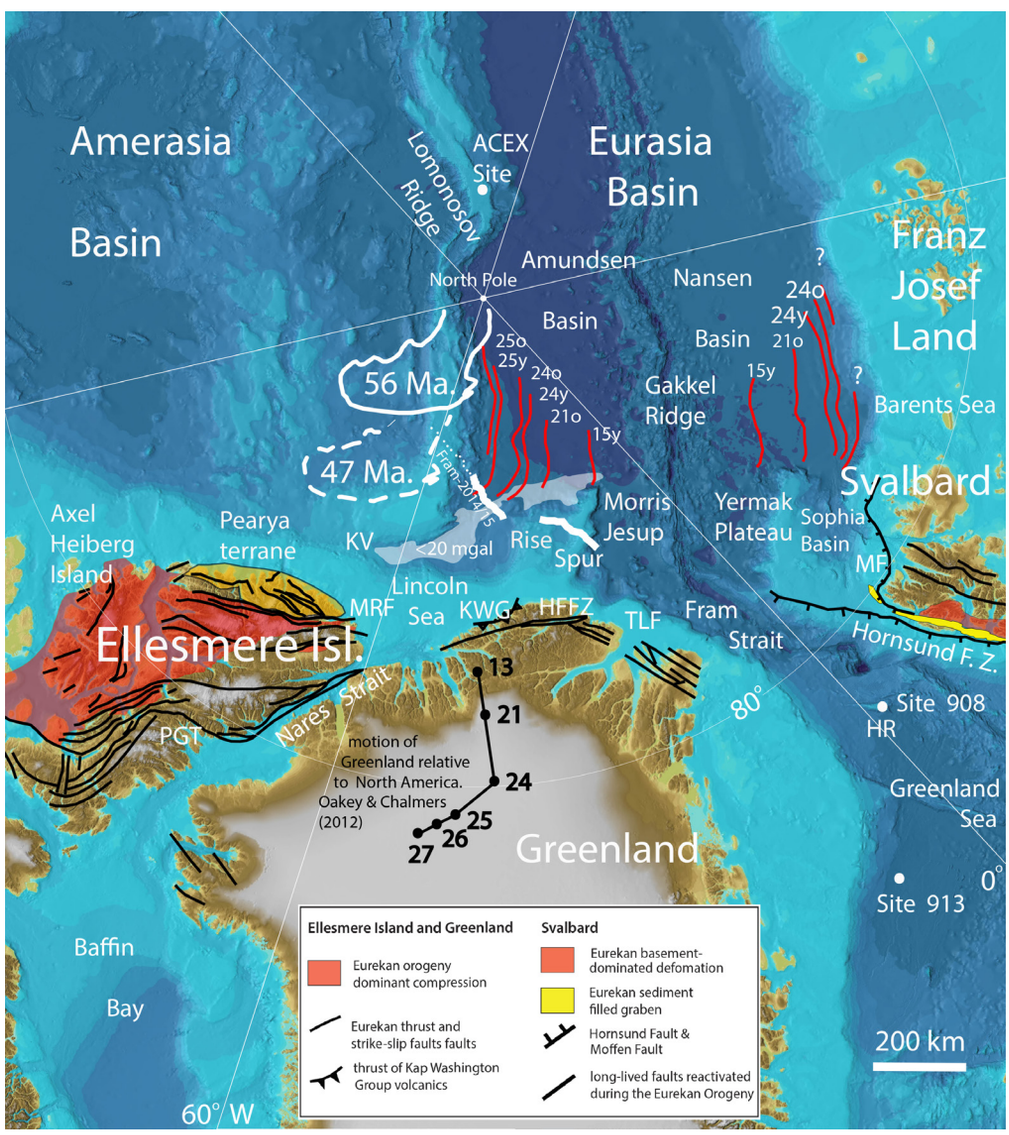

Figure 1. Overview of the Late Cretaceous-Cenozoic (Eurekan) deformation (red transparent overlay) related to the interaction between an independent Greenland plate with North America and Europe. The Arctic Ocean bathymetry is from Jakobsson et al. (2012), geological information from Ellesmere Island from Piepjohn et al. (2016) and from Svalbard from Dallmann (2015). The motion of Greenland relative to North America between Chron 27 and Chron 13 is from Oakey & Chalmers (2013) derived from the Labrador Sea Baffin Bay region. The position of the southern plateau of the Lomonosov Ridge relative to Greenland outlined by a thick white line (56 Ma) and dashed line (47 Ma) is derived from plate rotation parameters for the Eurasia Basin and the Norwegian/Greenland Sea from Gaina et al. (2002) and Barnett Moore et al. (2016), respectively. The gravity low (<20 mgal.) framing the Morris Jesup Rise is from Døssing et al. (2013), magnetic lineations (red) in the Eurasia Basin from Brozena et al. (2003) and major faults (black) from Dallmann (2015) and Piepjohn et al. (2016). The seismic traverse and ice drift of Fram–2014/15 is shown by the bold white line. Abbreviations: HFFZ; Harder Fjord Fault Zone, HR; Hovgard Ridge, KV; Klenova Valley, KWG; Kap Washington Group volcanics, MF; Moffen Fault, MRF; Mount Rawlinson Fault, PGT; Parrish Glacier Thrust, TLF; Trolle Land Fault

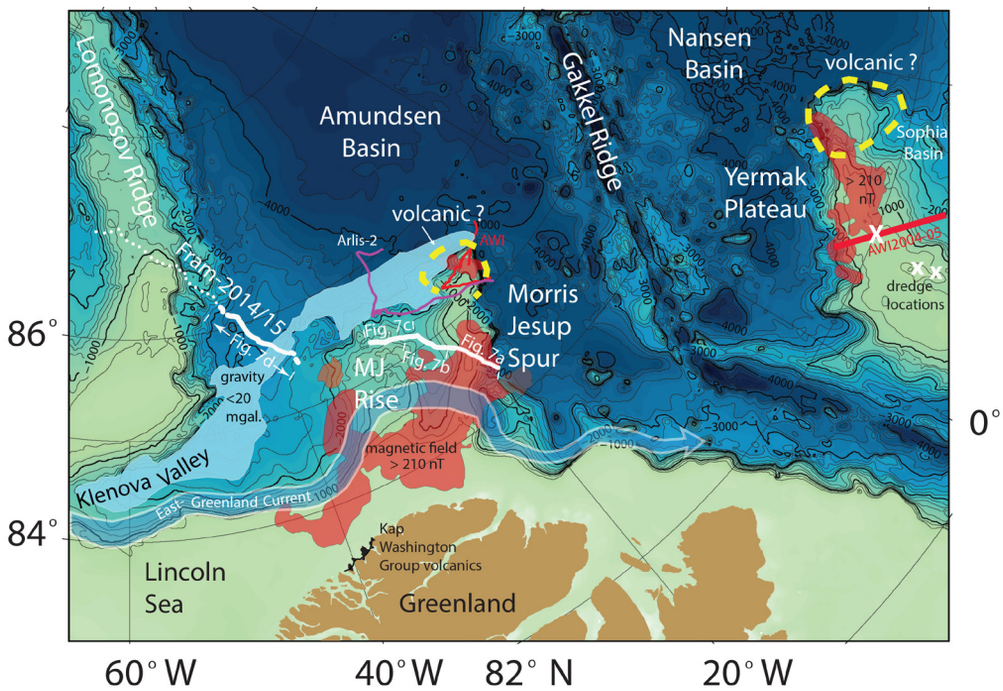

Figure 2. Location of the survey area north of Greenland with the track of ice-drift station Fram–2014/15 (white line) and locations of seismic sections shown in Fig. 7. Other surveys are by ice-drift station Arlis–2 (thin violet line) and by the icebreaker Polarstern (thin red line). The seismic line on the Yermak Plateau by Polarstern (Jokat et al., 2008) is indicated by a red line and the dredge sites of Kristoffersen et al. (2020) by white crosses. The areas of high magnetic intensity on the Yermak Plateau and Morris Jesup spur and rise are outlined by values > 210 nanoTesla in transparent red from Jokat et al. (2016). Bold dashed yellow circles outline the northern part of the Yermak Plateau and Morris Jesup Spur, postulated to be due to volcanism between Chron 22 and Chron 15 (Kristoffersen et al., 2020). Figure generated using GMT software (Wessel et al., 2011).

Jesup Rise for the broad western feature which forms a plateau at ~ 1400 m water depth (Fig. 3C). The spur and the rise are situated below the flow of old and heavily ridged sea ice out of the Arctic Ocean (Rigor et al., 2002), an area proven inaccessible for geophysical surveys from icebreakers (Jokat et al., 1995; Jakobsson & Marcussen et al., 2008). The bathymetry north of Greenland was first outlined from soundings made by the nuclear submarine *Skate* in 1959 and 1962 (Treshnikov et al., 1966; Beal, 1969). Only the northeasternmost 40 km of the spur has been traversed by surface platforms (Fig. 2), first by the US ice-drift station *Arlis–2* in October 1964 (Ostenso & Wold, 1977) and later by the icebreakers *Polarstern* in 1991 (Jokat et al., 1995) and *Oden* in 2009 (Jakobsson et al., 2010). At present, the major sources of information are airborne magnetic and gravity surveys (Vogt et al., 1979; Kovacs & Vogt, 1982; Brozena et al., 2003; Døssing et al., 2013; Jokat et al., 2016). In this contribution we present the first modern seismic reflection traverse which shows the eastern spur to be a truncated succession of dipping sedimentary and volcanic rocks and the western rise to be made up of deformed sediments and volcanics.

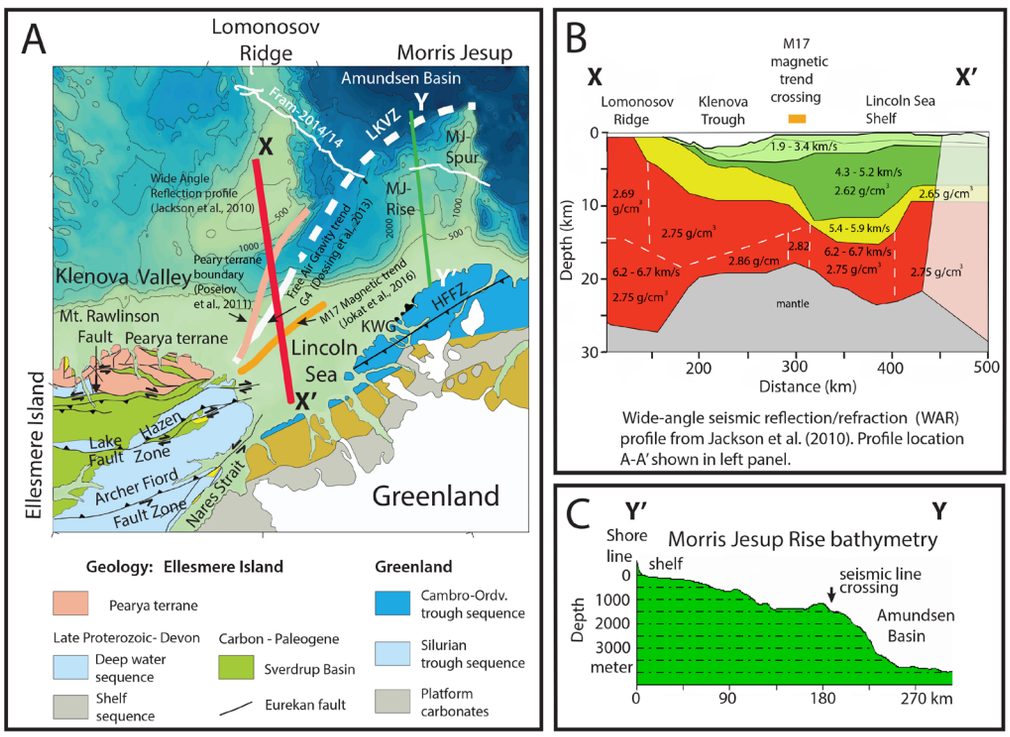

Figure 3. (A) Compilation of published geophysical information from the Lincoln Sea continental margin linking offshore geophysical trends to the geology of Ellesmere Island. The geology of Ellesmere Island is from Piepjohn et al. (2016), the geology of Greenland from Henriksen (2008) and the geophysical data from Døssing et al. (2013), Jackson et al. (2010), Jokat et al. (2016) and Poselov et al. (2011). Abbreviations: HFFZ; Harder Fjord Fault Zone, KWG; Kap Washington Group volcanics. Figure generated using GMT software (Wessel et al., 2011). (B) Crustal velocity and density structure along a transect X–X' from the Lincoln continental shelf on to the Lomonosov Ridge based on wide-angle seismic reflection/refraction measurements and gravity modelling (after Jackson et al., 2010). (C) North-south bathymetric transect (Y–Y') along the Morris Jesup Rise from the North Greenland coast to the Amundsen Basin based on IBCAO version 3.0. The profile was generated using Global Mapper software.

Outline of the geological and plate-tectonic framework

Oceanography

The circum-arctic boundary current (Rudels et al., 1999) flows east along the Lincoln Sea margin through the 1400 m-deep passage of the Klenova Valley (Fig. 2). The mean speed is <9 cm/s on the upper slope (Newton & Sotirin, 1997). By the Morris Jesup Spur and Rise, the boundary current merges with recirculated branches of warmer and more saline Atlantic Water as well as less saline water of Barents Sea origin before moving south along the continental slope of East Greenland (Rudels et al., 1999). The emergence and relative intensity of the East Greenland Current has been inferred from growth of the Erik Drift, a more than 1.5 km-high and over 400 km-long ridge of sediments deposited out from the continental slope at the southern tip of Greenland by contour-following bottom currents (Arthur et al., 1989). Initiation of sediment drift deposits in the area may have begun in the early Miocene (Müller-Michaels et al., 2013), but accelerated at ~4.5 Ma (Kaminski et al, 1989; Wold, 1994; Hunter et al., 2007). Another major Neogene oceanographic event in the Arctic Ocean is the opening of the Fram Strait which is manifested as a transition from an oxygen-poor basin to a state of ventilated circulation after about 17.5 Ma (Jakobsson et al., 2007).

The geology of northernmost Greenland and Ellesmere Island

Northernmost Greenland (Fig. 3A) was the southern platform margin of an Early Palaeozoic E–W-trending basin which accumulated carbonate-dominated sediments (Surlyk & Hurst, 1984; Henriksen, 2008). Turbidites and hemipelagic sediments were deposited in a deeper basin to the north at the present coast. Deformation between the north coast of Greenland and an orogenic borderland to the north during the late Devonian–early Carboniferous orogeny (Ellesmerian) reached greenschist/amphibolite facies in the rocks now exposed on the northernmost fifty kilometres from the coast of North Greenland. The metamorphic grade decreases to the south (Dawes & Peel, 1981; Soper & Higgins, 1991). Carboniferous to Tertiary sediments in northernmost Greenland are only preserved locally within the Harder Fjord Fault Zone (Fig. 3A) and north of the boundary thrust of the Kap Washington Group volcanics (Soper & Dawes, 1970; Batten et al., 1981; von Gosen & Piepjohn, 1999; Piepjohn & von Gosen, 2001). The Kap Washington Group (KWG) is a more than 5 km-thick section of tuff, breccias, rhyolite and basic lavas exposed over a distance of 45 km along the coast of North Greenland (Figs. 1–3). The 8 km-wide outcrop of KWG rocks as well as Permo–Carboniferous sediments are overridden from the south by Early Palaeozoic metamorphic rocks along the Kap Cannon Thrust (Soper & Dawes, 1970; Soper et al., 1982). The contact is represented by a 50–100 m-thick mylonite zone and the KWG outcrop is floored by another thrust to the north (von Gosen & Piepjohn, 1999). The amount of displacement along the mylonite zone is estimated to be more than 10 km (von Gosen & Piepjohn, 1999) or minimum 15 km (Soper & Higgins, 1991). Initial motion at deeper crustal levels facilitated ductile deformation and the rocks later experienced a brittle event at a shallower level. The KWG volcanic rocks are considered to be part of a High Arctic alkaline suite emplaced between 85 and 60 Ma and suffered later thrust displacement at 47–49 Ma inferred from resetting of ^{40}Ar–^{39}Ar ages (Tegnér et al., 2011).

On eastern Ellesmere Island, a structural transect across the Eurekan deformation zone (Fig. 1) from the Pearya terrane in the north to the Nares Strait in the south shows an ensemble of crustal blocks covered by folded Neoproterozoic to Devonian shelf and deep-water sedimentary rocks of the Franklinian Basin and Carboniferous to Paleogene sediments of the Sverdrup Basin (Piepjohn et al., 2016). The blocks are separated by ENE–WSW-trending fault-zones which demonstrate two generations of primary strike-slip motion accompanied by various degrees of orthogonal shortening during the Eurekan deformation (Piepjohn et al, 2016). However, the magnitude of relative displacements has proven difficult to quantify. The major thrust at the southern front of the Eurekan deformation is the Parrish Glacier Thrust (Fig. 1, PGT) or the Eurekan Frontal Thrust of Okulitch & Trettin (1991) along the north side of the Nares Strait (Fig. 1).

Morris Jesup Spur and Rise

Ideas for the origin and the geology of the submarine Morris Jesup Spur and Rise 100–200 km north of the shelf edge of North Greenland have been based on their present-day position at a continental margin, from variations in the intensity of the geomagnetic field over the area and from petrological inferences from the KWG volcanics exposed at the coast (Figs. 1 & 2). Feden et al. (1979) noted the proximity to the continental margin and recognised that plate-tectonic reconstructions of the Eurasia Basin for times prior to Chron 13 (34 Ma) would produce an overlap with the Yermak Plateau assuming both represented continental crust. The authors argued for the spur and rise being a young volcanic construction, as did Jackson & Gunnarsson (1990). The relatively high values of magnetic field intensity (>1000 nT, Kovacs & Vogt, 1982; Jokat et al., 2016) over the Morris Jesup Spur and the proximity (200 km) to the 150 km^2 area of Late Cretaceous/Early Cenozoic KWG volcanic rocks (Batten et al., 1981) on the north shore of Greenland (Fig. 1), have entertained the assumption that the KWG

volcanics extend from the coast across the shelf to the spur and rise (Riddihough et al., 1973, Ostenso & Wold, 1977; Dawes, 1990; Jokat et al., 2016). From a petrological standpoint, the dominantly alkaline KWG rocks include peralkaline compositions typical of continental rifts (Brown et al., 1987; Estrada et al., 1999; Thorarinsson et al., 2011), suggesting that the spur and the rise to the north may also be underlain by continental rocks (Dawes, 1990).

The *Arlis–2* seismic sparker profile of Ostenso & Wold (1977) shows hints of stratification down to 1 second travel time over parts of the western rise, but has no penetration across the northern end of the Morris Jesup Spur (Fig. 2, violet track). More modern seismic data from the northernmost tip of the spur (Fig. 2, AWI, red track) show laterally discontinuous stratified sediments disturbed by local faulting and current erosion overlying a rugged basement akin to volcanic rocks (Jokat et al., 1995).

A Late Cretaceous – early Cenozoic triple junction north of Greenland

The continuous effort of integration of marine magnetic lineations, gravity data and the characteristics of acoustic basement from seismic reflection measurements calibrated by scientific drilling have steadily improved our constraints for the motion of Greenland as an independent plate relative to North America and Europe during the Late Cretaceous – early Cenozoic. Recent updates of kinematic constraints for the Labrador Sea/Baffin Bay are given by Oakey & Chalmers (2012) and Hossienpour et al. (2013) and references therein, for the Norwegian/Greenland Sea by Gaina et al. (2017), Barnett-Moore et al. (2018) and references therein and for the Eurasia Basin by Glebovsky et al. (2006), Gaina et al. (2002) and references therein. We use the geomagnetic time scale of Gradstein et al. (2012). The magnetic isochron data document the motion of Greenland as an independent plate between early Eocene and the end of Oligocene (Chron 24 – Chron 13), effectively indenting the North American plate and the Eurasia plate via Spitsbergen (Dallmann, 2015; Piepjohn et al., 2016). This deformation in the Canadian Arctic Islands is known as the Eurekan deformation event (Thorsteinson & Tozer, 1970, Trettin, 1991; Okulitch & Trettin, 1991; Piepjohn et al., 2016). Although strictly related to Eocene events (Tessensohn & Piepjohn, 1998), the Eurekan orogenic event commonly includes deformation in the High Arctic preceeding Chron 24 and related to the relative motion of Greenland inferred from Late Cretaceous crustal extension, formation of transition zones and Paleocene sea-floor spreading in the Labrador Sea and Baffin Bay (Oakey & Chalmers, 2012). Piepjohn et al. (2016) recognised an Early Eocene and a Late Eocene phase of Eurekan deformation. The early phase was characterised by orthogonal compression along the west coast of Spitsbergen along with sinistral strike-slip faulting on Ellesmere Island, and the second by transtension between Svalbard and Greenland and on Ellesmere Island by dextral strike-slip and compression. The amount of compression between the North American and the Greenland plates as estimated using the combined kinematic constraints from the Labrador Sea/Baffin Bay (Oakey & Chalmers, 2013) or from the Norwegian/Greenland Sea and Eurasia Basin is of the order of 200–300 km (Fig. 1). Harrison (2006) made an attempt to reconcile the Late Cretaceous – Paleogene plate motion between Greenland and North America with the geological field evidence related to Eurekan deformation. He suggested that about 1/3 of the shortening was taken up across northern Ellesmere Island and implied a process of “extrusion tectonics” with 70 km of sinistral motion in the northern Nares Strait. The remainder was taken up by extension of basins around the southern end of Nares Strait.

The main Eurekan accommodation zone north of Greenland is constrained to the south by continental North Greenland, to the west by the geology of Ellesmere Island and to the north by the southern plateau on the Lomonosov Ridge, and to the east by the geology of Spitsbergen (Fig. 1). The Lomonosov Ridge is a continental sliver which rifted off the Barents–Kara Sea margin and became part of the Late Cretaceous/early Cenozoic North American plate (Wilson, 1965; Mair & Forsyth, 1982; Jackson et al.,

2010; Knudsen et al., 2017). The ridge has since remained an integral part of the North American plate as no sediment deformation indicative of younger crustal deformation on the Amerasia Basin side of the Lomonosov Ridge has so far been observed in the seismic reflection data (Jokat et al. 1992; Jokat et al., 2013; Evangelatos & Mosher, 2016). Whether the Lomonosov Ridge has moved relative to the Pearya terrane (Trettin, 1987; Gasser, 2014) on northern Ellesmere Island has not been resolved from a seismic refraction transect (Fig. 3B, line A–A') and the origin of the Klenova Valley remains an open question (Jackson et al., 2010; Døssing et al., 2013). The Caledonian and older basement of the Pearya terrane shows little sign of Eurekan compression (Piepjohn et al., 2013; Piepjohn et al., 2016). Piepjohn et al. (2016) envisaged the situation on Ellesmere Island at Chron 21 (47 Ma) as an interaction of largely intact blocks and an element of "extrusion" tectonics in response to N–S compression after Chron 21. Blocks between the Pearya terrane and the coast of Greenland and the Parrish Glacier Thrust on Ellesmere Island moved westwards along strike-slip faults. This motion was partly accommodated to the west by N–S-trending thrusts on Axel Heiberg Island (Fig. 1).

Large-scale compressional tectonics north of Greenland have been suggested by Brozena et al. (2003) and later Døssing et al. (2013) from features in the gravity field. A Free Air gravity low extends eastwards from the Klenova Valley to the foot of the slope of the Morris Jesup Rise (Figs. 1 & 2, shaded light area) and has been interpreted as a loading effect related to north-directed thrusting and crustal shortening during the Eurekan deformation event. However, the seismic data from the drift of ice-station *Arlis–2* (Fig. 2, violet track) show no apparent sediment deformation at the northern end of the Morris Jesup Rise (Ostenso & Wold, 1977). Døssing et al. (2013) further associated a positive gravity anomaly trend on the Lincoln Sea shelf (G4, Fig. 3A, white solid line) with a postulated offshore extension of the Mount Rawlinson Fault on Ellesmere Island, separating the Pearya terrane from the rest of the Ellesmerian fold-and-thrust belt (Piepjohn et al., 2013). This offshore tectonic extension was called the Lincoln Sea–Klenova Valley Fault Zone (LKVZ) on the continental slope and assumed to continue NNE to the foot of the slope of the Morris Jesup Rise and Spur (Fig.3A, dashed bold white line). Furthermore, the higher elevation of the southern plateau on the Lomonosov Ridge was postulated to be due in part to uplift and crustal shortening from compression during the Eurekan deformation event. A second significant feature of the geopotential field is a distinct change in total magnetic field intensity with short-wavelength linear trends present to the north from the eastern end of the Pearya terrane to the eastern end of the adjacent plateau of the Lomonosov Ridge (Poselov et al., 2011; Jokat et al., 2016). This transition (Fig. 3A, light orange line) was interpreted as the offshore extension of the Pearya terrane boundary (Poselov et al., 2011). Another magnetic trend (Fig. 3A, M17) along the Lincoln Sea shelf appears to align with the northern end of a closed Sophia Basin in a reconstruction for "Chron 25" (Kristoffersen et al., 2020).

Wide-angle seismic reflection/refraction experiments (Argyle et al., 1992; Jackson et al., 2010) have explored the general velocity structure of the crust in a transect across the Lincoln Sea continental shelf to the southern plateau of the Lomonosov Ridge (Fig. 3B). The Lincoln Shelf is underlain by a 12 km-deep sediment basin where the lower 8 km with high seismic velocity (4.3–5.2 km/s) is interpreted to represent Palaeozoic to Mesozoic strata (Jackson et al., 2010). The crust/mantle interface shallows by about 8 km below the Klenova Valley. Although, the seismic velocity of the lower crust remains rather constant and within the range of velocities of continental rocks along the entire transect, gravity modelling points to a northward increase in lower crustal density (4%) at the northern end of the deep basin below the continental shelf (Fig. 3B). This crustal transition is crossed by the magnetic anomaly trend M17 (Jokat et al., 2016) and may suggest a crustal-scale compositional change. In summary, the main ENE-WSW tectonic trends in northeastern Ellesmere Island (Piepjohn et al., 2016) project into at least three possible geophysical trends of unknown geological significance on the Lincoln Sea shelf (Fig. 3). Published geophysical data tend to include the Pearya terrane as part of the North American plate (Jackson et al., 2010), but new seismic reflection data across the Klenova Valley are required to resolve any Eurekan crustal deformation between Pearya and the Lomonosov Ridge such as uplift of the southern end of the latter (Døssing et al., 2014).

Materials and methods

Data acquisition

We have used a platform drifting with the flow of old sea ice out of the Arctic Ocean to acquire the first transect of seismic reflection data north of Greenland (Fig. 1). The heavily ridged sea ice is inaccessible for seismic surveys by icebreakers (Jakobsson et al., 2008) and the field party was deployed upstream near the North Pole by icebreaker *Polarstern* six months earlier (Fig. 4, inset). The area between the Lomonosov Ridge and the Morris Jesup Spur discussed here was traversed in about 2.5 months of ice drift (Kristoffersen et al., 2016). The operation was carried out using a hovercraft fully equipped as a scaled-down polar research vessel and manned by two persons (Kristoffersen & Hall, 2014).

The average sea ice drift was 4–5 km/day and the seismic air-gun source (0.3 litre) was fired under GPS-control at 25-metre intervals. Air temperatures were generally below minus 30 °C, but the air-gun operation (water temperature -1.7 °C) remained remarkably stable for weeks. An ocean capped by sea ice has the advantage of low ambient noise levels generally below the equivalent of sea state zero in the open ocean (Buck & Greene, 1964; Buck, 1968; Makris & Dyer, 1986; Dyer, 1984). As a result, we achieved up to 2 km of sub-bottom penetration in 3 km water depth with the small sound source and only a single hydrophone as receiver. The hydrophone was suspended just below the ice-water interface to avoid cable strumming. The complete seismic system (compressor, air bottles, air gun and data logging instrumentation) weighed less than 150 kilos and a semi-automatic procedure enabled a single person to run the seismic operation 24/7 for a total period of 7.5 months acquiring 1000 km of good-quality single-channel data (Fig. 4). To explore the seabed, we mounted a GoPro camera with a

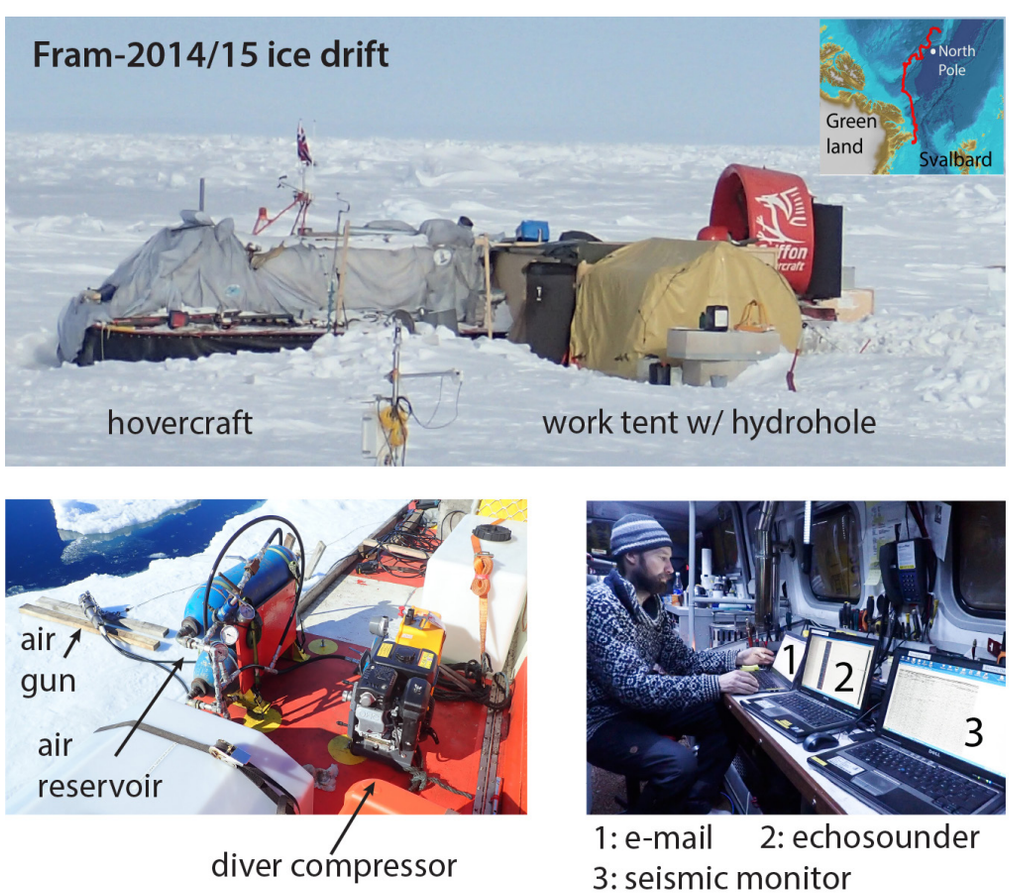

Figure 4. The Fram–2014/15 ice camp with the seismic source and data logging facilities. The hovercraft is 12 m long, has a practical hover height of 0.5 m and can carry a payload of 2.2 tons.

3000 m depth capability on a sled for video recording over distances of 0.25–0.5 km pr. deployment. Good internet connection was available via Iridium at all times whenever external technical advice was needed. Ice activity was frequent as the drift of sea ice approached the coast of Greenland and in one case forced subduction of the camp area below an adjacent ice floe. The time lost for relocation led to a 78 km gap in the seismic data acquisition over the Morris Jesup Rise.

Seismic processing

The seismic source was powered by a diver compressor via an air reservoir regulated by a pressure reduction valve to keep a constant air-gun input pressure at 140 bar (Figs. 4 & 5). If the reservoir was not recharged in time, the air-gun pressure would fall below its nominal value and cause a frequency and time variation in the relatively strong bubble pulse created by release of compressed air into the water (Fig. 5). Removal of the bubble pulse therefore required accurate tracking of its time variation and a trial and error procedure to estimate its effective frequency content which best enhanced the signal obscured by the bubble pulse. A minimum phase predictive deconvolution was then applied. Removal of random noise was achieved by stacking on common reflection surfaces (de Bazelaire, 1988; Gelchinsky, 1988), f–k filtering and 2D time migration.

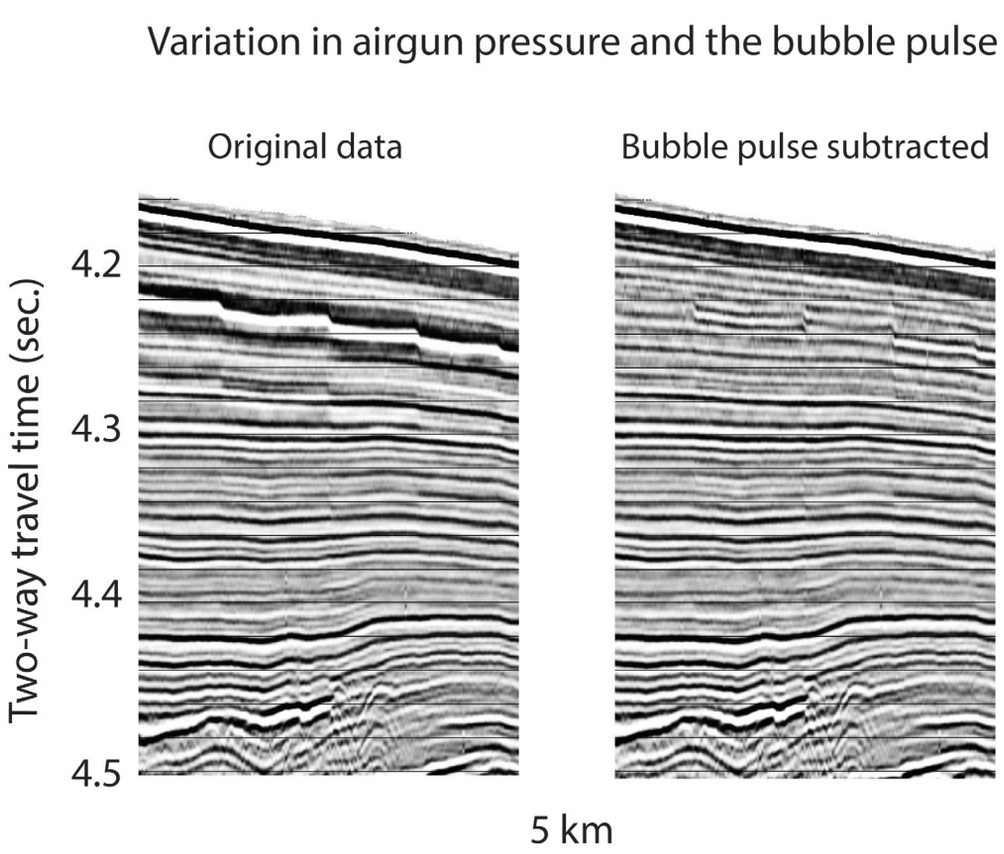

Figure 5. Comparison of a raw seismic record with the results after removal of the bubble pulse.

Results

Description of the seismic data

The acoustic stratigraphy on the continental slope north of Greenland show three very different domains: tilted laterally uniform sequences, truncated at the top of the Morris Jesup Spur, limited acoustic penetration below the undulating topography of the Morris Jesup Rise and thick deposits below the southwestern end of the Amundsen Basin between the Morris Jesup Rise and the Lomonosov Ridge (Figs. 6 & 7).

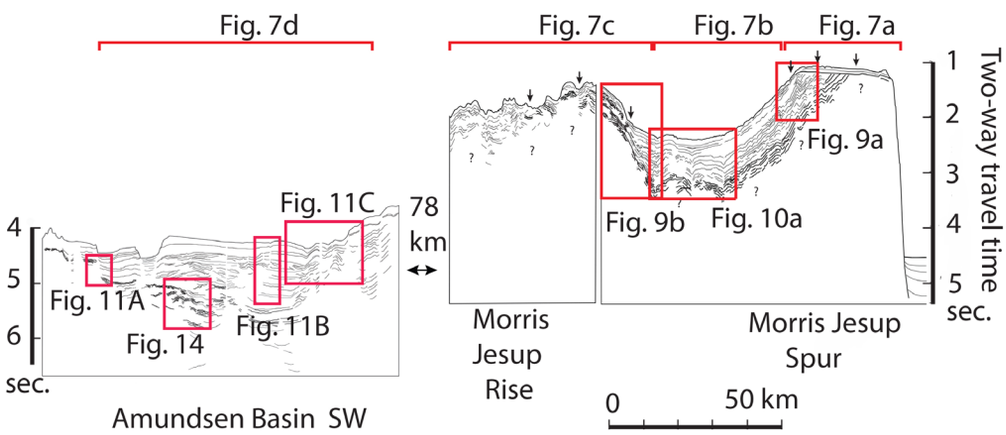

Figure 6. Line drawing of selected reflections in the seismic record in the transect from the foot of the Lomonosov Ridge to beyond the Morris Jesup Spur (Fig. 1). The seismic data panels outlined by red frames are displayed in the respective labelled figures. The locations of individual seismic sections are shown in Fig. 2. Bottom-camera sled deployments are shown by vertical arrows above the bathymetry on the Morris Jesup Spur and Rise.

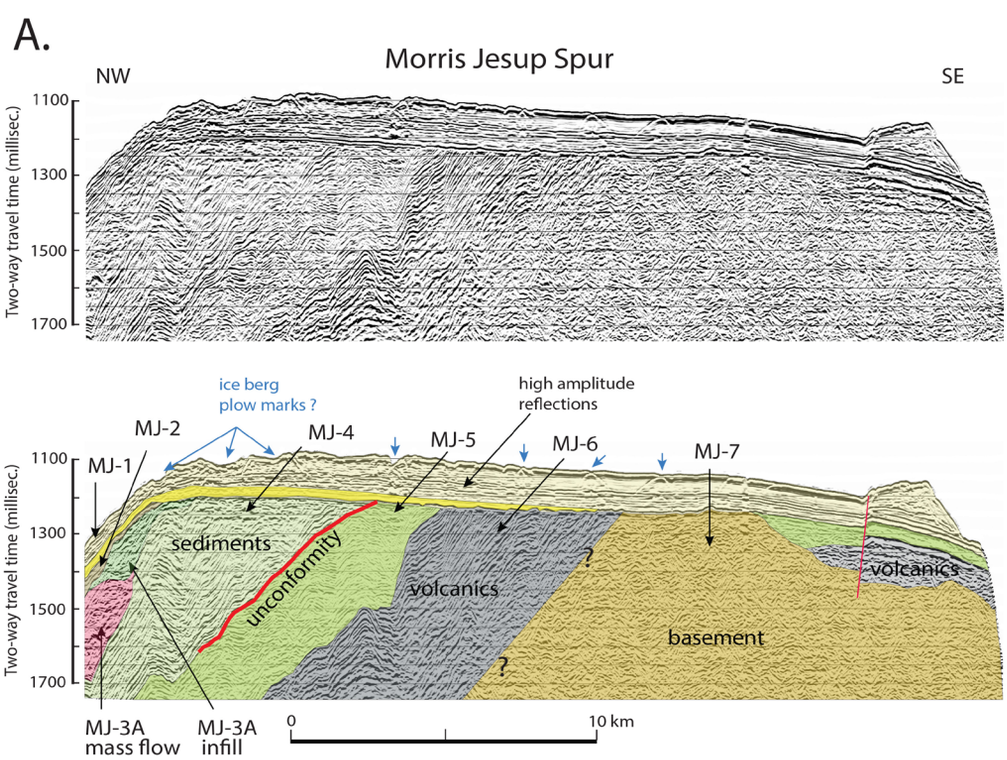

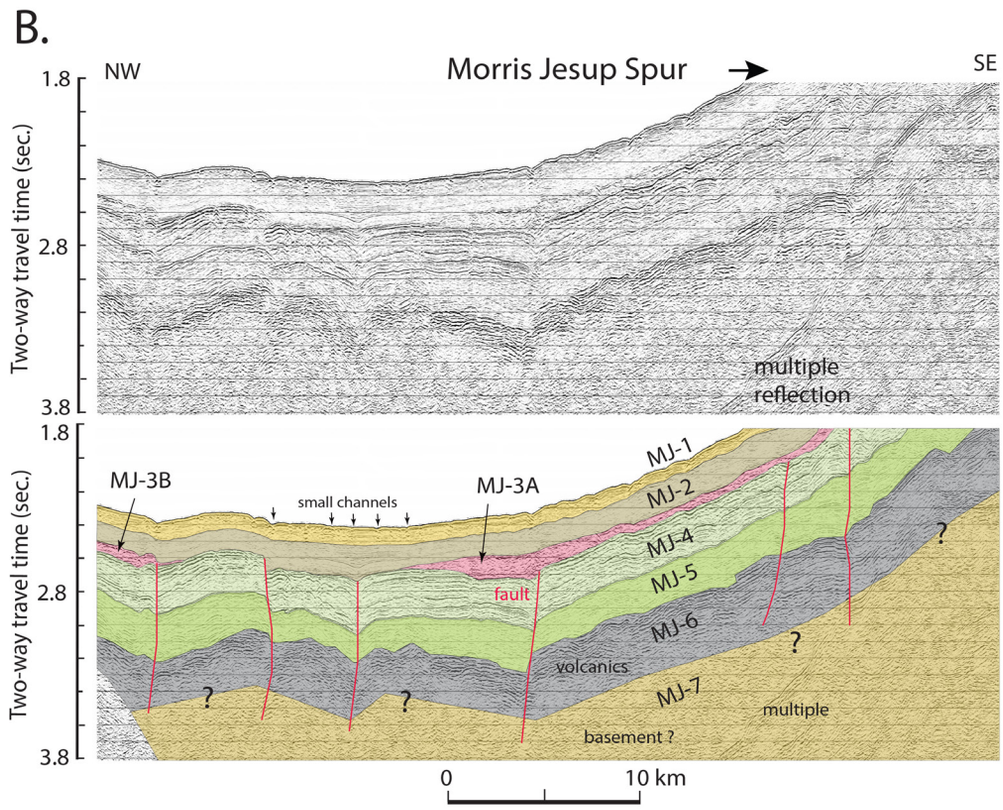
B.
NW
Morris Jesup Spur
SE
Two-way travel time (sec.)
1.8
2.8
3.8
multiple
reflection
MJ-3B
small channels
MJ-3A
MJ-1
MJ-2
MJ-4
MJ-5
MJ-6
MJ-7
fault
volcanics
basement ?
multiple
?
0
10 km

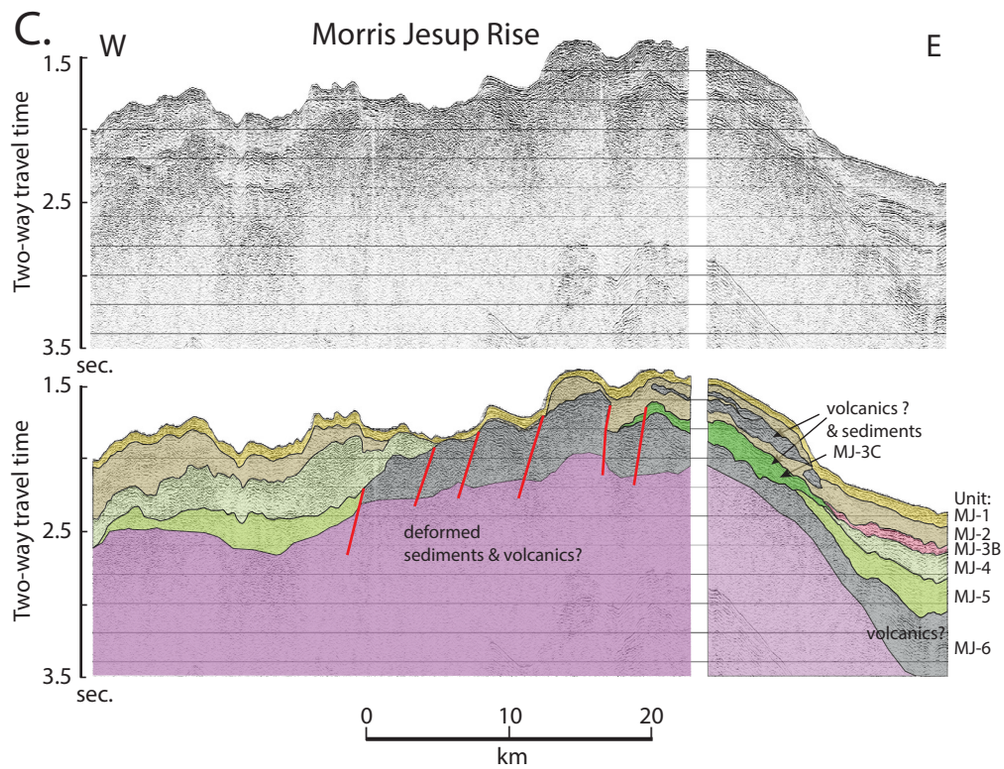
C.
W
Morris Jesup Rise
E
Two-way travel time
1.5
2.5
3.5
sec.
deformed
sediments & volcanics?
volcanics ?
& sediments
MJ-3C
Unit:
MJ-1
MJ-2
MJ-3B
MJ-4
MJ-5
volcanics?
MJ-6
0
10
20
km

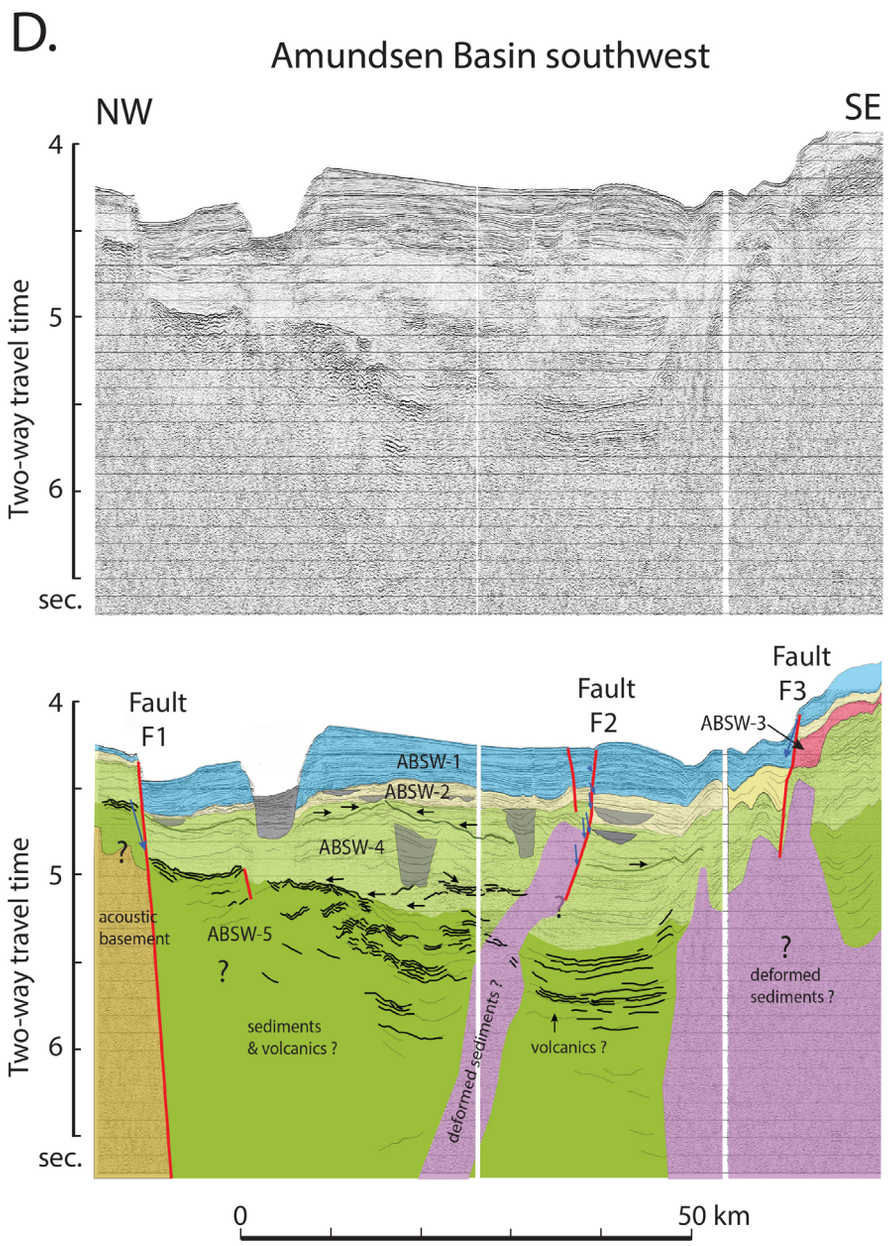

Figure 7. Seismic sections and interpreted depositional sequences for: (A) Morris Jesup Spur; (B) between the Morris Jesup Spur and Rise; (C) Morris Jesup Rise; (D) southwestern end of Amundsen Basin. Locations of the seismic sections are shown in Figs. 2 & 6.

The seabed

The seabed on the flat-topped Morris Jesup Spur has multiple incisions with flanking berms, particularly on the upstream western half where the water depth is less than ~800 m. (Fig. 7A). The largest incision is about 15 m deep. The true width is indeterminate as our seismic profile is roughly parallel to observed directions of ice scour at the northern tip of the Morris Jesup Spur (Jakobsson et al., 2010). Our video coverage over distances of 0.25–0.5 km along the seabed from three locations on the top of the spur show brownish-grey mud covered with varying quantities of coarse material ranging from sand and pebbles to football-size boulders (Fig. 8). Other findings from the top of the spur are broken up centimetre thick whitish crust, isolated decimetre-size sediment cones and small cave-like openings. A site on the upper western slope of the spur, appears free of any coarse material (Fig. 8, 25 April).

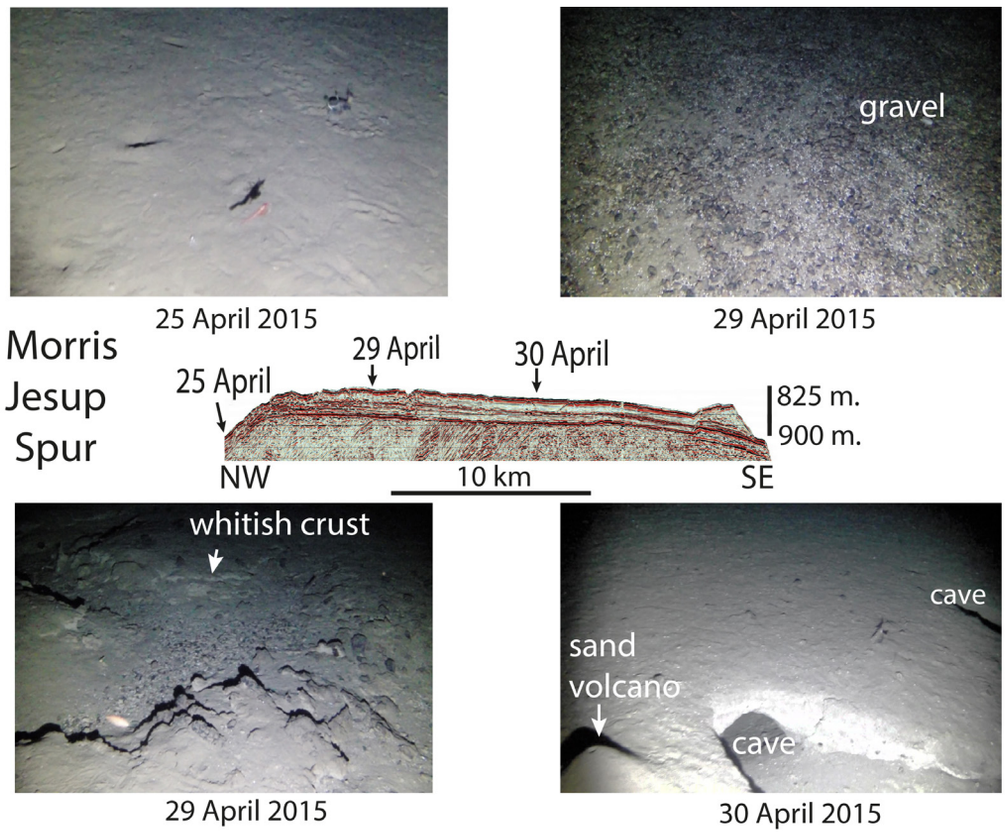

Figure 8. Bottom photos from the Morris Jesup Spur. Individual pictures are referenced by the date taken. The station locations are shown by vertical arrows above the bathymetry in Fig. 6.

The spur is bounded to the east by a precipitous ~60° slope (Fig. 6). The gentle western slope of the spur has a maximum inclination of 3° and shows seabed undulations of apparent wavelengths of >2.5 km above 2.0 sec. (~1500 m) water depth and <2 km on the lower slope (Figs. 6 and 7B). The deepest part between the spur and the rise is characterised by small bow-tie reflections <1 km apart which represent narrow channels not properly resolved in the seismic data (Fig. 7B).

The Morris Jesup Rise to the west of the spur (Fig. 7C) was crossed in water depths between 1020 and 1440 metres and the undulating seabed has no sharp local incisions.
The seabed is littered with sand to gravel-size material at the three locations where video footage was obtained (Fig. 6, black vertical arrows).

The southwestern end of the Amundsen Basin is bounded to the west by a steep fault (Fig. 7D, fault F1, dip 30°) and to the southeast by gentle seabed undulations at the foot of the Morris Jesup Rise . The abyssal plain is interrupted by the NP–28 Channel (Kristoffersen et al., 2004) where the lower slope of the ~5 km- wide channel floor is ~30° on the western side and ~10° on the eastern side. The water depth is about 3000 m and beyond the depth capability of our photo equipment.

Morris Jesup Spur

The acoustic record from the western slope of the Morris Jesup Spur shows stratigraphic intervals of distinct sub-bottom acoustic facies bounded by sharp reflections. We divide the acoustic stratigraphy into six units based on reflection characteristics (amplitude & wavelength) and acoustic interface geometry (Figs. 7 A, B, 9A & 10A).

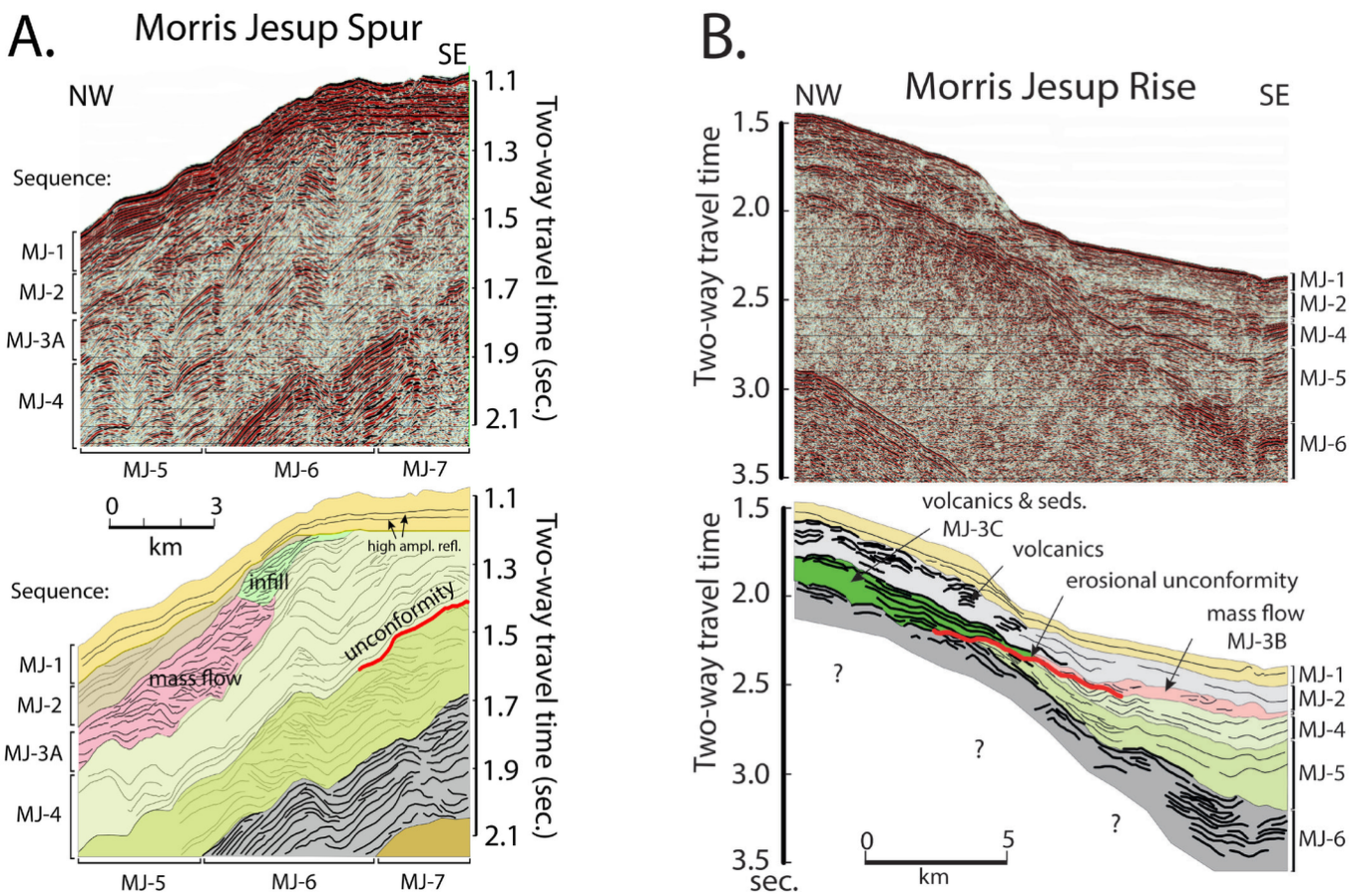

Figure 9. (A) Details of seismic sections and interpreted acoustic sequence boundaries from the western edge of the Morris Jesup Spur. (B) Details of seismic sections and interpreted acoustic sequence boundaries from the eastern edge of the Morris Jesup Rise. The profile locations are shown in Fig. 6.

Unit MJ–1

Unit MJ–1 represents the deposits on top of the flat, ~25 km-wide Morris Jesup Spur separated from the underlying rocks by a sharp angular unconformity (Figs. 7A & 9A). The thickness of the unit is only 0.13 sec. (~104 m, assuming velocity 1.6 km/s) and decreases by about 0.03 sec. (~24 m.) across the spur from west to east. The change in thickness is due to a thin basal wedge with its apex at a small high in the acoustic basement (Fig. 7A, yellow colour). Two high-amplitude reflections occur within the middle of the Unit MJ–1 on top of the spur (Figs. 7A & 9A). They are separated by 0.02 sec. (~16 m.) on the western half and merge gradually eastwards. The acoustic response of Unit MJ–1 on the western slope of the spur is characterised by uniform, medium amplitudes (Fig. 7A).

Unit MJ–2

Unit MJ–2 onlaps the western slope of the Morris Jesup Spur and is about 0.15 sec. (~120 m) thick with monotonous vertical acoustic stratification on a scale of <10 metres throughout (Figs. 7B, 9A & 10A). The bedding of units MJ–1 and –2 shows gentle undulations of wavelengths < 2.0 km and amplitudes < 10 m on the western slope of the spur (Figs. 7B & 10A). Unit MJ–2 also onlaps the Morris Jesup Rise to the west and includes irregular volumes of high-amplitude reflections below the highest part of the rise (Figs. 7C & 9B).

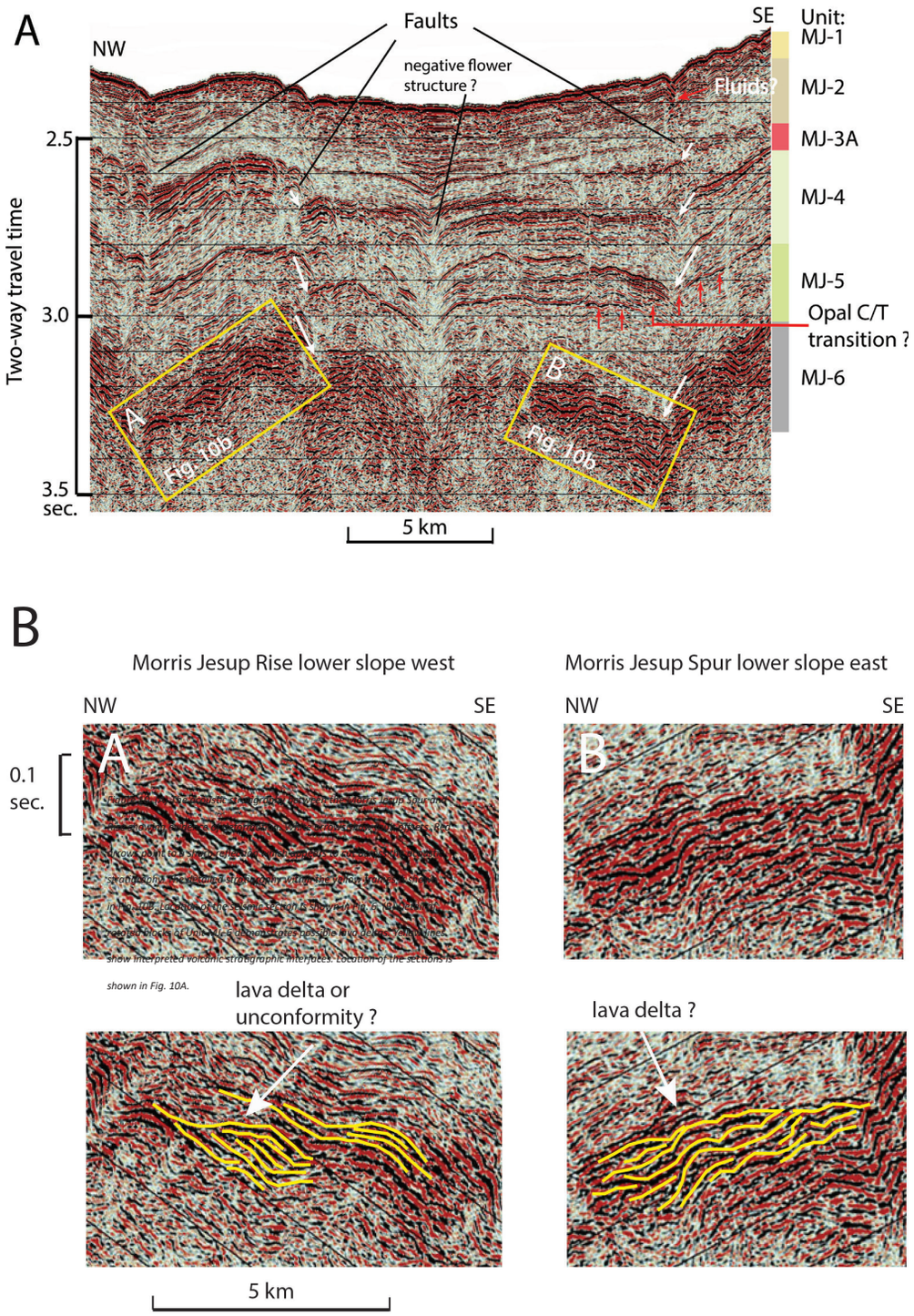

Figure 10. (A) The acoustic stratigraphy between the Morris Jesup Spur and Rise showing evidence of deformation. White arrows show fault offsets. Red arrows point to a sharp reflection which appears to cut across the acoustic stratigraphy. The detailed stratigraphy within the yellow frames is shown in Fig. 10B. Location of the seismic section is shown in Fig. 6. (B) Detail of rotated blocks of Unit MJ–6 demonstrates possible lava deltas. Yellow lines show interpreted volcanic stratigraphic interfaces. Location of the sections is shown in Fig. 10A.

Unit MJ–3

We divide Unit MJ–3 into three subunits. Subunits MJ–3A & –B are two lenticular sediment bodies restricted to the western slope of the spur and near the foot of the slope on the east side of the rise (Figs. 7B and 9). The largest body (MJ–3A) below the western slope of the Morris Jesup Spur is 25

km long and up to 0.2 sec. (~180 m.) thick (Figs. 7B, 9A & 10A). It is characterised by a semi-chaotic reflection pattern with dismembered volumes of parallel reflection segments which are apparently parts of rotated blocks. The upper interface is formed by a linear trend of contorted reflector segments while the lower part of the subunit smooths out vertical offsets in the topography of the underlying Unit MJ–4 (Fig. 7B). Higher up on the slope is a smaller triangular-shaped sediment volume (Fig. 9A, MJ–3A infill,) which onlaps the spur from the shelf break and downlaps on the top of the main chaotic zone (MJ–3A, mass flow).

The second semi-chaotic sediment body (MJ–3B) is 0.1 sec. (~90 m) thick and extends for c. 9 km on the lower eastern slope of the Morris Jesup Rise (Figs. 7B & 9B).

Subunit MJ–3C extends for about 20 km over the high eastern flank of the Morris Jesup Rise (Figs. 7C & 9B). The 0.15 sec. (~225 m, assuming velocity of 3.0 km/s) thick unit has persistent high-amplitude reflections in its upper part and is unconformably overlying older units (MJ–4 and –5) below the eastern slope of the rise.

Unit MJ–4

Unit MJ–4 is characterised by high-amplitude and relatively low-frequency reflections, has a wedge-shaped geometry and downlaps the western slope of the Morris Jesup Spur (Figs. 7B & 9A). The unit has a thickness of about 0.25 sec. (~250 m, assuming velocity of 2.0 km/s), and is truncated upslope by a horizontal peneplain which forms the top of the spur and wedges out against the upper slope of the western rise (Figs. 7C & 9B). The unit is gently folded below the western slope of the spur (wavelengths < 2.5 km, amplitudes < 100 m) and cut by several sub-vertical faults (vertical component < 80 m and hanging wall down) in the depression between the spur and the rise (Fig. 10A).

Unit MJ–5

The top of Unit MJ–5 is a sharp reflection about 0.6 sec sub-bottom and appears to locally cross–cut the general acoustic stratigraphy in the low between the spur and the rise (Figs. 7B & 10A, red arrows). High up below the western edge of the spur is a major unconformity which separates Unit MJ–4 from MJ–5 (Fig. 9A). Unit MJ–5 onlaps the rise and is represented by high-amplitude reflections at its upslope termination. The amplitude and frequency variations in the acoustic image of Unit MJ–5 are very similar to those of Unit MJ–2 (Fig.7B).

Unit MJ–6

Unit MJ–6 is characterised by high-amplitude reflections which display lateral continuity below the spur, but become piece-wise continuous and more complex in the bathymetric low between the spur to the east and the rise to the west (Figs. 7A, B & 10). The depth extent of laterally coherent seismic energy suggests a minimum unit thickness of about 0.5 sec. (~1 km, assuming velocity of 4.0 km/s) below the spur (Fig. 7A). Folds and vertical offsets in Unit MJ–6 are also present in units MJ–5 and MJ–4 above.

Unit MJ–7

The acoustic expression of stratigraphic levels below MJ–6 beneath the major unconformity on the Morris Jesup Spur change from the high-amplitude, westward-dipping, coherent reflections of Unit

MJ–6 to near-vertical stacks of low-amplitude reflections with alternating dips (Fig.7A). This general pattern persists below the eastern half of the spur with the exception of a 7 km segment at the far eastern edge.

Morris Jessup Rise

Deposits on the Morris Jesup Rise have a complex geometry with high-amplitude reflections at shallow sub-bottom depths and pockets of up to 0.7 sec. (~630 m, assuming velocity of 1.8 km/s) of acoustically transparent material. The stratigraphic relations below the high part of the rise suggested in Fig. 7C are very speculative because of prevailing incoherent reflected energy. Unit MJ–1 drapes the undulating topography, but the true vertical thickness variation is very difficult to define. Unit MJ–2 appears to continue from the east on to the high part of the rise, but includes volumes of high-amplitude reflections (Figs. 7C & 9B). The true thickness and continuity of Unit MJ–2 over the rise is not possible to resolve acoustically and thus considered speculative.

Units MJ–4 and –5 terminate against the eastern slope of the rise, and the upper part of MJ–5 is unconformably overlain by the large volume of high-amplitude reflections of Unit MJ–3C which thickens to the west (Fig. 7C). The extent of Unit MJ–4 and –5 on the western part of the rise is also speculative as the main part of the rise is clouded by incoherent reflected energy (Fig. 7C).

Amundsen Basin southwest

The southwestern end of the Amundsen Basin (ABSW) has a sediment thickness of more than 2 sec. two-way travel time with large vertical and lateral changes in the layer geometry (Figs. 6 & 7D). The basin is bounded to the west by a normal fault at the foot of the Lomonosov Ridge (Figs. 7D & 11, fault F1) and to the east by the deformation front at the base of the Morris Jesup Rise (Figs. 6 & 7D). We tentatively divide the acoustic section into four depositional units.

Unit ABSW–1

A 0.4 sec. (~300 m) deep and 10 km-wide submarine channel (NP–28 Channel) is flanked by an up to 0.35 sec. (~280 m) thick package of laterally continuous reflections with remarkably uniform amplitude variations (Fig. 7D). The levee deposits are thickest on the east side of the channel. The 5 km-wide channel floor is characterised by high amplitudes with significant signal attenuation after only 0.1 sec sub-bottom two-travel time. Unit ABSW–1 has its maximum thickness in the deep basin bounded to the west by a fault at the foot of the slope of the Lomonosov Ridge and tapers off to the southeast towards the foot of the slope of the Morris Jesup Rise as a drape over the gently folded underlying sediments (Fig. 7D). The NP–28 Channel is a sediment pathway which extends to the North Pole and beyond (Fig. 12).

Unit ABSW–2

Unit ABSW–2 has an amplitude pattern similar to the overlying unit, but more complex lateral geometry which includes several smaller paleo-channels. The thickness is 0.1–0.15 sec. (~120 m) or less (Fig. 7D).

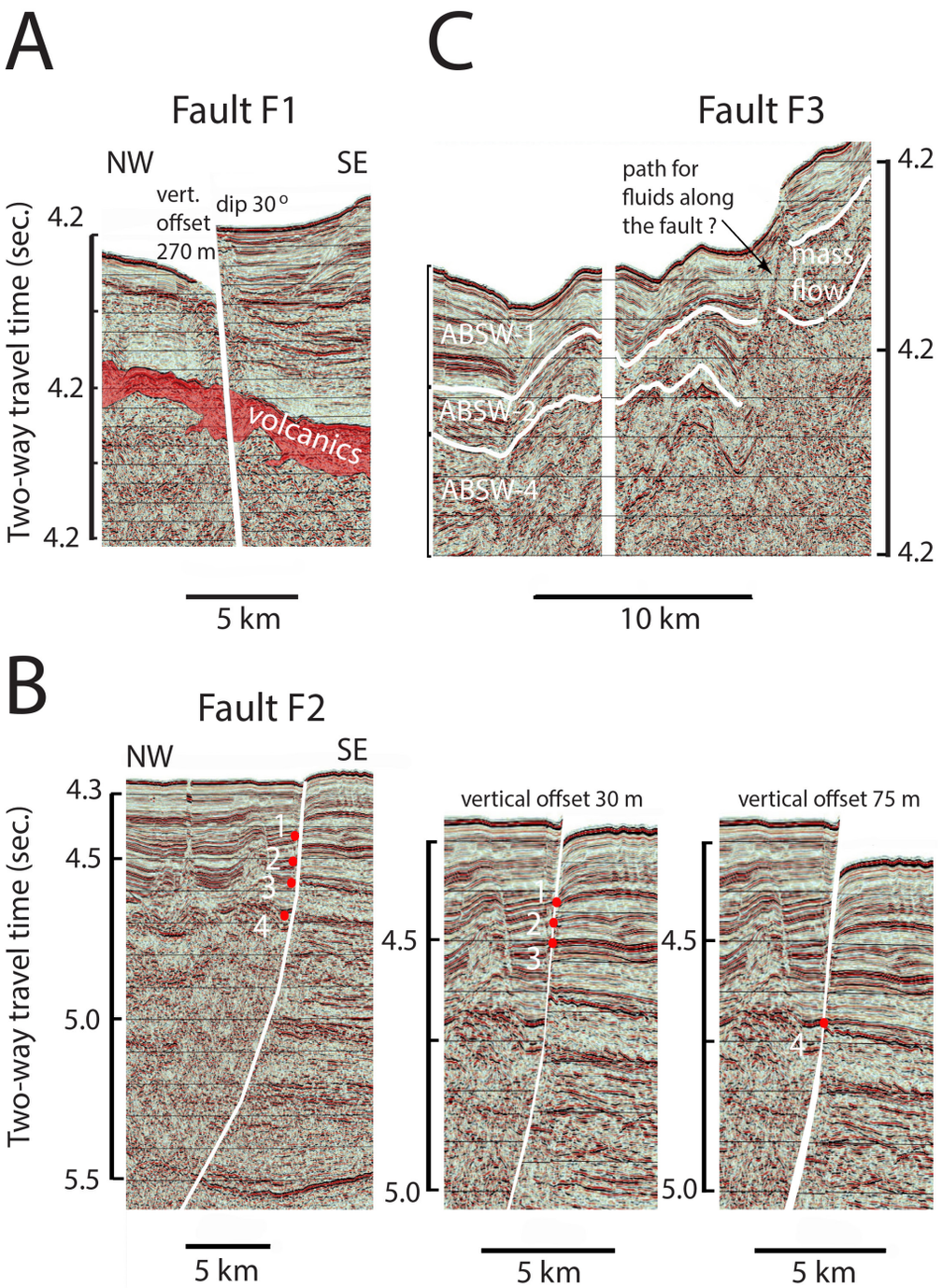

Figure 11. Seismic detail of the main normal faults (fault F1, F2 & F3) in the southwestern Amundsen Basin. The stratigraphic correlations across faults F1 and F2 indicate the amount of offset. Fault F2, left panel: original data with selected reflection events 1-4. Fault F2, middle and right panel show cross-fault correlation of events 1-3 and event 4, respectively. The seismic panel locations are shown in Fig. 6.

Unit ABSW–3

Unit ABSW–3 is a local sediment body below the lower northwestern slope of the Morris Jesup Rise (Figs. 7D & 11). The unit is a lenticular, 0.1 sec. (~90 m) thick volume of chaotic reflections which extends for about 20 km with significant lateral thickness variation. The rough upper surface of the unit is represented by nested diffraction hyperbolae. The internal acoustic image of Unit ABSW–3 has strong similarities to Unit MJ–3A on the western side of the Morris Jesup Spur (Figs. 7A, 7B, 7D & 9A).

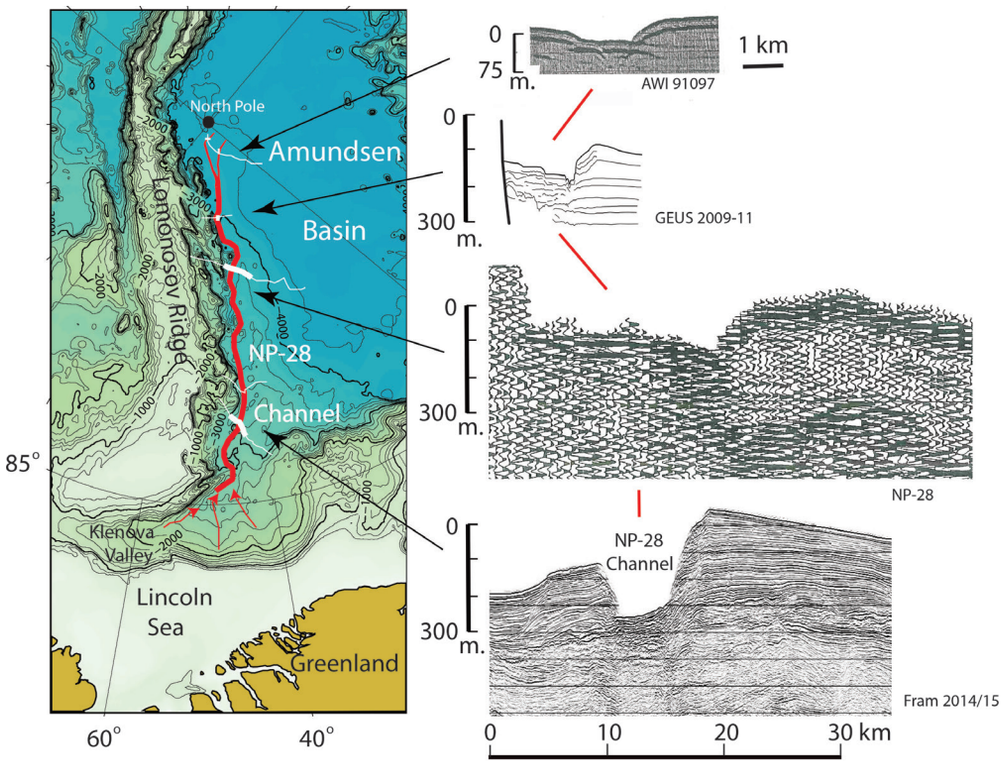

Figure 12. A compilation of available crossings of the NP–28 Channel and associated levee complexes extending from the Lincoln Sea margin to the North Pole. The bathymetry is contoured at 200 m intervals and the submarine fan is approximately outlined by the 3800 m depth contour. Crossings AWI 91097 and NP–28 from Kristoffersen et al. (2004) and GEUS 2009–11 redrawn from Castro et al. (2018).

Unit ABSW–4

Unit ABSW–4 is characterised by relatively small amplitude contrasts, but very complex reflection geometries over a thickness of 0.6 sec. (~600 m) two-way travel time (Fig. 7D). The unit comprises several channel-levee complexes, both contemporary and separate in time. Laterally uniform reflection sequences are limited to the first 10 km east of the foot of the Lomonosov Ridge and also to a 15 km-long section next to the foot of the Morris Jesup Rise before the layering becomes bent to shallower levels below the slope (Fig. 7D). In the centre of the basin is a roughly 5 km-wide zone where the reflected energy becomes laterally non-coherent (Fig. 7D, violet region). The zone has a slope ~10° in the lower part and is associated with fault F2 with an apparent dip of ~45° in the upper part. Similarly, the deeper layers below the lower slope of the Morris Jesup Rise become clouded by non-coherent energy returns.

Unit ABSW–5

Bands and clusters of high-amplitude reflections within Unit ABSW–5 extend out to c. 40 km from the foot of the Lomonosov Ridge and step down into the deeper part of the southwestern end of the Amundsen Basin. Two horizons reach the foot of the Morris Jesup Rise (Fig. 7D). Individual high-amplitude reflection clusters have an apparent width of 2–5 km and thickness of 0.1 sec. (~175 m, assuming a velocity of 3.5 km/s) (Fig. 13). In between and below these reflective volumes of material are complex vertical stacks of piecewise coherent low-amplitude reflections. The acoustic layering within Unit ABSW–5 loses definition below the central part of the basin by a sloping incoherent zone which also penetrates the overlying Unit ABSW–4 (Fig. 7D). The signal coherency is lost below the foot of the Morris Jesup Rise. The minimum thickness of Unit ABSW–5 is 1.2 sec. (~2.1 km).

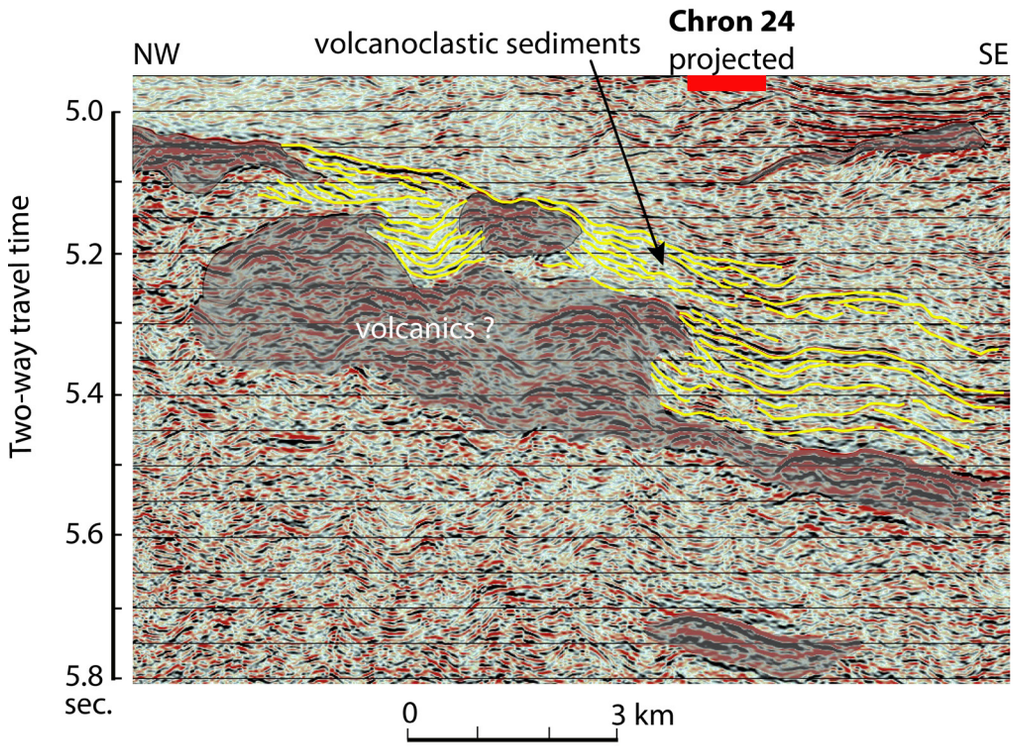

Figure 13. Seismic detail of volcanic accumulations (grey shade) and associated basinward sediment deposits (yellow traces) at the southwestern end of the Amundsen Basin. The projected trace of Chron 24 is shown in Fig. 19B (dashed thin black line) and the location of the seismic section in Fig. 6.

Interpretation

The seabed

The muddy seabed on the Morris Jesup Spur and Rise is littered with gravel and in places almost completely covered with debris (Fig. 8). Icebergs moving in the East Greenland Current are sometimes loaded with hundreds of cubic metres of gravel (Clark & Hanson, 1983; Stein, 2019). The material presently visible on the seabed may have been discharged from melting icebergs in transit within the last half of the Holocene epoch given a sedimentation rate of 1.4 cm/ka (Sellén et al., 2010). The seabed towards the western edge of the spur is locally covered by a few centimetre-thick slabs of whitish broken crust (Fig. 8). The material may either have been brought in and dropped from passing icebergs or more likely be hardground formed in situ and subsequently disrupted by icebergs keels. The geometry of individual slabs seems to be part of a larger entity and argues for an origin in situ either from syn-sedimentary cemented carbonate layers (Wilson & Palmer, 1991) or cementation by methane-derived authigenic carbonate (Judd & Hovland, 2007). Cementation of carbonate layers exposed on the seabed is unlikely from the deficiency of carbonate material. Sediment cores from Morris Jesup only contain biogenic carbonate in 10–20 cm-thick intervals representing interglacial conditions (Spielhagen et al., 2004; Sellén et al. 2010). At deeper levels, the ACEX drill sites on the Lomonosov Ridge show that biogenic carbonate is generally absent in the silty clay down to 190 metres below the seabed (Backman et al., 2006). If the thin whitish crust at the seabed on the Morris Jesup Spur is formed by authigenic carbonate cementation, the presence of methane is required (Judd & Hovland, 2007). Our video recordings from two locations on the seabed show several small cone-shaped features in association with nearby small caves (Fig. 8). The cones have a small opening at the apex. The caves are similar to observations made on the continental rise off North Norway and interpreted as fluid-escape features

(Bøe et al., 2012). The cones may be analogous to miniature 'sand volcanos' on land constructed by erupting groundwater and observed in association with an earthquake in Japan (Judd & Hovland, 2007, page 230). We suggest the caves and cones may originate from expulsion of fluids including methane and contribute to local authigenic carbonate cementation of the surficial sediments on the seabed. The available data do not resolve any obvious spatial relationship between these seabed features and possible faults below the unconformity (Fig. 8).

Morris Jesup Spur

The flat top of the Morris Jesup Spur derives from horizontal truncation of the entire stratigraphic section (Fig. 7A). We interpret the truncation to be a result of subaerial exposure as in the case of the Jan Mayen Ridge (Talwani et al., 1976) or the Broken Ridge (Driscoll et al., 1989). The truncation appears smooth for the sediments above the base of Unit MJ–5 and has minor undulations (max. amplitude 10 m, wavelength 500 m) across the truncated volcanics of Unit MJ–6 and acoustic basement below (Fig. 7A). The basal <30 millisec. (~25 m) thick wedge onlapping the unconformity below the western half of the spur (Fig. 7A, yellow colour) suggests that the western flank subsided first while a section on the eastern half above sea level acted as a sediment source. Subsequently, the eastern half of the spur proximal to the Oligocene rift between the spur and the Yermak Plateau subsided at a faster rate to create the present eastward tilt of the main unconformity (Fig. 7A).

Sediments deposited on bathymetric highs are most likely hemi-pelagic mud and clay carried in suspension within the near-bottom nepheloid layer of boundary currents such as the East Greenland Current (Hunkins et al., 1969; McCave, 1986). The material accumulates as a continuous drape with gentle lateral variation in thickness. At the ACEX site on the central part of the Lomonosov Ridge, silty clay/mud dominate the first 190 m below the sea floor (Backman et al., 2006). Biogenic carbonate as well as biogenic silica are absent and low-amplitude reflections generally correlate with variation in bulk density associated with the relative proportions of the clay and silt fractions (Jakobsson et al., 2007). We expect a similar situation at the Morris Jesup Spur, but the origin of the acoustic impedance contrast for the two high-amplitude reflections on top of the spur is unclear (Figs. 7A & 9A).

A peculiar fault-bounded sediment accumulation of triangular cross-section at the eastern edge of the Morris Jesup Spur (Fig. 7A) presents an enigma as its maximum thickness above an upper bright reflection appears to exceed the corresponding thickness within unit MJ–1 on the rest of the plateau. The accumulation has a steep eastern side (~5°) and slopes more gently (~0.7°) towards the central part of the spur. The internal architecture resembles grounding-zone wedges observed elsewhere on the Greenland shelf (Dowdeswell & Fugelli, 2012; Batchelor & Dowdeswell, 2015), from Svalbard (Ottesen & Dowdeswell, 2009) or in Antarctica (Anderson & Jakobsson, 2016). Alternatively, the accumulation may be a bottom-current deposit as observed c. 100 km to the north at the northern tip of the spur, except that the acoustic response of clay to silt size material brought in by bottom currents tends to display more regular and distinct stratification than observed here (Jokat et al., 1995). A grounding-zone wedge at the edge of the high spur adjacent to a precipitous slope of ~ 60° would represent an extraordinary delicate balance of ice-front stability in a dynamic marine environment during the time needed to build up an excess crestal thickness of ~ 25 m (Fig. 7A). The accumulation has subsequently been displaced by a normal fault.

Local incisions in the seabed on top of the spur suggest mechanical reworking from iceberg keels as observed in Parasound records from the northern tip of Morris Jesup Spur down to 980-metre water depth (Spielhagen et al., 2004) or as linear grooves down to 1045-metre depth from multibeam data (Jakobsson., 2016). The ice transport out of the Arctic Ocean passes over the Morris Jesup Spur from the WNW (Rigor et al., 2002) and we note the difference in the magnitude of the seabed incisions

between the western part of the spur and the light imprint on the slightly deeper eastern part (Fig. 7A). More importantly, the uniform thickness of unit MJ–1 across the spur suggests insignificant erosion and displacement of material across the spur by grounded ice (present water depth <800 m) during the entire record represented by Unit MJ–1 (since late Miocene?).

The undulating bedforms of unit MJ–1 on the upper western slope of the Morris Jesup Spur (water depth shallower than 2 sec.) show slight upslope migration and apparent wavelengths are decreasing with water depth (Figs. 7B & 10A). Although these are characteristics of turbidity current waves (Wynn & Stow, 2002; Rebesco et al., 2014; Shanmugam, 2017), their origin is more likely a combination of a steady bottom-current flow fed by sporadic scavenging of down-slope turbidity current loads. The bow-tie reflections in the depression between the spur and the rise most likely represent narrow down-slope channels of dimensions tens of metres wide and a few metres deep (Fig. 7B, black arrows).

The Morris Jesup Spur was subaerially exposed during deposition of the onlapping sequence MJ–2 which also wedges out to the west against the elevated Morris Jesup Rise (Figs. 7C & 9B). Unit MJ–2 must, in part, have been sourced from erosion of the spur, but shows no significant down-slope changes in impedance contrasts indicative of variations in sand content with increasing distance from the potential sediment source area.

The geometry and semi-chaotic internal structure of Unit MJ–3A suggest a slump deposit (Posamentier & Martinsen, 2011). The upper 11 km of this 25 km-long unit contains detached, heavily deformed, sediment volumes with partial intact internal layering, changing downslope into a more chaotic pattern. The MJ–3A slump has moved about 2.5 km down the upper slope and the accommodation space at the shelf edge was subsequently infilled by shelf progradation (Fig. 9A, infill). The base of the slump cuts though different acoustic stratigraphic levels on the uppermost slope, but generally follows a single stratigraphic level. The subunits MJ–3A and –B have similar stratigraphic positions and possible trigger mechanisms will be discussed later.

Evidence of prograding sediment deposits from an emergent shelf edge at the spur is present in the upper part of the underlying units MJ–4 and MJ–5 (Fig. 9A). The base of Unit MJ–4 is a high-amplitude reflection event which may argue for possible silica-bearing sediments rather than deposition of coarser grain-size material transported by turbidity currents (Fig. 7B). The reflection (Fig. 10A, red arrows) can be interpreted as cutting across the general acoustic stratigraphy. This acoustic response is similar to the serrated seismic response of the diagenetic change of amorphous Opal A to Opal CT observed in siliceous marine sediments (Meadows & Davies, 2009; Ireland et al, 2010). This chemical dissolution-reprecipitation process is accompanied by a porosity reduction of 20% or more, and may take place over a stratigraphic interval of the order of 10 m (Nobes et al.,1992) to form a transition zone stronger and more brittle than the surrounding rocks (Ishii et al., 2011).

The 0.3 sec. (~300 m) thick Unit MJ–5 is onlapping the highly reflective unit below and is truncated by erosion at both ends both below the spur as well as on the upper slope of the rise (Figs. 7C & 9B). Even though the unit forms a wedge capped by an unconformity on the upper slope of the spur, there is little downslope change in acoustic reflectivity associated with distance from a sediment source.

The package of high-amplitude reflections of Unit MJ–6 dipping westwards from below the central part of the Morris Jesup Spur (Figs. 7A & 9A) differ from impedance contrasts associated with sediments which most often include only a few high-amplitude cycles. Similar high-amplitude acoustic facies have been documented by drilling in numerous studies from the North Atlantic rifted margins (Boldreel & Sparre Andersen, 1994; Kjørboe, 1999; Planke et al., 2000; Wright et al, 2012; Abdelmak et al, 2016; Walker et al, 2019). We interpret the acoustic response of Unit MJ–6 to represent low-viscosity basaltic

lava flows extruded subaerially, and the thickness of Unit MJ–6 is > 0.35 sec. or >700 m if we assume a compressional velocity of 4.0 km/s. The amplitude pattern appears laterally uniform below the slope of the Morris Jesup Spur and also below the eastern slope of the Morris Jesup Rise, but the continuity becomes degraded and partly complicated by block rotation in the intervening depression (Fig. 10A). In Fig. 10B, we restore the blocks flanking the depression to an approximate horizontal position, and part of the depositional geometry may be interpreted as lava fronts prograding from subaerial flow into a marine environment (Jones & Nelson, 1970; Walker et al, 2019). If an unconformity is present, an alternative may be erosion from subaerial exposure. Thus, volcanic flows must have been extruded over a distance of 100 km between the continental margin north of Spitsbergen and Ellesmere Island (Fig. 6). The acoustic reflection pattern suggests the emplacement was subaerial on the slope of the spur and the rise, but into shallow water in a topographic low in between the elevated areas.

The basal Unit MJ–7 below the unconformity on the Morris Jesup Spur shows little coherent energy returns except faint layering which we speculate may indicate rotated blocks of stratified material (Fig. 7A). A layered wedge is present below the unconformity at the last 7 km of the eastern side of the spur (Fig. 7A). The wedge is interpreted as sediments (MJ–5) and includes a bright horizontal reflection characteristic of a volcanic flow.

Morris Jesup Rise

Any stratigraphic correlation across the rise is speculative due to the complex stratigraphy and general lack of lateral coherent energy in the reflected seismic signal below 0.2–0.3 sec. sub-bottom (Fig. 7C). Lateral signal coherency in the shallow part is limited to blocks of apparent width < 5 km. We relate the loss of coherency at depth to intense tectonic deformation creating steep or disrupted interfaces of cross-section less than the width of the first Fresnel zone (>150 m) of the reflected signal. The deformed rock volumes may represent tectonic mélanges.

The continuity of Unit MJ–1 across the rise is likely, but the thickness variation is uncertain. Unit MJ–2 extends on to the rise, but any continuity is obscured by volcanic complexes (Figs. 7C & 9B). The volcanic bodies are framed by high-amplitude bounding reflections suggesting lava flows enclosing or intercalated with volumes of sediments (Fig. 9B). The presence of volcanic complexes within units MJ–2 and –3C suggest a prolonged volcanic history associated with the Morris Jesup Rise, or alternatively that the rise stratigraphy is offset relative to the stratigraphy of the spur by undetected fault(s).

The 78 km gap between the seismic transect across the southern end of the Amundsen Basin and the shallow part of the Morris Jesup Rise precludes any meaningful stratigraphic correlation between the two areas (Fig. 7C, D).

Amundsen Basin

The sediment deposits below the southwestern end of the Amundsen Basin include a number of channel/levee complexes throughout the upper 1 sec. of the stratigraphy (Fig. 7D). The recent environment is represented by a single 10 km-wide and 0.4 sec. (~300 m) metre-deep channel flanked by levees (Fig. 7D). The eastern >40 km-wide levee spans the entire lower part of the Klenova Valley and occupies the southwestern side of the Amundsen Basin all the way to the North Pole (Fig. 12). The NP–28 Channel is only matched in size by the Barrow Canyon off Alaska (Eitreim et al., 1982) as the largest in the Arctic Ocean and also on the continental margin of the entire island of Greenland. The width/depth aspect ratio of the NP–28 Channel is at the high end for modern and ancient submarine channels (Clark & Pickering, 1996; Solli et al, 2007). Channels associated with

glaciomarine deposits fed by continental ice sheets may have reliefs up to 1000 m and widths >30 km which is several times larger than river-sourced submarine fans (Normark et al., 1983; Kuvaas & Leitchenkov, 1992; Escutia et al., 2000). Channel relief may be a result of the wide spectrum of grain sizes fed to a glacial fan as compared to finer material transported by river input on a non-glaciated margin (Normark et al., 1983). Alternatively, the extreme relief may arise from a combination of coarse material moving and eroding the channel floor and the fines being deposited by overbank flow (Stow, 1981). Another factor for enhanced overbank flow in high latitudes is the Coriolis force which reaches its maximum value at the poles (Peakall et al., 2012). We interpret deposition of unit ABSW–1 to be associated with a single large trunk channel and reflect input to the Lincoln Sea continental margin from a major ice stream through the northern part of the Nares Strait (England, 1999). The ice stream was confined by the landmasses of North Greenland and Ellesmere Island and continued to the shelf edge across the Lincoln Sea (Fig. 12). The volume of material associated with the NP–28 Channel in the Amundsen Basin is reflected by a >1 km excess bathymetric elevation of the seabed along the south-western margin of the Amundsen Basin relative to the deepest abyssal plain (Fig. 12). The deepest large channel floor recognised in the seismic stratigraphy about 300 km north of our crossing is 0.35 sec. (~300 m) below the seabed (Castro et al., 2018), with a smaller channel also discernible at 0.45 sec. (~360 m) directly below the present channel floor (Fig. 4 in Castro et al., 2018).

Unit ABSW–2 is less than 0.15 sec. (~135 m) thick, contains smaller paleochannels and appears as a transition between the overlying uniform unit ABSW–1 and the underlying 0.6 sec. (~600 m.) thick unit ABSW–4 with several large paleo-channels and major lateral shifts in sediment pathways (Fig. 7D). Channels on the lower continental slope probably collect material from numerous tributaries (Clark & Pickering, 1996). The more easterly position of the channels in Unit ABSW–4 relative to the present NP–28 Channel suggests past sediment input to the lower continental slope from several places on the upper slope between the Morris Jesup Rise and the shelf edge north of Ellesmere Island. Tectonic growth of the Morris Jesup Rise may have repeatedly altered the slope morphology, destabilised upper-slope deposits and created temporary sediment pathways. We infer that glacial conditions with trough-mouth fan development on the Lincoln Sea continental slope favour a major trunk channel following the Klenova Valley, whereas periods of persistent tectonic activity on the Morris Jesup Rise and/or reduced glacial input are manifested as sediment input channelled through more easterly pathways (Figs. 7D & 12).

We interpret Unit ABSW–3, a semi-chaotic 11 km-long and 0.1 sec. (~ 90 m)-thick body on the lower northwestern slope of the Morris Jesup Rise (Figs. 7D & 11, right panel) to be a mass flow of partly intact rotated blocks (Posamentier & Martinsen, 2011; Alves, 2015). Slope failure was probably triggered by movements on nearby faults. The stratigraphic position is below ABSW–2 and above ABSW–4. A fault has subsequently cut through the toe and the fault trace (F3) appears associated with a trail of enhanced seismic amplitudes indicating the presence of escaping fluids (Fig. 11, fault F3).

The strata of units ABSW–4 and –5 are bent upwards below the foot of the slope of the Morris Jesup Rise and continue into a frontal deformation zone (Fig. 7D). The deformation zone involves two or three folds of wavelengths <3 km and peak-to-peak amplitudes of 0.12 sec. (~150 m) whereas the strata for the next ~8 km upslope are only mildly deformed. The loss of coherency of the seismic signal at depth in the frontal zone as well as farther northwest in the ~ 5 km-wide zone (dip ~12°) in the middle of the basin, reflects more intense deformation (Fig. 7D). The loss of signal coherency below the rise proper indicates pervasive deformation. There may be a small bathymetric step at around 2000 m water depth on the lower northwestern slope of the Morris Jesup Rise (Fig. 2), but the gap in our seismic data precludes any direct indications as to the tectonic significance of any step in the rise architecture. The seismic data suggest that the outer part of the rise is likely an accumulation of deformed sediments. Also, values of the magnetic field intensity along this part of the seismic transect are low (Fig. 2) and show small lateral variations (Jokat et al., 2016).

Irregular high-amplitude reflections interfinger with more monotonous acoustic intervals within Unit ABSW–5. We interpret the bright reflections as compound volcanic flows or complexes intercalated with sediments. The volcanic flows have travelled from the west into a sedimentary basin during four separate phases which span deposition of a 0.8 sec. (~1.4 km.) thick section of sediments (Figs. 7D & 13). In two instances the flows reach across the basin and their distal ends are consumed by the advancing deformation zone (Fig. 7D).

The volcanics appear as nested local (1–3 km wide) accumulations with uneven upper surfaces which may represent local volcanic centers, subaerial silicic flows of relatively high viscosity or extrusion of less viscous basaltic flows into shallow water (Boldreel & Sparre Andersen, 1994; Wright et al., 2012; Abdelmalak et al., 2016). Hypabyssal intrusions may also be a component. The basinward face of each volcanic mound is associated with an onlapping wedge of reduced signal amplitude (Fig. 13). The wedges are interpreted as volcanoclastic material (Jones & Nelson, 1970) and the setting is most likely shallow water at the basin margin. Two weak reflection segments at ~6.5 sec. two-way travel time indicate at least 3.4 km of sediments in the southwestern Amundsen Basin if we assume an average velocity of 2.0 km/s for units ABSW–1, –2 and –4, and 3.5 km/s for unit ABSW–5 (Fig. 7D). The depth to crystalline basement is unknown, except that inversion of gravity data suggests a total sediment thickness of ~7 km (Døssing et al., 2014).

Discussion

The sedimentary deposits on the continental margin north of Greenland range from the laterally uniform layers below the western slope of the Morris Jesup Spur to a complex and deformed stratigraphy of the Morris Jesup Rise and in the west a large channel/levee accumulation overlying weakly deformed sediments and volcanics below the lower slope of the Lincoln Sea margin (Fig. 7). A striking feature is the large amount of glacial input to the Lincoln Sea margin and insignificant glacial input to the Morris Jesup spur and rise area.

Morris Jesup Spur: Age of the acoustic facies

Deposits above the unconformity on the Morris Jesup Spur (MJ–1) are expected to be hemipelagic sediments and within its upper part a contribution of material carried by sea ice and icebergs. If we compare the thickness of Unit MJ–1 with deposits on the top of other Arctic ridges like the Pleistocene section at the ACEX drillsite on the Lomonosov Ridge (Fig. 1) with a sedimentation rate of ~1.5 cm/ka (Frank et al., 2008; O'Regan et al., 2008) or the 180 m-thick late Miocene– Recent section at Site 908 (Knies et al., 2014) on the top of the Hovgard Ridge (2.65 cm/ka), we arrive at an age range of 3.8–6.7 Ma. for a delayed submergence of the Morris Jesup Spur. The spur split from the Yermak Plateau before Chron 13 (~34 Ma.) when Greenland became part of the North American plate and should theoretically have subsided to its present depth 25 million years ago (Voelker, 2016). The contemporary subsidence history of another continental fragment, the Hovgard Ridge, is similar (Myhre et al., 1995; Knies et al., 2014). Thermal subsidence of the lithosphere is time dependent and the effect may be limited by the positive bouyancy of the continental crust, plate forces (Weissel & Karner, 1989; Reston, 2009) or post-breakup uplift from temperature-related changes in mantle mineral composition (Minakov & Podladchikov, 2012).

There is a distinct acoustic contrast between units MJ–2 and –4 (Fig. 7B) which suggests a change in depositional environment. To obtain an age estimate for the base of Unit MJ–2, we extrapolate the late Pleistocene sedimentation rate of 1.4 cm/ka for the Morris Jesup Spur from Sellén et al. (2010) which

is close to the average Cenozoic sedimentation rate (1.5 cm/ka) on the Lomonosov Ridge (Backman et al., 2008), and arrive at about 16 Ma. Thus, the MJ–2/MJ–4 transition may relate to opening of the Fram Strait at ~17.5 Ma and the emerging ventilation of the Arctic Ocean as interpreted from scientific drilling on the Lomonosov Ridge (Moran et al., 2005; Jakobsson et al., 2007).

Deposition of the mass flow units MJ–3A and –B is interpreted as an instantaneous event at around 17.5 Ma. A likely trigger mechanism is tectonic movements (Masson et al., 2006) since pervasive folding and several major faults appear to terminate at the base of Unit MJ–2 (Figs. 7A, B & 9A). The mass flow (MJ–3A) smooth offsets at the top of the underlying unit MJ–4 and the trailing scar created on the uppermost slope of the spur was subsequently filled in by a small prograding wedge (Fig. 9A, MJ–3A infill).

Continued projection of a sedimentation rate of 1.4 cm/ka yields an estimated age of ~37 Ma for the base of Unit MJ–4 and ~56 Ma for the top of the volcanics of Unit MJ–6. Alternatively, the mean Paleogene sedimentation rate of 17.7 m/Ma for the Lomonosov Ridge (Jakobsson et al., 2007) implies an age of ~50 Ma for the top of Unit MJ–6. The Morris Jesup Spur rifted away from the Yermak Plateau prior to ~34 Ma and the top of Unit MJ–5, estimated at ~37 Ma, displays an erosional unconformity (Fig. 9A) which may indicate rift-related uplift. Also, the difference in acoustic facies between units MJ–4 and –5 may reflect a subsequent change in environment associated with the Morris Jesup Spur rifting away from the Yermak Plateau (Fig. 7B). '

We estimate the age of the volcanic Unit MJ–6 to be Late Cretaceous–Eocene. The unit may possibly be part of an alkaline phase of volcanism (85–60 Ma.) attributed to continental rifting (Tegnér et al., 2011). The estimates of stratigraphic ages are summarised in Fig. 14.

Morris Jesup Rise: Age of the acoustic facies

Units MJ–1 and –2 appear to continue westwards to the Morris Jesup Rise with little change in thickness. On the rise, Unit MJ–2 (late early Miocene–Pliocene) also includes high-amplitude reflections interpreted as volcanic material (Fig. 9B). Units MJ–4 and –5 which span the early Eocene to early Miocene onlap the rise, are truncated at the top and overlain by a volcanic Unit MJ–3C restricted to the rise. As the volcanics of Unit MJ–6 appear to continue from the spur to the crest of the rise, the eastern part of the rise appears connected to a history of volcanism which may extend from the Late Cretaceous/early Cenozoic to the Miocene (Fig. 14). The accumulation of volcanic material on the outer rise does not appear to have any significant magnetic signature (cf., Fig. 2). However, the lack of significant magnetic intensity anomalies does not preclude the presence of volcanic rocks. The Kap Washington volcanics on the north coast of Greenland ~ 200 km to the SW may illustrate this (Fig. 1). The KWG rocks are pyroclastic rocks and siliceous lavas which tend to have a relatively low intensity of magnetization (Flinn & Morgan, 2002; Ganerød et al., 2010). As a result, the westernmost 5 km-wide KWG outcrop on Lockwood Island, which is estimated to be more than 3 km thick (Brown et al., 1987), is associated with a magnetic intensity variation of only a few tens of nanotesla (Fig. 5B in Jokat et al., 2016).

Southwest Amundsen Basin: Age of the acoustic facies

The large channel/levee complex on the Lincoln Sea margin feeding the submarine fan in the southwestern Amundsen Basin is most likely formed by glacial sediments. However, the timing of mountain glaciers or continental ice sheets reaching the Arctic Ocean is poorly known. Given that the general pattern of ocean circulation and sea-ice drift in the Arctic Ocean has prevailed since the opening

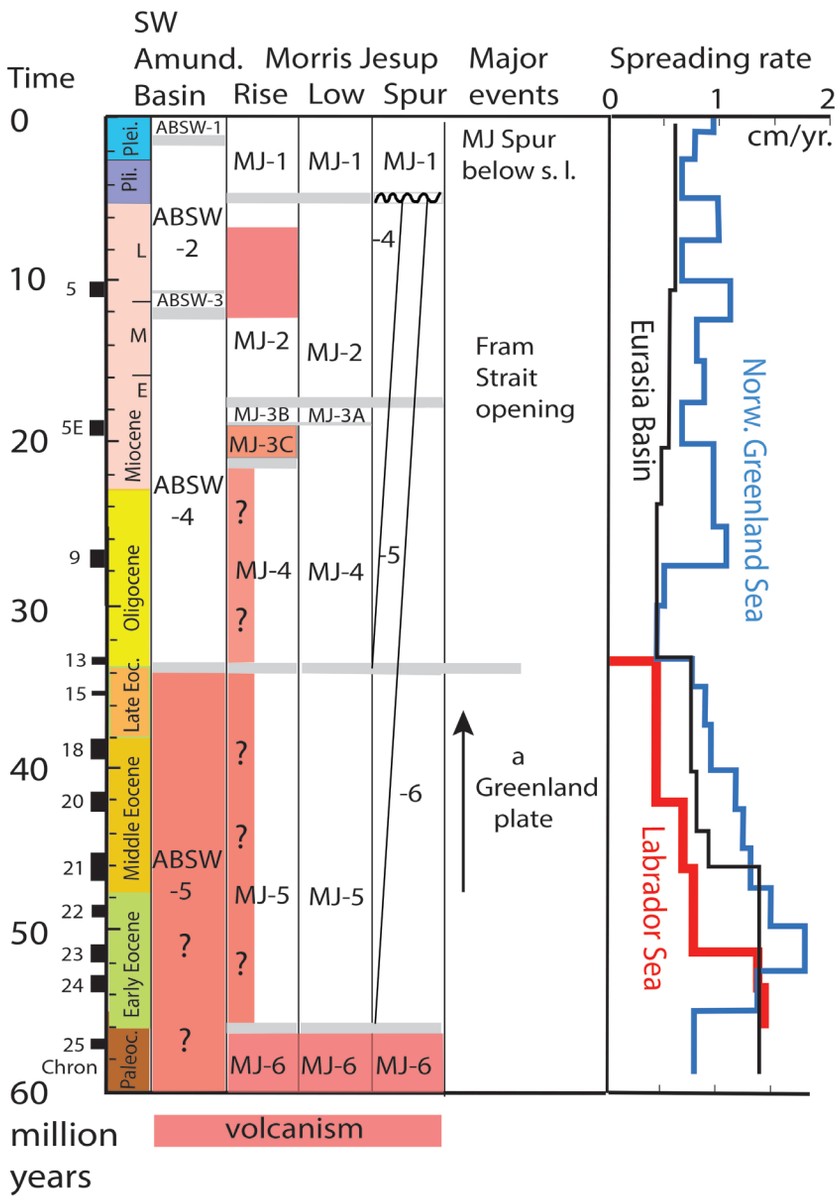

Figure 14. Summary of tentative stratigraphic ages assigned to acoustic facies on the continental margin north of Greenland. Spreading rates in the Eurasia Basin from Glebovsky et al. (2006), in the Norwegian/Greenland Sea from Gaina et al. (2017) and in the Labrador Sea from Roest & Srivastava (1989).

of the Fram Strait, we assume that outlet glaciers along the Siberian and the northern Kara and Barents Sea margins had little influence on sediment deposition on the continental slopes of the Lincoln Sea, North Greenland or the southern end of the Amundsen Basin. The Mackenzie region drained into the Hudson Bay area throughout the Cenozoic and became diverted into the Arctic Ocean by Quaternary glaciations on the North American continent (Dixon & Dietrich, 1990; Duk-Rodkin & Hughes, 1994; Batchelor & Dowdeswell, 2014). The North American ice sheets were smaller during the first 2 Ma of the late Cenozoic than they were during the last 0.7 Ma (Barendregt & Irvin, 1998). The largest known extent of glacial ice on Ellesmere Island, possibly older than 400 ka, was most likely facilitated by a reduced sea-ice cover in the Arctic Ocean (Lemmen & England, 1992). The advance of glacial ice across the Lincoln Sea continental margin is manifested by an over-deepened trough projecting northeast from the Nares Strait, turning north and ending in a convex upper continental slope most likely representing a trough mouth fan (Fig. 12). During the last glacial maximum, the Greenland and the Innutian ice sheets on Ellesmere Island coalesced and supported an ice stream flowing northeast and constrained by the topography of the Nares Strait (England, 1999).

The glacial deposits on high-latitude continental margins show a general pattern of initial restricted glaciations with glacio-fluvial sediment deposition evolving into expansive periods where the glaciers advanced beyond the coastline multiple times (Nielsen et al., 2005). The entire eastern continental margin of Greenland from south to north is shaped by prograding wedges of sediments documented by scientific drilling to be of glacial origin and considered younger than middle Miocene (Larsen et al., 1994; Solheim et al., 1998; Berger & Jokat, 2008, 2009). The largest thickness below the shelf edge north of 69° N appears to be >1.35 sec. (~1.35 km) with a shelf edge advance of >60 km (Table 1). The advance is largest north of 73° N.

Table 1. Estimates of the advance of the shelf edge along the coast of East Greenland due to glacial sediment input. The estimates are based on seismic sections published by Berger & Jokat (2008, 2009). Reflection R1 separates an upper aggrading unit from two underlying prograding units separated by reflector R2. Reflector R3 marks the transition from prograding to deeper non-prograding strata and is considered to represent the base of the glacial sediments.

	Shelf edge advance (km)			Wedge thickness** (km)			Age calibration
Latitude	**Since R3***	**Since R2***	**Since R1***	**Above R3***	**Above R2***	**Above R1***	**ODP Site**
79° N	?	~50	~6	?	~0.8	~0.4	909, 913
78° N	?	~60	~4	?	~1.1	~0.3	
77° 30’	~110	~25	~1	~1.6	~0.8	~0.2	
73° 30’	~90	~20	~4.5	~1.35	~1.0	~0.35	
69°	~60	~15	~5	~1.5	~1.0	~0.6	
68°	~50	~5	~2.5	~1.0	~0.4	~0.15	

**from Berger & Jokat (2008, 2009). **wedge thickness is measured at the present shelf edge and assumes a seismic velocity of 2.0 km/s.*

ODP Site 913 at 75° 30’ N (Fig. 1) is currently the northernmost age calibration point for direct glacial input to the East Greenland margin and used for estimating the age of the base of the glacial wedge off Northeast Greenland (Berger & Jokat, 2008, 2009: Døssing et al., 2016). Unfortunately, the recovery in hole 913B was only 2% in the interval 86–375 m below the sea floor. It was drilled from 375 m down to 423.5 m and a wash core recovered 7.16 m of undisturbed section, but the true position of the wash core within the drilled interval is unknown (Shipboard Scientific Party Site 913, 1995). As recovery was high below 423.5 m depth, the core could equally well represent stratigraphy just above 423.5 m depth rather than at 375 m depth as listed. This particular core yielded a mid–Miocene age from diatoms and ebridians. Another tie-point is a wash core from 288 m depth containing poorly preserved benthic foraminifera with a listed age range of Quaternary to Pliocene? These considerations suggest the presumed mid–Miocene age inferred from Site 913 for the base of the glacial wedge off Northeast Greenland is most likely too old. We propose a revised framework where the deepest reflector R3 of Berger & Jokat (2009) at the base of the glacial wedge is set at ~7 Ma instead of ~15 Ma. If this is correct, a general temporal pattern emerges for sediment input to the East Greenland continental margin since the late Miocene (Larsen et al., 1994; Vanneste et al., 1995; Channel et al., 1999; Butt et al., 2001), which is also in general agreement with observations from southwest Greenland by Nielsen & Kuijpers (2013).

i) 7– ~5 Ma: mountain glaciers in Greenland advance beyond the coastline followed by enhanced glacio-fluvial input to the shelf and slope;
ii) ~5 Ma: the Greenland Ice Sheet expands and reaches the shelf edge, oscillates and retreats followed by glacifluvial and hemipelagic sedimentation;

iii) 2.74 Ma: intensification of Northern Hemisphere glaciation and the ice-sheet readvance to the shelf edge, the ice front oscillates and retreats followed by glacifluvial and hemipelagic sedimentation;
iv) Mid–Pleistocene Transition (1.25–0.7 mill. years ago) and later; several readvances to the shelf edge.

The channel-levee complex of Unit ABSW–1 is a manifestation of prolonged high sediment input to the Lincoln Sea margin. This could have occurred from either ~5 Ma or 2.74 Ma and onwards. However, as the Northern Hemisphere glaciations intensified at 2.74 Ma (Flesche Kleiven et al., 2002), prograding wedges developed on the Norwegian Shelf but wedge growth did not accelerate until after 1.6 Ma on the Svalbard margin (Solheim et al., 1998; Dahlgren et al., 2005). The main Scoresby Sound Fan developed after 1.77 Ma (Laberg et al., 2018). For this reason, we consider Unit ABSW–1 to be younger than 2 million years and probably younger than 0.7 Ma following the argument of Barendregt & Irvin (1998) about the relative size of past North American ice sheets (Fig. 14).

Past glacial advances with confluence of the Greenland and Innutian ice sheets as documented for the Last Glacial Maximum by England (1999) would enhance a main Nares Strait ice stream and increase the sediment transport capacity. The implied sedimentation rate for ABSW–1 being younger than 0.7 Ma is ~46 cm/ka and greater than glacial deposition rates (10–30 cm/ka) for the East Greenland margin, but significantly lower (30–170 cm/ka) than for the Svalbard–Barents Sea margin (Solheim et al., 1998). The NP–28 trunk channel has also been active through deposition of units ASW–2 and –4 as the deepest paleo-channel floor appears to be as deep as 4.95 sec. travel time (Fig. 7D). There would still be a 0.9 sec. (~900 m) elevation difference relative to the deepest (5.8 sec. depth) channel floor observed ~300 km to the north (Castro et al., 2018), and the corresponding bathymetric gradient (> 1:1000) would be sufficient to sustain sediment transport by abyssal gravity flow (Bye, 1971).

Unit ABSW–2 is characterised by several smaller channels which suggest several active sediment pathways on the Lincoln Sea margin (Fig. 7D). Sediment input at this time may have been related to increased erosion from emerging mountain glaciers in North Greenland and advance to the coastline after ~7 Ma as observed elsewhere (Larsen et al, 1994; Channel et al., 1999). Slope instabilities from tectonic movements on the Morris Jesup Rise may also have contributed to the input of sediment.

The mass flow ABSW–3 is stratigraphically below ABSW–2 and likely to have been a short event triggered by tectonic movement on the Morris Jesup Rise. Potential triggers are motion on a fault (F3) at the lower end of ABSW–3, a long-lived major growth fault (F2) in the basin 5 km NW of the unit F2 or major faults upslope not detected here because of the data gap (Figs. 2 & 6).

The activity of the NP–28 Channel extends back into the lower half of Unit ABSW–4, but most channels in the unit are predominantly in the eastern half of the basin (Fig. 7D). We speculate that this reflects sediment input related to mobilisation of deposits on the Morris Jesup Rise or the adjacent continental slope of the Lincoln Sea generated from an ongoing tectonic convergence between Greenland and the North American plate. This suggests that Unit ABSW–4 may be older than considered here (Fig. 14) and could extend back into the late Eocene.

Volcanism north of Greenland

Volcanism on the Morris Jesup Spur is limited to the basal part of the stratigraphy and the volcanic unit MJ–6 extends westward on to the Morris Jesup Rise (Figs. 7A, B, 9B & 10A). The spur was initially part of a Yermak crustal block and represented the continental slope north of Svalbard in the early Cenozoic (Kristoffersen et al., 2020). Although opening of the Sophia Basin by crustal extension was not associated with any significant volcanism (Geissler & Jokat, 2004), the Morris Jesup Spur in the northwestern half of a Yermak crustal block, was covered by a > 0.5 km-thick sequence of volcanic rocks

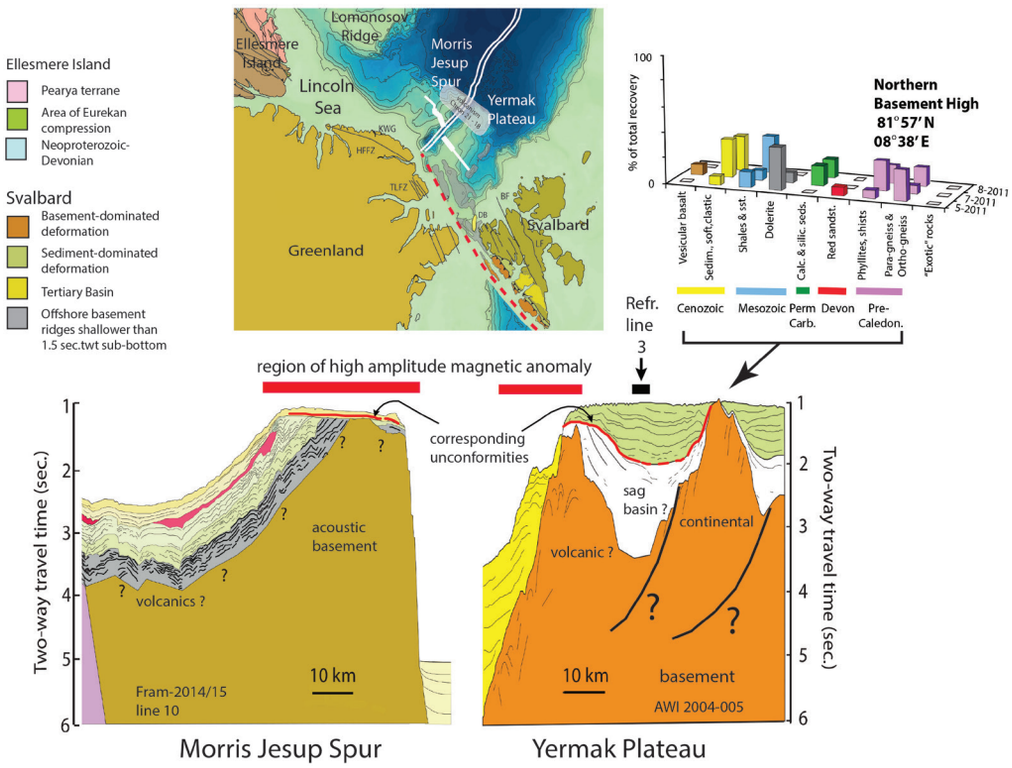

Figure 15. Reconstruction of the position of the Morris Jesup Spur relative to the Yermak Plateau at Chron 13 (~34 Ma.) and comparison of their respective cross-sections. Europe (Svalbard) is kept fixed and the rotation of North America (Greenland) is from parameters given by Gaina et al. (2009) using GPlates software (www.gplates.org). The section from the Yermak Plateau is modified from Geissler et al. (2011) and dredge results (upper right) from Kristoffersen et al. (2020). The position of seismic refraction line 3 of Jackson et al. (1984) as indicated by a black arrow. Abbreviations: BF; Billefjorden Fault. DB; Danskøya Basin, HFFZ; Harder Fjord Fault Zone, KWG; Kap Washington Group volcanics, LF; Lomfjorden Fault, TLFZ; Trolle Land Fault Zone.

(Unit MJ–6) from a subaerial source to the southeast of the spur (Fig. 15). This volcanism must have extended northwestwards at least to the paleo-position of the Morris Jesup Rise with local centres of extrusion. Unit MJ–6 could be part of the alkaline phase (85–60 Ma) of volcanism in the High Arctic and a forerunner to sea-floor spreading in the Eurasia Basin (Tegnér et al., 2011). A volcanic source region may have been the northwestern volcanic margin of an elevated Yermak crustal block (Fig. 15, lower right). Alternatively, Unit MJ–6 could be part of a younger local suite of volcanics in the western and northern parts of the Yermak block (Fig. 2) sampled by the dredged basalts (~51 Ma.) from the Sverdrup Bank (Riefstahl et al., 2013). If so, the volcanism may have started at the end of amagmatic crustal extension in the Sophia Basin by about Chron 22 (~49 Ma) and included construction of the submarine northern tip of both the Yermak Plateau and the Morris Jesup Spur (Kristoffersen et al., 2020).

Following deposition of Unit MJ–6, the Morris Jesup Rise was uplifted as units MJ–5 & 4 are onlapping, wedging out upslope and truncated by an unconformity on the northeastern flank of the rise (Fig. 9B). Volcanism may have continued on the high northernmost part of the rise where Unit MJ–6 is directly overlain by two units (MJ–3C & MJ–2) with large volcanic components (Fig. 9B). The top of the volcanic stratigraphy on the Morris Jesup Rise reaches an elevation (~ 1400 m water depth) which appears as a plateau of >60 km in N–S extent in the rise bathymetry (Fig. 3C). Our postulated stratigraphic age of Unit MJ–2 suggests that volcanism on the rise persisted into the late Miocene (Fig. 14).

Volcanism at the southwestern end of the Amundsen Basin was associated with syn-volcanic deposition of >1.4 km of sediments (assuming a velocity of 3.5 km/s). The eastern termination of the stacked flow fronts in Unit ABSW–5 appears to be in general alignment with the SW projection of

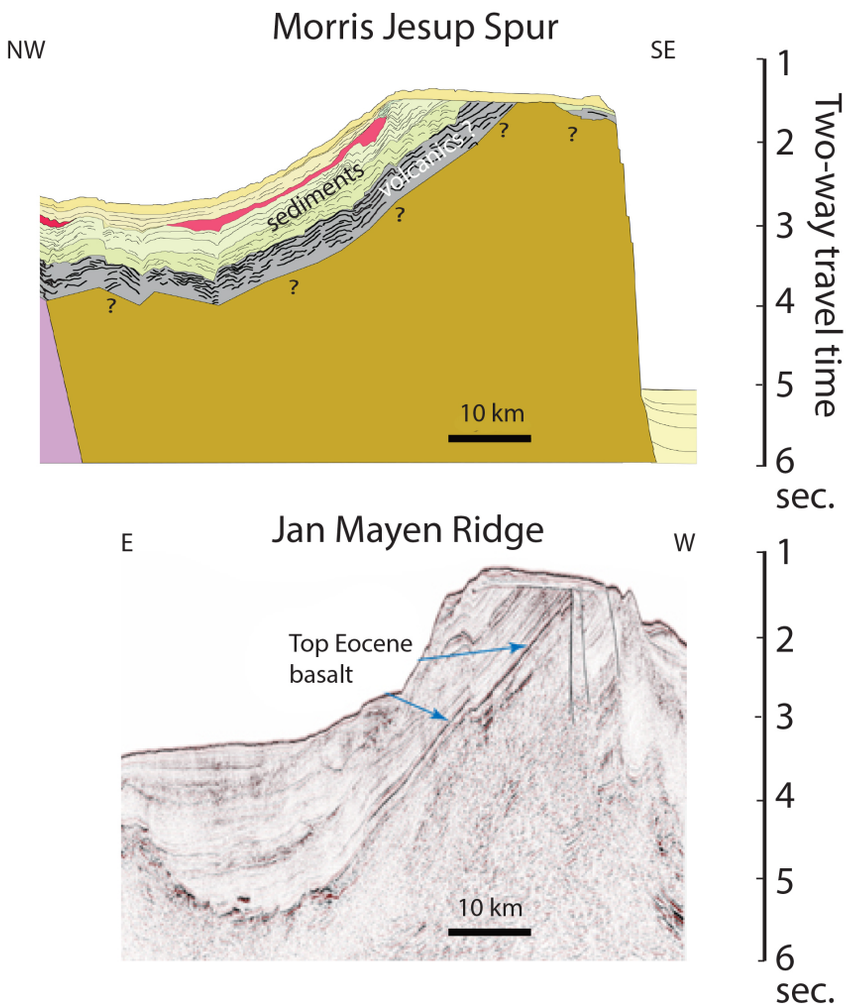

Figure 16. A comparison of the Morris Jesup Spur structure with a cross-section of the northern part of the Jan Mayen microcontinent. The Jan Mayen section is from Oljedirektoratet (2013).

Chron 24 into the area (Figs. 13 & 17). We suggest that the volcanic flows (Unit ABSW–5) are younger than the corresponding top of the volcanics below the Morris Jesup Spur for two main reasons:

1) the pre–glacial section (ABSW–4) above the volcanics at the southwestern end of the Amundsen Basin is thinner (0.45 sec.) than its presumed equivalent (MJ–2, –4 & –5) between the spur and the rise (0.7 sec.);
2) the volcanic input in Unit ABSW–5 extends over a stratigraphic thickness of 0.8 sec. two-way travel time indicating protracted volcanic activity.

From this, we speculate that volcanism during deposition of Unit ABSW–5 in the southwestern Amundsen Basin extended from the Late Cretaceous at least into the Oligocene.

There is a striking contrast between the non-volcanic northern Barents Sea margin (Berglar et al., 2016; Lutz et al., 2018) and the conjugate Lomonosov Ridge margin with protracted volcanism in the SW Amundsen Basin (Fig. 17). This suggests that volcanism at the foot of the slope of the Lomonosov Ridge is younger than the initial rifting and early sea-floor spreading in the southwest Amundsen Basin. The late volcanism appears quite extensive as flows reached >30 km into the basin from the projected position of Chron 24 (Figs. 7D & 13).

Tectonic deformation on the continental margin north of Greenland

The sediments on the continental margin north of Greenland show evidence of tectonic deformation (Fig. 7). The stratigraphy below Unit MJ–2 of the Morris Jesup Spur and its western slope has been gently folded (wavelengths <2.5 km, amplitudes <100 m) with a unique fault-bounded structure at the eastern edge (Fig. 7A). The folds become attenuated below the western slope of the spur and the stratigraphy partitioned by normal faults (vertical offsets <150 m) into rotated 4–9 km-wide blocks between the spur and the rise (Figs. 7B & 10A). The true strikes of these folds and faults are not known. Possible alternative trends could be either parallel to the eastern perimeter of the Morris Jesup Spur and generated by forces which induced splitting of the former Yermak block, or folds developed normal to the compressional stresses from the convergence between Greenland and the southwestern part of the Amundsen Basin (Fig. 1). The case of strike-slip faulting is difficult to recognise in the seismic record unless either positive or negative flower structures are present (Harding, 1985; Zalan, 1987). A negative flower structure is considered to reflect a transtensional event. A fault in the low between the spur and the rise (Fig. 10A) could possibly be interpreted as a negative flower structure. Gentle deformation of the stratigraphy below the Morris Jesup Spur is pre-Unit MJ–2 or pre-opening of the Fram Strait and ended with triggering of the mass flows MJ–3A & –B (Figs. 7D & 14).

The Morris Jesup area is presently aseismic. The recent seismicity is concentrated along the Greenland coast (INTAROS event catalogue; Gregersen, 1982) and considered to have arisen from post-glacial unloading (Stein et al. 1989; Chung, 2002).

The Morris Jesup Rise is a massively deformed construction of unknown architecture delimited to the north and west by a deformation front. To the east, the uplifted western slope of the rise forms the transition to the relatively mild tectonic deformation of the Morris Jesup Spur (Fig. 6). The central part of the rise forms a plateau (Figs. 2 & 3C) mantled by deformed sediments and volcanics and dissected by a complex fault pattern (Fig.7C). The site of the rise had slightly elevated topography already by the start of deposition of Unit MJ–5 in the early Eocene (Figs. 9B & 14). The rise could be the result of sediment input from a tectonically active proto-Lincoln Sea continental margin into a short oceanic spreading segment which was later deformed as the Eurekan convergence progressed and in addition obscured by later volcanism (Figs. 14 & 18). We have interpreted the loss of coherent seismic energy below the

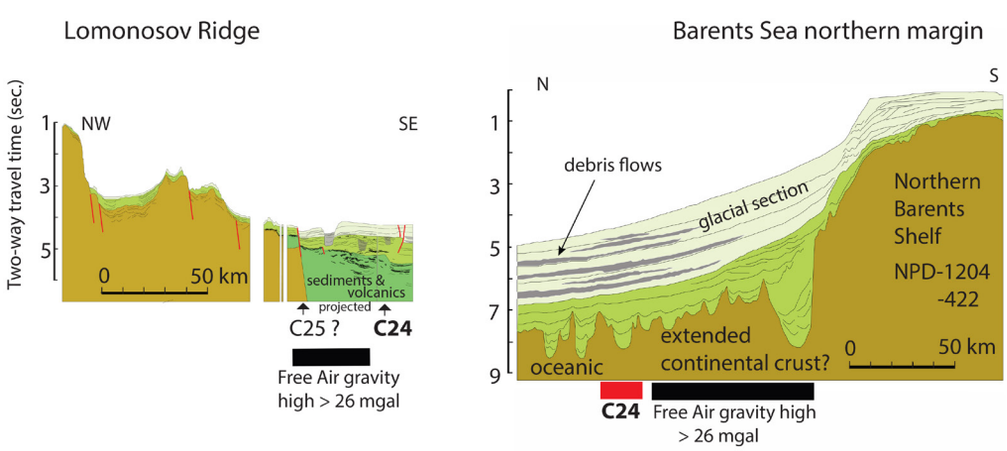

Figure 17. Compilation of geophysical information from the conjugate northern Barents Sea margin and the Lomonosov Ridge. Seismic line NPD–1204 422 is by courtesy of the Norwegian Petroleum Directorate. The relative locations of the two conjugate seismic sections in the Eurasia Basin are shown in Fig. 18 for Chron 21 time and in Fig. 20 at "Chron 25" or just prior to the onset of sea-loor spreading. The extent of the glacial section on the Barents Sea margin is defined from seismic-stratigraphic intervals interpreted as debris flows.

rise as evidence of extensive deformation, but evidence of possible thrust planes separating tectonic mélanges is not apparent so far. Unfortunately, our seismic data gap includes the critical northwest-facing frontal part of the rise (Figs. 2 & 6). A time line for deformation of the Morris Jesup Rise is difficult to constrain, but is expected to span the entire Cenozoic.

The tectonic impact on the sediments at the southwestern end of the Amundsen Basin is manifested as:

i) a normal fault (fault F1) with an offset of ~270 m and dip of <30° at the foot of Lomonosov Ridge (Figs. 7D & 11);
ii) ii) as a ~5 km-wide shallow angle (12° – 24°) deformation zone in the middle of the basin comprising Unit ABSW–4 and older strata. This zone is bounded in the upper part by a normal fault (fault F2) which penetrates all the way to the seabed (Figs. 7D & 11);
iii) iii) a normal fault (fault F3) on the lower slope of the deformation zone (Figs. 7D & 11). In addition, there are many other minor faults particularly in Unit ABSW–1. Past displacements on all the main faults in the SW Amundsen Basin have occurred up to and including the time of deposition of the glacial unit ABSW–1 (Fig. 7D).

Faults F1, F2 & F3 all demonstrate late-stage extension and the entire displacement on fault F1 includes the lower part of Unit ABSW–1 which suggests an age of less than 1 million years. We expect these late-stage normal displacements in part reflect readjustments of crustal stresses from relatively rapid loading of the SW Amundsen Basin crust by glacial sediments.

The pre-glacial stratigraphy of the basin between the foot of the Lomonsov Ridge and the Morris Jesup Rise shows only mild deformation from compression except for the ~5 km-wide zone in the middle of the basin (Fig. 7D). Also, Unit ABSW–4 appears to double in thickness from west to east and may reflect loading of the lithosphere from an advancing Morris Jesup deformation zone. The lack of evidence for significant convergence may imply that either the upper part of Unit ABSW–5 is younger than considered here (Oligocene?) or the main contractional deformation between Greenland and the Lomonosov Ridge is located below the continental slope and shelf landward of the Morris Jesup deformation front. The Morris Jesup Rise deformation front starts with an upward flexure of the entire stratigraphic column followed by a succession of open folds (wavelength <2.5 km, amplitude < 100 m). Sediments immediately southeast of Fault F3 do not appear to be deformed. We speculate that the observed sediment deformation, vergence of the folds and elevated bathymetry of the deformation front on the northern slope of the Morris Jesup Rise reflect the response of the sediments of the SW Amundsen Basin to convergence against the north-facing apex of a deep wedge-shaped basement backstop below continental margin north of Greenland. A shallow basement backstop would have induced frontal thrusts. The rise may be a northern promontory of more extensively deformed crustal unit below the Lincoln Sea margin (Fig. 18).

Possible plate-tectonic scenarios: the end of the Eocene:

In Fig. 15, we show the reconstructed relative position of the conjugate plateaus north of Greenland (Morris Jesup) and Svalbard (Yermak) at the time of Chron 13 (34 Ma) using the GPlates software (www.gplates.org; Boyden et al., 2011). The rotation parameters for North America (incl. Greenland) relative to Europe (fixed) are from Gaina et al. (2009). Although, Chron 13 is generally cited as the first isochron on the Mid–Atlantic Ridge to bypass the Paleogene triple junction south of Greenland, this detail of the triple junction is poorly surveyed and any independent motion of the Greenland plate may have ended by Chron 15 (Kristoffersen & Talwani, 1977). Also, the apparent gap between the Yermak Plateau and the Morris Jesup Spur at Chron 13 (Fig. 15, upper panel) supports an earlier time for the separation.

The juxtaposition of the two marginal structures suggests that the Yermak Plateau displays a similar unconformable surface compared to the Morris Jesup Spur (Fig. 15, red line). The northwestern basement peak on the Yermak Plateau is outlined by nested diffraction hyperbolae and associated with a relatively large magnetic signature interpreted by Jokat et al. (2008) as volcanic basement. The overlying sediments (Fig. 15, light green colour) are considered to be middle Miocene and younger (Geissler et al., 2011). The unconformable surface dips south and the triangular cross-section of the basin between the two basement peaks suggests the basin is located on a rotated basement block and the initial peneplained top surface on the Yermak Plateau may have reached the continental basement peak to the south (Fig. 15). The acoustic returns from the southeastern basement peak have hints of parallel faults, and dredged material from an outcrop at the seabed includes schists and gneisses as well as unmetamorphosed sediments and volcanics representing continental basement (Kristoffersen et al., 2020). Thus, prior to Chron 15, the Morris Jesup Spur and the northwestern part of the Yermak Plateau formed a single subaerial entity of continental rocks and the NW basement peak on the Yermak Plateau probably a volcanic centre which may have contributed material to Unit MJ–6 (Fig. 15). Magmatism along the northwestern edge of the Yermak Plateau is also suggested by the refraction results of Jackson et al. (1984) where the crust below the 'sag basin' (Fig. 15, lower right, refraction line 3) was interpreted as thickened oceanic crust.

Moreover, the geometry of acoustic layers below the Morris Jesup Spur shows striking similarities to the geometry in acoustic images of crustal fragments like the Jan Mayen Ridge (Fig. 16) in the Norwegian Sea (Gudlaugsson et al., 1988; Gaina et al.,2009; Peron-Pinvindic et al., 2012) and also the Broken Ridge in the Indian Ocean (Driscoll et al.,1989; Tikku & Cande, 2000). The Jan Mayen Ridge has had a prolonged tectonic history, starting with extension at the southern end as early as Paleocene (56 Ma) and later during the middle Eocene (40 Ma) before complete detachment from the continental margin of Greenland in the early Miocene (~20 Ma). The unconformity at the bevelled top of the Jan Mayen Ridge separates early– and late–Oligocene sediments (Talwani et al., 1976). The lasting uplift

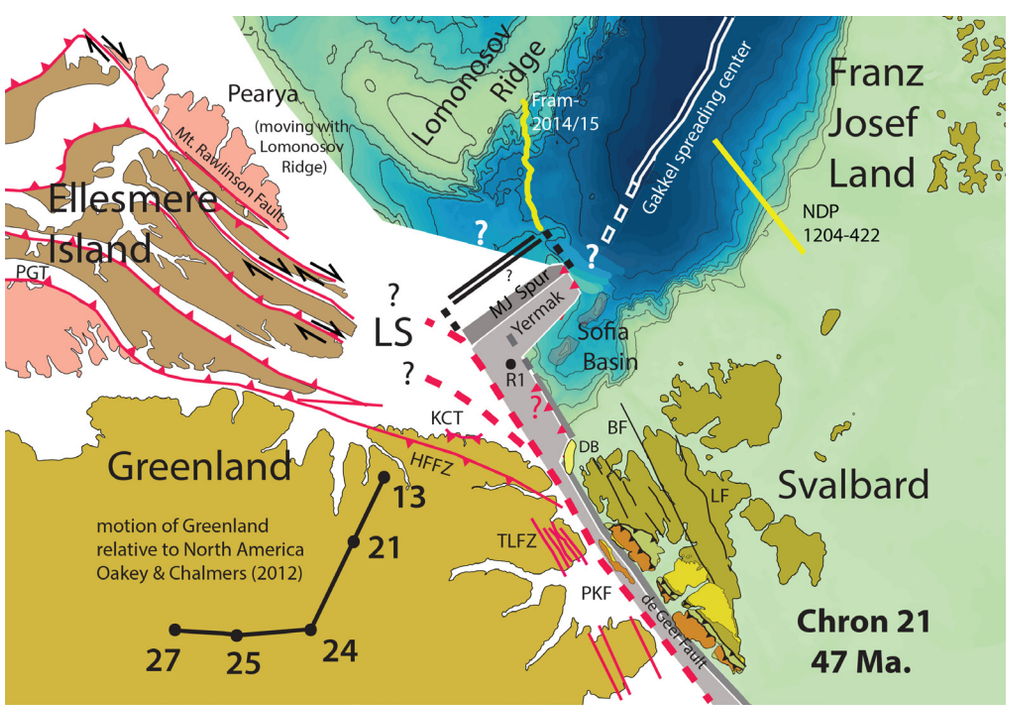

Figure 18. Reconstruction of the Greenland and the North American plates relative to Europe (fixed) at Chron 21 time (~ 47 Ma) using GPlates software and rotation parameters from the sources given in the text. The GPlates display was used as a template for redrawing of the relevant geological structures, bathymetry and continental outline. Active faults at Chron 21 time from Piepjohn et al. (2016) are shown by red colour; and the bathymetry is from Jakobsson et al. (2012) Abbreviations: BF; Billefjorden Fault. DB; Danskøya Basin, HFFZ; Harder Fjord Fault Zone, KCT; Kap Cannon Thrust, LF; Lomfjorden Fault, PKF; Prins Karls Forland, R1; dredge site on Sverdrup Bank (Riefstahl et al., 2013), TLFZ; Trolle Land Fault Zone.

of these ridges during extension is probably due to the positive buoyancy of the continental crust and mechanical unloading and isostatic rebound of the footwall, as contributions from dynamic or thermal support would decay with time (Weissel & Karner, 1989). Magmatic thickening is not present below the Jan Mayen Ridge (Kodeira et al., 1998).

A subaerial Morris Jesup Spur would have impeded the circum-arctic boundary current north of Greenland (Fig. 2). Our estimated delayed submergence of the spur during the latest Miocene–earliest Pliocene appears to coincide in time with accelerated build-up of the Erik Ridge south of Greenland at ~4.5 Ma (Arthur et al., 1989; Kaminski et al., 1989; Müller-Michaels et al., 2013), suggesting a possible connection between submergence of the spur and the intensification of the East Greenland Current.

The structure of the Morris Jesup Spur also occupies a central position for exit of deep draft ice out of the Arctic Ocean (Rigor et al., 2002). As a result, icebergs have impacted the upstream and shallow western part (~800 m water depth) and to a lesser extent the slightly deeper eastern part of the Morris Jesup Spur (Fig. 7A). The constant thickness of Unit MJ–1 on top of the spur demonstrates insignificant cross-spur sediment transport and argues against a postulated kilometre-thick ice shelf and its expected erosional power (Jakobsson et al., 2014). Linear features down to 1045 m water depth observed in the multibeam data (Spielhagen et al., 2004; Jakobsson., 2016) still need to be explained, but suggest the impacting ice had limited kinetic energy.

The end of the early middle Eocene:

The plate boundary geometry at Chron 13 (Fig. 15) implies that the Morris Jesup Spur was part of a Yermak crustal block prior to the Oligocene. Figure 18 shows the reconstructed relative position of the North American and Greenland plates relative to Europe (fixed) at Chron 21 (47 Ma) using the rotation parameters of Gaina et al. (2002) for the Eurasia Basin and Gaina et al. (2009) for the Norwegian–Greenland Sea. Oakey & Chalmers (2012) inferred a relative motion between the Greenland plate and North America (Pearya terrane and Lomonosov Ridge) to be NNW–SSE convergence by about 105 km between Chron 21 and Chron 13 (Fig. 18).

The dextral shear motion between Greenland and Svalbard from Chron 24 to Chron 21 was nearly 200 km and involved crustal extension of 100–150 km in the Sophia Basin north of Spitsbergen (Kristoffersen et al., 2020). Continental basement is continuous from Spitsbergen northwards to 82° N on the Yermak Plateau (Geissler et al., 2011; Kristoffersen et al., 2020) and extension in the Sophia Basin requires shear close to the coast of Spitsbergen along the postulated de Geer Fault (Fig. 18). The Yermak crustal block, which also included the Morris Jesup Spur, moved as part of the Greenland plate while the Sophia Basin opened (Kristoffersen et al., 2020). By Chron 22, the locus of the main transform motion shifted westwards to the Hornsund Fault and the Yermak block became part of the European plate (Fig. 18). The Hornsund Fault may have been initiated in the Late Cretaceous but became active as extension in the Sophia Basin ceased at about Chron 22. At this time, excessive volcanism started at the junction of the Gakkel spreading centre and the Yermak/Morris Jesup continental block. This volcanism created the circular 65 km-wide northeastern end of the Yermak Plateau and also the northern tip of the Morris Jesup Spur (Figs. 2 & 15, transparent white area). The postulated volcanism follows from an overlap when the Yermak Plateau is reconstructed back to the continental margin north of Spitsbergen (Kristoffersen et al., 2020). We suggest the Hornsund Fault cut through the Greenland side of the Yermak block and from Chron 22 onwards connected to a zone of distributed crustal extension or a Gakkel oceanic spreading segment to the northwest of the undisturbed northwestern slope of the Morris Jesup Spur (Figs. 7A–C & 18). The salient features may since have been modified by Eurekan convergence and further obscured by late-stage volcanism (Unit MJ–3C & MJ–2) to make up the intensely deformed present structure of the Morris Jesup Rise (Fig. 7C).

As the Hornsund Fault became the main plate boundary between Svalbard and Greenland, it is likely that splays of this transform fault connected up with the main strike-slip faults on Ellesmere Island (Fig. 18). We speculate that a change in fault trends below the Lincoln Sea shelf created restraining bends for dextral motion and induced deformation of the Morris Jesup Rise, thrusting of the KWG volcanics (Tegnér et al., 2011), movements on the Harder Fiord Fault Zone (Piepjohn & von Gosen, 2001) and eastward thrusting of the NNW-SSE-trending part of the Yermak Plateau forming the Danskøya Basin as a pull-apart basin (Kristoffersen et al., 2020).

The Paleocene:

To explore scenarios for the early Cenozoic tectonic evolution north of Greenland, we keep Europe fixed and rotate the Free Air gravity and total magnetic field intensity (CAMP–GM; Gaina et al., 2009) grid of the respective plates to a reconstruction for Chron 21 time (Fig. 19). Brozenas et al. (2003) identified a low-amplitude magnetic lineation tentatively designated as Chron 25? along the foot of the slope of the Lomonosov Ridge. A conjugate Chron 25? lineation on the Barents Sea continental slope was not discerned (Fig. 19B). The juxtaposition of thick continental crust against thinner oceanic crust and its shallower mantle generates an edge effect manifested as a broad seaward Free Air gravity high. This is illustrated in models for the northern Barents Sea margin by Minakov et al. (2012), Berglar et al.

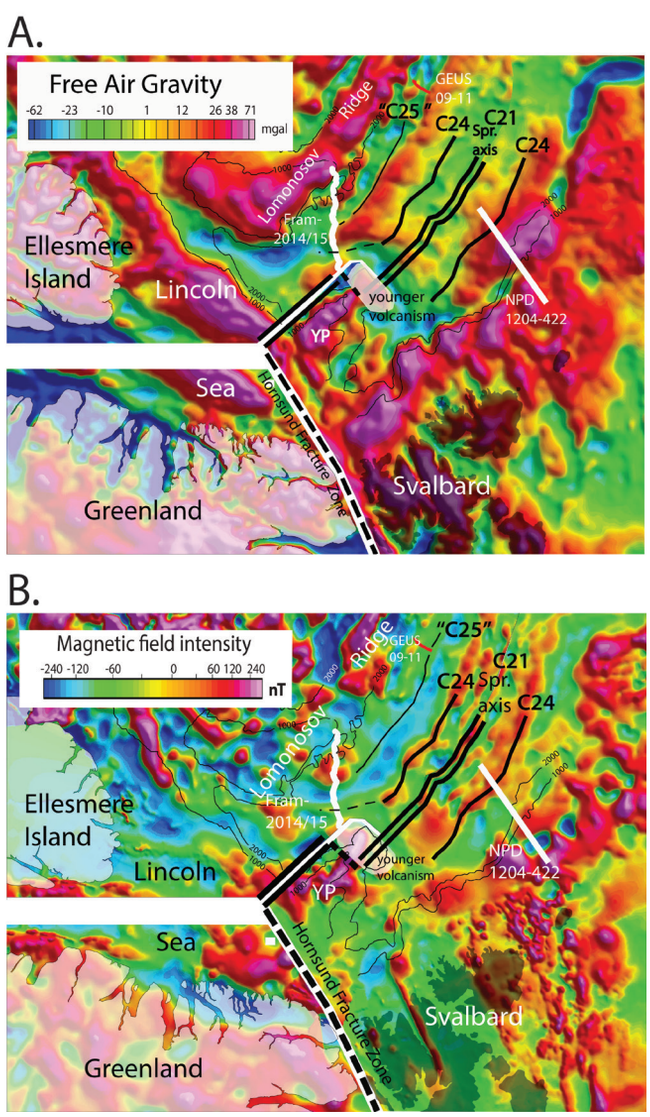

Figure 19. Reconstruction for Chron 21 (~47 Ma) as for Fig. 18 with overlay of the potential field data for the respective plates from CAMP–GM (Gaina et al. (2009). Magnetic isochrones are from Brozena et al. (2003). (A) Free Air gravity. (B) Magnetic field intensity. Abbreviation: YP –Yermak plateau.

(2016) and Lutz et al. (2018). The gravity high on the northern Barents Sea continental slope is located between oceanic crust of Chron 24 age and the shelf edge where a 80–100 km-wide tract of deep basement made up of rotated fault blocks meets the steeply rising continental basement (Figs. 17 & 19). The Free Air gravity edge effect appears well developed along the foot of the slope of the Lomonosov Ridge and parallels the low-amplitude Chron 25? magnetic lineation (Fig.19). However, the seismic stratigraphies of the two conjugate margins are dramatically different (Fig. 17). The projected southwestward extension of Chron 24 in the Amundsen Basin appears to coincide with the basinward edge of stacked stratigraphic levels of volcanics and Chron 25? with fault blocks capped by volcanics (Fig. 17). This spatial relationship of 'Chron 25' to basement and the ~100 km of separation between Chron 24 and 'Chron 25?' on the Lomonosov Ridge side being equal to the width of old deep crust on the northern Barents Sea margin suggest that 'Chron 25?' on the Lomonosov Ridge side is most likely a magnetic edge effect generated from crustal block topography and not an isochron within the oceanic crust (Fig. 17). In any case, the presence of ~100 km-wide tracts of deep crust beyond Chron 24 below the conjugate margins of the western Eurasia Basin suggest that the ~200 km of pre–Eocene extension may be a far-field consequence of the relative plate motion between North America and Europe (incl. Greenland) accommodated in the Labrador Sea (Chalmers & Laursen, 1995) and the Baffin Bay (Hussienpour et al., 2013) area by formation of transition zones followed by pre–Chron 24 sea-floor spreading.

We keep Europe fixed and reconstruct the relative position of the Lomonosov Ridge at the time of 'Chron 25' (56 Ma) using the finite rotation of Gaina et al. (2002) and the position of Greenland relative to Svalbard at continental break-up from parameters given by Barnett-Moore et al. (2016). To close the Sophia Basin, we move the Yermak Plateau towards Svalbard along the trend of the de Geer Fault (Fig. 20). Greenland moved ~155 km closer to the Pearya terrane/Lomonosov Ridge between Chron 21 and Chron 24 with only a minor apparent change in direction at Chron 21 (Oakey & Chalmers, 2012). Thus, the marine magnetic data from the Labrador Sea/Baffin Bay suggest that an initial phase of sinistral strike-slip motion between Greenland and North America changed to pure convergence and crustal shortening from Chron 24 onwards rather than from Chron 21 as advocated by Piepjohn et al. (2016).

The reconstruction at 'Chron 25' shows our seismic transect across the foot of the slope of the Lomonosov Ridge to be about 250 km away from the northern end of the Morris Jesup Spur and of marginal relevance to tectonic events at the triple junction (Fig. 20). However, at Chron 21 (early middle Eocene) the situation is different (Fig. 18). We may summarise our observations in the new seismic data relevant to the Eurekan deformation event as follows:

i) The Morris Jesup Spur has suffered only mild deformation. The folding is pre-opening of the Fram Strait (early Miocene), and has apparent wavelengths < 2.5 km and amplitudes < 100 m. The intensity of deformation increases from the lower western slope of the spur towards the Morris Jesup Rise (Fig. 7).
ii) The Morris Jesup Rise is a strongly deformed structure where volcanic activity continued into the late Miocene. A deformation time line is presently not possible to define, but the stratigraphy of the deformation front at the foot of the slope to the northwest suggests activity throughout the Cenozoic (Figs. 7D &11).
iii) The southwestern end of the Amundsen Basin has suffered only mild Cenozoic compressive deformation (Fig. 7D). Syn-volcanic deposition of >1.4 km of sediments (Unit ABSW–5) suggests a regime of extension along the foot of the Lomonosov Ridge into the Oligocene (Figs. 7D, 13 & 14).
iv) Given a predicted 200–300 km of Late Cretaceous/early Cenozoic convergence between the Lomonosov Ridge and the north coast of Greenland (Fig. 1), we are led to postulate that the Morris Jesup Rise may be a northern outlier of a convergent tectonic domain hidden below the Lincoln Sea continental shelf. The southern extent of this domain may relate to the Kap Cannon Thrust (Figs. 18 & 20).

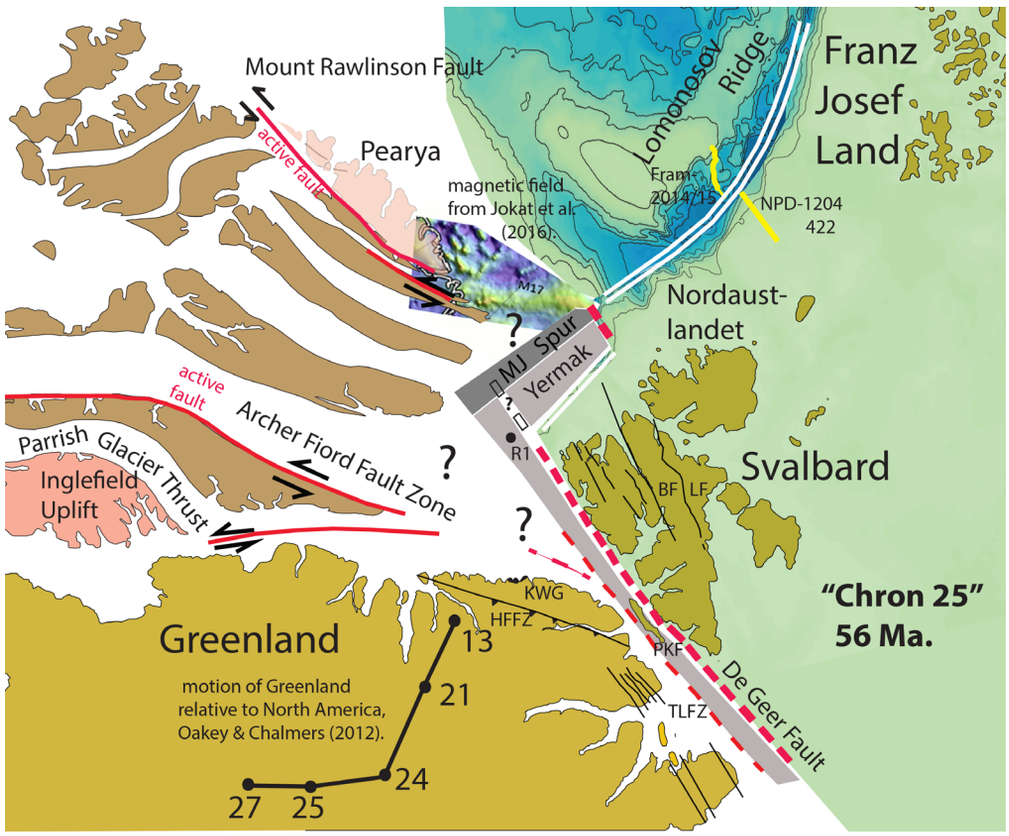

Figure 20. Reconstruction for "Chron 25" (Europe fixed) using rotation parameters given in the text. Procedure and abbreviations as for Fig. 18.

Conclusions

The Morris Jesup Spur and Rise north of Greenland along with the Yermak Plateau north of Svalbard are submarine structures involved in the development of a postulated triple junction when Greenland moved relative to North America and Eurasia as an independent plate during the Late Cretaceous–early Cenozoic. We have used a hovercraft research platform drifting passively with the sea ice to acquire the first seismic reflection transect across the area north of Greenland. The flat ~25 km-wide Morris Jesup Spur is formed by a west-dipping sedimentary succession (0.8 sec. thick) overlying >0.35 sec. (~ 0.7 km) of volcanic rocks truncated at the top by a horizontal unconformity. The spur split away from the Yermak Plateau before Chron 13 (34 Ma) but did not become submerged until late Miocene. The rise to the west of the spur is for the most part acoustically opaque with patches of laminated sediments above irregular high-amplitude reflections considered to represent volcanics. We interpret the lack of coherent seismic energy as the acoustic response of random scatterers generated by extensive sediment deformation. The rise was the site of volcanic activity from the early Cenozoic to the late Miocene and is framed by a deformation front to the north and west. The southwestern end of the Amundsen Basin is dominated by the largest channel-levee complex known in the Arctic Ocean and multiple smaller channel-levee complexes dominate the upper 1 sec. (~ 1 km) of the stratigraphy. The input of glacial sediments on to the Lincoln Sea margin has been considerable, but insignificant input to the Morris Jesup Spur and Rise area. At deeper levels in the southwestern Amundsen Basin, volcanics intercalated with sediments are present over a stratigraphic range of at least 0.8 sec. (>1.4 km) and some of the flows extend across the basin to the rise. The strata of the entire sediment section in the southwestern Amundsen Basin becomes bent upwards and folded at a deformation front at the foot of the slope of the Morris Jesup Rise. A slope morphology repeatedly altered by tectonic growth may have destabilised upper slope deposits and altered sediment pathways.

The Morris Jesup Spur and Yermak Plateau constituted a Yermak crustal block as an integral part of the continental margin north of Spitsbergen in the Late Cretaceous. The block rifted off as part of the Greenland plate during the initial opening of the Eurasia Basin including the minor Sophia Basin and became part of Europe at about Chron 22. The Morris Jesup Spur split from the Yermak Plateau prior to Chron 13 and became part of North America. The Morris Jesup Rise may have been the site of a spreading centre from Chron 22 to Chron 15 and later deformed during the early Cenozoic convergence between Greenland and the North American plate. The 200–300 km of Late Cretaceous/early Cenozoic deformation between north Greenland and the Lomonosov Ridge predicted from plate-tectonic considerations is difficult to reconcile with the mild tectonic effect observed on the Morris Jesup Spur and in the southwestern Amundsen Basin. The Morris Jesup Rise is likely a northern outlier of a larger terrane involved in Eurekan deformation now hidden below the Lincoln Sea continental shelf.

Acknowledgements. The seismic results reported here were obtained over 2.5 months during the Fram–2014/15 ice drift, with another 3.5 months needed to drift far enough south into the Fram Strait to be successfully recovered. We greatly appreciate the logistic support of our cooperating partner, the A. Wegener Institute of Polar and Marine Research. Assistance from the 333 Squadron of the Norwegian Air Force and the Danish Air Force ensured the highest possible continuity of the 7.5 months science program with acquisition of 1000 km of good-quality seismic data. Audun Tholfsen provided crucial logistic support during the ice drift and senior engineer Ole Meyer, student Gaute Hope and the technical staff at Griffon Hoverworks contributed advice on technical issues. We thank Alexander Minakov for assistance to access the gravity and magnetic data. The Fram–2014/15 ice drift was funded by Blodgett-Hall Polar Presence LLC, Lundin-Energy-Norway and the Norwegian Petroleum Directorate. The enthusiasm of Halvor Jahre, Geir Birger Larsen and Harald Brekke was essential for a Norwegian ice drift to happen only 118 years after Nansen's drift with the "Fram". Constructive reviews by H. Maher and G.E. Shepard significantly improved the manuscript.

References

Abdelmalak, M.M., Planke, S., Faleide, J.I, Jerram, D.A., Zastrozhnov, D., Eide, S. & Myklebust, R. 2016: The development of volcanic sequences at rifted margins: New insights from the structure and morphology of the Vøring Escarpment, mid-Norwegian Margin. *Journal of Geophysical Research Solid Earth 121*,5212–5236. https://doi.org/10.1002/2015JB012788.

Alves, T. 2015: Submarine slide blocks and associated soft-sediment deformation in deep-water basins: A review. *Marine Petroleum Geology*. https://doi.org/10.1016/j.marpetgeo.2015.05.010

Anderson, J.B. & Jakobsson, M. 2016: Grounding-zone wedges on Antarctic continental shelves. *In:* J. Dowdeswell, M. Canals, M. Jakobsson, B.J. Todd, E.K. Dowdeswell and K.A. Hogan (eds.): A*tlas of Submarine Glacial landforms: Modern, Quaternary and Ancient.* Geological Society of London Memoirs, 46, 243–244. https://doi.org/10.1144/M46.7

Argyle, M., Forsyth, D.A., Okulitch, A.V. & Huston, D. 1992: A new crustal model of the Lincoln Sea polar margin. *In:* Thurston, D.K. &Kazuya, F. (eds.): *Proceedings of the International Conference on Arctic Margins, Report MMS 94-0040,* Minerals Management Service, U.S. Department of Interior, p. 277–282.

Arthur, M., Srivastava, S.P., Kaminski, M., Jarrard, R. & Osloer, J. 1989: Seismic stratigraphy and history of deep circulation and sediment drift development in the Baffin Bay and the Labrador Sea. *In:* S.P. Srivastava, M. Arthur, B. Clemens (eds.): *Proceedings of the Ocean Drilling Program, Scientific Results 105,* Ocean Drilling Program, College Station, TX, 957–988. https://doi.org/10.2973/odp.proc.sr.105.118.1989

Backman, J., Moran, K., McInroy, D.B., Mayer L. & Expedition 302 Scientists 2006: Sites M0001-M0004. *In:* J. Backman, K. Moran, D.B. McInroy, L. Mayer, and the Expedition 302 Scientists. *Proceedings of the Integrated Ocean Drilling Program, Volume 302*. https://doi.org/10.2204/iodp.proc.302.2005

Barendregt, R.W. & Irving, E. 1998: Changes in the extent of North American ice sheets during the late Cenozoic. *Canadian Journal of Earth Science 35,* 504-509. https://doi.org/10.1139/e97-126.

Barnett-Moore, N., Muller, D., Williams, S., Skogseid, J., & Seton, M. 2016: A reconstruction of the North Atlantic since the earliest Jurassic. *Basin Research 30,* 160–185. https://doi.org/10.1111/bre.12214.

Batchelor, C.L. & Dowdeswell, J. 2014: The physiography of High Arctic cross-shelf troughs. *Quaternary Science Reviews 92,* 68–96. https://doi.org/10.1016/j.quascirev.2013.05.025.

Batchelor, C.L. & Dowdeswell, J. 2015: Ice-sheet grounding-zone wedges on high latitude continental margins. *Marine Geology 363*, 65–92. https://doi.org/10.1016/j.margeo.2015.02.001.

Batten, D., Brown, P., Dawes, P., Higgins, A., Koch, B., Parsons, I., & Soper, N. 1981: Peralkaline volcanicity of the Eurasia Basin margin. *Nature 294*, 150–152. https://doi.org/10.1038/294150a0.

de Bazelaire, E. 1988: Normal-moveout correction revisited: Inhomogeneous media and curved interfaces: *Geophysics 53*, 143–157. https://doi.org/10.1190/1.1442449.

Beal, M.A. 1969: *Bathymetry and Structure of the Arctic Ocean*. Msc. Thesis, Oregon State University, 188 pp.

Berger, D. & Jokat, W. 2008: A seismic study along the East Greenland margin from 72◦N to 77◦N. *Geophysical Journal International 174,* 733–748. https://doi.org/10.1111/j.1365-246X.2008.03794.x.

Berger, D. & Jokat, W. 2009: Sediment deposition in the northern basins of the North Atlantic and characteristic variations in shelf sedimentation along the East Greenland margin. *Marine and Petroleum Geology 26,* 1321–1337. https://doi.org/10.1016/j.marpetgeo.2009.04.005.

Berglar, K., Franke, D., Lutz, R., Schreckenberger, B. & Damm, V. 2016: Initial opening of the Eurasian Basin, Arctic Ocean. *Frontiers in Earth Science 4*, 1–14. http://dx.doi.org/10.3389/feart.2016.00091.

Boldreel, L.O. & Sparre Andersen, M. 1994: Tertiary development of the Faeroe-Rockall Plateau based on reflection seismic data. *Bulletin Geologial Society of Denmark 41*,162–180.

Boyden, J.A., Müller, R.D., Gurnis, M., Torsvik, T.H., Clark, J.A., Turner, M., Ivey-Law, H., Watson, R. & Cannon, J.S. 2011: Next-generation plate-tectonic reconstructions using GPlates. *In: Geoinformatics: Cyberinfrastructure for the Solid Earth Sciences,* Cambridge University Press, Cambridge, pp.95–114, https://doi.org/10.1017/CBO9780511976308.008.

Brown, P.E., Parsons, I. & Becker, S.M. 1987: Peralkaline volcanicity in the Arctic Basin – the Kap Washington Volcanics, petrology and palaeotectonics. *Journal Geological Society, London 144,* 707–715. https://doi.org/10.1144/gsjgs.144.5.0707.

Brozena, J., Childers, V., Lawver, L., Gahagan, L., Forsberg, R., Faleide, J. & Eldholm, O. 2003: New aerogeophysical study of the Eurasia Basin and Lomonosov Ridge: Implications for basin development. *Geology 31* (9), 825–828. https://doi.org/10.1130/G19528.1.

Buck, B. M. 1968: Arctic acoustic transmission loss and ambient noise. *In:* Sater, J. E. (ed.): *Arctic Drifting Stations.* Arctic Institute of North America, Calgary, 427–439.

Buck, B. M. & Greene, C. R. 1964: Arctic deep-water propagation measurements. *Journal of the Acoustical Society of America 36*, 1526–1533. https://doi.org/10.1121/1.1919237.

Butt, F.A., Elverhøi, A., Forsberg, C.F. & Solheim A. 2001: Evolution of the Scoresby Sund Fan, central East Greenland – evidence from ODP Site 987. *Norsk Geologisk Tidsskrift 81*,3–15.

Bye, J.A.T. 1971: The Slope of Abyssal Plains. *Journal of Geophysical Research 76* (18), 4188–4194. https://doi.org/10.1029/JC076i018p04188.

Bøe, R., Bellec, V.K., Rise, L., Buhl.Mortensen, L., Chand, S. & Thorsnes, T. 2012: Catastrophic fluid escape venting-tunnels and related features associated with large submarine slides on the continental rise off Vesterålen-Troms, North Norway. *Marine and Petroleum Geology 38,* 95–103. https://doi.org/10.1016/j.marpetgeo.2012.08.008.

Castro, C.F., Kuntz, P.C., Hopper, J. & Funck, T. 2018: Depositional evolution of the western Amundsen Basin, Arctic Ocean: Paleoceanographic and Tectonic implications. *Paleoceanography and Paleoclimatology 33* (12), 1357–1382. https://doi.org/10.1029/2018PA003414.

Chalmers, J.A. & Laursen K.A. 1995: Labrador Sea: The extent of continental and oceanic crust and the timing of the onset of seafloor spreading. *Marine Petroleum Geology 12,* 205–217. https://doi.org/10.1016/0264-8172(95)92840-S.

Channell, J.E.T., Smelror, M., Jansen, E., Higgins, S.M., Lehman, B., Eidvin, T. & Solheim, A. 1999: Age models for glacial fan deposits off East Greenland and Svalbard (Sites 986 and 987). *In:* M. Raymo, E. Jansen, P. Blum, T. Herbert (eds.): *Proceedings of the Ocean Drilling Program, Scientific Results 162,* 149–165. https://doi.org/10.2973/odp.proc.sr.162.008.1999

Chung, W-Y. 2002: Earthquakes Along the Passive Margin of Greenland: Evidence for Postglacial Rebound Control. *Pure & Applied Geophysics 159*, 2567–2584. https://doi.org/10.1007/s00024-002-8748-1.

Clark, D.L. Hanson, A. 1983: Central Arctic Ocean sediment texture: a key to ice transport mechanisms. *In* Molnia, B.F., ed. *Glacial–marine sedimentation*. New York and London, Plenum Press, 301–30.

Clark, J.D. & Pickering, K.T. 1996: *Submarine Channels: Processes and Architecture.* Vallis Press, London, 229 pp.

Dahlgren, K.I.T., Vorren, T.O., Stoker, M.S., Nielsen, T., Nygård, A. & Sejrup, H.P. 2005: Late Cenozoic prograding wedges on the NW European continental margin: their formation and relationship to tectonics and climate. *Marine and Petroleum Geology 22*, 1089–-1110.

Dallmann, W.K. 2015: Geoscience atlas of Svalbard. *Norsk Polarinstitutt Report Series 148,* 292 pp. https://doi.org/10.1016/j.marpetgeo.2004.12.008.

Dawes, P.R. & Peel, J.S. 1981: The Northern margin of Greenland from Baffin Bay to the Greenland Sea. *In:* Nairn, A.E.M., Churkin Jr., M., Stehli, F. (eds.): The Ocean Basins and Margins, *The Arctic Ocean vol. 5,* 201–264. https://doi.org/10.1007/978-1-4757-1248-3_5.

Dawes, P.R. 1990: The North Greenland Continental Margin. *In:* Grantz, A., Johnson. G.L., Sweeney, J. (eds.): The Arctic Region. *The Geology of North America, vol. L*, pp. 211–227. https://doi.org/10.1130/DNAG-GNA-L.211.

Dixon, J. & Dietrich, J.R. 1990: Canadian Beafort Sea and adjacent areas. *In:* Grantz, A., Johnson. G.L., Sweeney, J. (eds.): *The Arctic Region. Geology of North America, vol. L,* 15, 239–256. https://doi.org/10.1130/DNAG-GNA-L.239.

Dowdeswell, J. & Fugelli, E.M.G. 2012: The seismic architecture and geometry of grounding-zone wedges formed at margins of past ice sheets. G*eological Society of America Bulletin 124*, 1750-1761. https://doi.org/10.1130/B30628.1.

Driscoll, N.W., Karner G.D. & Weissel J.K. 1989: Stratigraphic and tectonic evolution of Broken Ridge from seismic stratigraphy and Leg 121 drilling. *In:* Peirce, J., Weissel, J. (eds.): *Proceedings of the Ocean Drilling Program, Part A: Initial Reports Leg 121*, pp. 63-70. https://doi.org/10.2973/odp.proc.ir.121.104.1989.

Duk-Rodkin, A. & Hughes, O.L. 1994: Tertiary-Quaternary drainage of the pre-glacial Mackenzie Basin. Quarternary International 22/23, 221-241. https://doi.org/10.1016/1040-6182(94)90015-9.

Dyer, I. 1984: The song of sea ice and other Arctic Ocean melodies. *In:* Dyer, I., Chryssostomidis, C. (eds.): Arctic Technology and Policy, *Proceedings of the Second Annual MIT Sea Grant College Program Lecture and Seminar.* Hemisphere, Washington, DC, 11–37.

Døssing, A., Hopper, J.R., Olesen, A.V., Rasmussen, T.M. & Halpenny, J. 2013: New aero-gravity results from the Arctic: Linking the latest Cretaceous- early Cenozoic plate kinematics of the North Atlantic and Arctic Ocean. *Geochemistry Geophysics Geosystems 14,* 4044-4064, https://doi.org/10.1002/ggge.20253.

Døssing, A., Hansen, T., Olesen, A., Hopper, J.R. & Funck, T. 2014: Gravity inversion predicts the nature of the Amundsen Basin and its continental borderlands near Greenland. *Earth and Planetary Science Letters 408,* 132-145. https://doi.org/10.1016/j.epsl.2014.10.011.

Døssing, A., Japsen, P., Watts, A., Nielsen, T., Jokat, W., Thybo, H. & Dahl-Jensen, T. 2016: Miocene uplift og the NE Greenland margin linked to plate tectonics: Seismic evidence from the Greenland Fracture Zone, NE Atlantic. *Tectonics.* https://doi.org/10.1002/2015TC004079.

Eittreim, S., Grantz, A. & Greenberg, J. 1982: Active geological processes in Barrow Canyon, Northeast Chukchi Sea. *Marine Geology 50,* 61-76. https://doi.org/10.1016/0025-3227(82)90061-5.

England, J., 1999: Coalescent Greenland and Inutian ice during the Last Glacial Maximum: revising the Quaternary of the Canadian High Arctic. *Quaternary Science Review 18,* 421-456. https://doi.org/10.1016/S0277-3791(98)00070-5.

Escutia, C., Eittreim, S.L., Cooper, A. & Nelson, C.H. 2000: Morphology and acoustic character of the Antarctic Wilkes Land Turbidite System: Ice-sheet-sourced versus River-sourced Fans. *Journal of Sedimentary Research 70,* 84-93. https://doi.org/10.1306/2DC40900-0E47-11D7-8643000102C1865D.

Estrada, S., Höhndorf & Henjes-Kunst, F. 1999: Cretaceous/Tertiary Volcanism in North Greenland: the Kap Washington Group. *Polarforschung 69*, 17-23.

Evangelatos, J. & Mosher, D.C. 2016: Seismic stratigraphy, structure and morphology of Makarov Basin and surrounding regions: tectonic implications. *Marine Geology 374*, 1-13. https://doi.org/10.1016/j.margeo.2016.01.013.

Feden, R.H., Vogt, P.R. & Fleming, H.S. 1979: Magnetic and bathymetric evidence for the "Yermak hot spot" northwest of Svalbard in the Arctic Ocean. *Earth and Planetary Science Letters 44,* 18-38. https://doi.org/10.1016/0012-821X(79)90004-9.

Flesche Kleiven, H., Jansen, E., Fronval, T. & Smith, T.M. 2002: Intensification of Northern Hemisphere glaciations in the circum Atlantic region (3.5-2.4 Ma) – ice rafted detritus evidence. *Palaeogeography Palaeoclimatology Palaecology 184,* 213-223. https://doi.org/10.1016/S0031-0182(01)00407-2.

Flinn, C. & Morgan, L.A. 2002: High-resolution aeromagnetic mapping of volcanic terrain, Yellowstone National Park. *Journal of Volcanology and Geothermal Research 115,* 207-231. https://doi.org/10.1016/S0377-0273(01)00317-1.

Frank, M., Backman, J., Jakobsson, M.,Moran, K., O'Reagan, M., King, B., Haley, P., Kubik, W. & Garbe-Schønberg D. 2008: Beryllium isotiopes in central Arctic Ocean sediments over the past 12.3 million years: Stratigraphic and paleoceanographic implications. *Paleoceanography 23* PA 1S02. https://doi.org/10.1029/2007PA001478.

Gaina, C., Roest, W.R. & Müller, R.D. 2002: Late Cretaceous-Cenozoic deformation of northeast Asia. *Earth and Planetary Science Letters 197*, 273-286. https://doi.org/10.1016/S0012-821X(02)00499-5.

Gaina, C., Gernigon, L. & Ball, P. 2009: Paleocene-Recent plate boundaries in the NE Atlantic and the formation of the Jan Mayen microcontinent. *Journal Geological Society London 166,* 601-616. https://doi.org/10.1144/0016-76492008-112.,

Gaina, C., Werner, S. & the CAMP-GM Group 2009: Circum-Arctic Geophysical Maps 2009. *Norwegian Geological Survey report 2009.*010, pp. 21.

Gaina, C., Nasuti, A., Kimbell, G.S. & Blischke, A. 2017: Break-up and seafloor spreading domains in the NE Atlantic. *In:* Péron-Pinvindic, G., Hopper, J.R., Stoker, M., Gaina, C., Doornenbal, J.C., Funck, T., Arting, U.E. (eds.): The NE Atlantic Region: A Reappraisal of Crustal Structure, Tectonostratigraphic and Magmatic Evolution, *Special Publication 447, Geological Society London,* https://doi.org/10.1144/SP447.12.

Ganerød, M., Smethurst, M.,Torsvik, T., Prestvik, T., Rousse, S., McKenna, C., van Hinsbergen, D. & Hendriks, B. 2010: The North Atlantic Igneous Province reconstructed and its relation to the Plume Generation Zone: the Antrim Lava Group revisited. *Geophysical Journal International 182,* 183–202. https://doi.org/10.1111/j.1365-246X.2010.04620.x.

Gasser, D. 2014: The Caledonides of Greenland, Svalbard and other Arctic areas: status of research and open questions. *In:* Corfu, F., Gasser, D., Chew, D. M. (eds.): New Perspectives on the Caledonides of Scandinavia and Related Areas. *Geological Society, London, Special Publications 390,* 93–129. https://doi.org/10.1144/SP390.17.

Geissler, W.H., & Jokat, W. 2004: A geophysical study of the northern Svalbard continental margin. *Geophysical Journal International 158*, 50–66. https://doi.org/10.1111/j.1365-246X.2004.02315.x.

Geissler, W.H., Jokat, W. & Brekke, H. 2011: The Yermak Plateau in the Arctic Ocean in the light of reflection seismic data – implication for its tectonic and sedimentary evolution. *Geophysical Journal International 187,* 1334–1362. https://doi.org/10.1111/j.1365-246X.2011.05197.x.

Geissler, W.H., Estrada, S., Riefstahl, F., O'Connor, J., Spiegel, C., van den Boogard, P. & Klugel, A. 2019. Middle Miocene magmatic activity on the Sophia Basin, Arctic Ocean – evidence from dredged basalt at the flanks of Mosby Seamount. *Arktos 5,* 31–48. https://doi.org/10.1007/s41063-019-00066-8.

Gelchinsky, B. 1988: The common-reflecting-element (CRE) method: *ASEG/SEG Internationl Geophysical Conference, Extended Abstracts,* 71–75. https://doi.org/10.1071/EG988071.

Gion, A.M., Williams, S.E. & Muller, R. 2017: A reconstruction of the Eurekan Orogeny incorporating deformation constraints. *Tectonics 36,* 304–320. https://doi.org/10.1002/2015TC004094

Glebovsky, V.Yu., Kaminsky, V.D., Minakov, A.N., Merkur`ev, S.A., Childers, V.A. & Brozena, J.M. 2006: Formation of the Eurasia Basin in the Arctic Ocean as inferred from geohistorical analysis of the anomalous magnetic field. *Geotectonics 40*(4), 263–281. https://doi.org/10.1134/S0016852106040029.

Gradstein, F., Ogg, J., Schmitz, M. & Ogg, G. 2012: *The Geologic Time Scale 2012*. Elsevier Publishing Company, 1176 pp.

Gregersen, S. 1982: Earthquakes in Greenland. *Bulletin Geological Society of Denmark 31*, pp. 11–27.

Gudlaugsson, S., Gunnarsson, K., Sand, M. & Skogseid, J. 1988: Tectonic and volcanic events at the Jan Mayen Ridge microcontinent. *In:* Morton, A., Parson, L. (eds.): Early Tertiary Volcanism and the Opening of the NE Atlantic, *Geological Society London Special Publication 39,* pp. 85–93. https://doi.org/10.1144/GSL.SP.1988.039.01.09.

Harding, T.P. 1985: Seismic Characteristics and Identification of Negative Flower Structures, Positive Flower Structures, and Positive Structural Inversion. *American Association of Petroleum Geologists Bulletin 69,* 582–600. https://doi.org/10.1306/AD462538-16F7-11D7-8645000102C1865D.

Harrison, J.C. 2006: In Search of the Wegener Fault: Re-Evaluation of Strike-Slip Displacements Along and Bordering Nares Strait. *Polarforschung 74* (1-3), 129 – 160.

Henriksen, N. 2008: *Geological History of Greenland. Geus*, 272 pp.

Hosseinpour, M.. Müller, R.D., Williams, S.E. & Whittaker, J.M. 2013: Full-fit reconstruction of the Labrador Sea and Baffin Bay. *Solid Earth 4*, 461–479. https://doi.org/10.5194/se-4-461-2013.

Hunkins, K., Thorndike, E.M. & Mathieu, G. 1969: Nepheloid Layer and Bottom Currents in the Arctic Ocean. *Journal Geophysical Research 74*, 6995–7007. https://doi.org/10.1029/JC074i028p06995

Hunter, S.E., Wilkinson, D., Stanford, J., Stow, D., Bacon, S., Akhmetzhanov, A.M. & Kenyon, N.H. 2007: The Erik Drift: a long-term barometer for North Atlantic deepwater flux south of Cape Farewell, Greenland. *In:* Viana, A.R., Rebesco, M. (eds.): Economic and Paleoceanographic Significance of Contourite Deposits. *Geological Society, London Special Publications 276*, 245–263. https://doi.org/10.1144/GSL.SP.2007.276.01.12.

IOC-IHO/GEBCO SCUFN-XVI/3, 2003: Summary Report, Sixth meeting of the GEBCO Sub-Committee on Undersea Feature Names (SCUFN), *International Hydrographic Office,* Monaco, 10–12 April, 2003. http://www.gebco.net/data_and_products/undersea_feature_names/

Ireland, M.T., Goulty, N. & Davies, R. 2010: Influence of pore water chemistry on silica diagenesis: evidence from the interaction of diagenetic reaction zones with polygonal fault systems. *Journal Geological Society, London 167*, 273–279. https://doi.org/10.1144/0016-76492009-049.

Ishii, E., Kurikami, H. & Iwatsuki, T. 2011: Mechanical strength of the transition zone at the boundary between opal-A and opal-CT zones in siliceous rocks. *Engineering Geology 122,* 215–221. https://doi.org/10.1016/j.enggeo.2011.05.007.

Jakobsson, M., Backman, J., Rudels, B., Nycander, J., Frank, M., Mayer, L., Jokat, W., Sangiorgi, F., O'Reagan, M., Brinkhuis, H., King, J. & Moran, K. 2007: The early Miocene onset of a ventilated circulation regime in the Arctic Ocean, *Nature 447,* 986–990. https://doi.org/10.1038/nature05924.

Jakobsson, M., Marcussen, C. & LOMROG Scientific Party 2008: Lomonosov Ridge off Greenland 2007 (LOMROG) Cruise Report. *Geological Survey of Denmark and Greenland Special Publication,* 122 pp.

Jakobsson, M., Nilsson, J., O'Regan, M., Backman, J., Löwemark, L., Dowdeswell, J., Mayer, L., Polyak, L., Colleoni, F., Anderson, L.F., Björk, G., Darby, D., Eriksson, B., Hanslik, D., Hell, B., Marcussen, C., Sellén, E. & Wallin, Å. 2010: An Arctic Ocean ice shelf during MIS 6 constrained by new geophysical and geological data. *Quaternary Science Review 29*, 3505–3517 (2010). https://doi.org/10.1016/j.quascirev.2010.03.015

Jakobsson, M., Mayer, L., Coakley, B., Dowdeswell, J. A., Forbes, S., Fridman, B., Hodnesdal, H., Noormets, R., Pedersen, R., Rebesco, M., Schenke, H. W., Zarayskaya, Y., Accettella, D., Armstrong, A., Anderson, R. M., Bienhoff, P., Camerlenghi, A., Church, I., Edwards, M., Gardner, J. V., Hall, J. K., Hell, B., Hestvik, O., Kristoffersen, Y., Marcussen, C., Mohammad, R., Mosher, D., Nghiem, S. V., Pedrosa, M. T., Travaglini, P. G., & Weatherall, P. 2012: The International Bathymetric Chart of the Arctic Ocean (IBCAO) Version 3.0. *Geophysical Research Letters 39,* L12609. https://doi.org/10.1029/2012GL052219.

Jakobsson, M. 2016: Submarine glacial landform distribution in the central Arctic Ocean shelf-slope-basin system. *In:* Dowdeswell, J., Canals, M., Jakobsson, M., Todd, B., Dowdeswell, E.K., Hogan, K.A. (eds.): *Atlas of Submarine Glacial landforms: Modern, Quaternary and Ancient.* Geological Society of London Memoirs 46, 469-476. https://doi.org/10.1144/M46.179.

Jackson, H.R. & Gunnarsson, K. 1990: Reconstruction of the Arctic: Mesozoic to Present. *Tectonophysics 172,* 303-322. https://doi.org/10.1016/0040-1951(90)90037-9.

Jackson, H.R., Dahl-Jensen, T. & the LORITA working group 2010: Sedimentary and crustalstructure from the Ellesmere Island and Greenland continental shelves onto the Lomonosov Ridge, Arctic Ocean. *Geophysical Journal International 182*,11-35. https://doi.org/10.1111/j.1365-246X.2010.04604.x.

Jokat, W., Uenzelmann-Neben, G., Kristoffersen, Y. & Rasmussen, T. 1992: Lomonosov Ridge—A double sided continental margin, *Geology 20,* 887–890. https://doi.org/10.1130/0091-7613(1992)020%3C0887:LRADSC%3E2.3.CO;2.

Jokat, W., Weigelt, E., Kristoffersen, Y., Rasmussen, T. & Schöne, T. 1995: Geophysical and Bathymetric Results from Morris Jesup Rise, Yermak Plateau and Gakkel Ridge. *Geophysical Journal International 123*(2), 601–610. https://doi.org/10.1111/j.1365-246X.1995.tb06874.x.

Jokat, W., Geissler, W. & Voss, M. 2008: Basement structure of the north-western Yermak Plateau. *Geophysical Research Letter 35*, L050309. https://doi.org/10.1029/2007GL032892.

Jokat, W., Ickrath, M. & O'Connor, J. 2013: Seismic transect across the Lomonosov and Mendeleev Ridges: Constraints on the geological evolution of the Amerasia Basin, Arctic Ocean. *Geophysical Research Letters 40*, 5047–5051. https://doi.org/10.1002/grl.50975.

Jokat, W., Lehmann, P., Damaske, D. & Bradley Nelson, J. 2016: Magnetic signature of North-East Greenland, the Morris Jesup Rise, the Yermak Plateau, the central Fram Strait: Constraints for the rift/drift history between Greenland and Svalbard since the Eocene. *Tectonophysics 691*, 98–109. https://doi.org/10.1016/j.tecto.2015.12.002.

Jones, J.G. & Neslon, P.H.H. 1970. The flow of basalt lava from air into water – its structural expression and stratigraphic significance. *Geological Magazine 107*: 13–20. https://doi.org/10.1017/S0016756800054649.

Judd, A. & Hovland, M. 2007: Seabed Fluid Flow: The Impact on Geology, Biology and the Marine Environment. Cambridge University Press, 475 pp. https://doi.org/10.1017/CBO9780511535918.

Kaminski, M. A., Gradstein, F. M., Scott, D. B. & Mackinnon, K. D. 1989: Benthic foraminifera of the Baffin Bay and Labrador Sea. PANGAEA, https://doi.org/10.1594/PANGAEA.743960, Supplement to: Kaminski, MA et al. (1989): Neogene benthic foraminifer biostratigraphy and deep-water history of sites 645,646, and 647, Baffin Bay and Labrador Sea. *In:* Srivastava, S.P., Arthur, M., Clement, B. et al. (eds.): *Proceedings of the Ocean Drilling Program, Scientific Results Leg 105,* College Station, TX (Ocean Drilling Program), 731–756, https://doi.org/10.2973/odp.proc.sr.105.123.1989.

Kjørboe, L. 1999: Stratigraphic relationsships of the Lower Tertiary of the Faeroe Basalt Province and the Faeroe-Shetland Basin. *In:* Fleet, A.J. & Boldy, S.A.R. (eds.): *Petroleum Geology of Northwest Europe. Proceedings of the 5th Conference, Geological Society; London*, 559–572. https://doi.org/10.1144/0050559.

Knies., J., Mattingsdal,R., Fabiana, K., Grøsfjeld, K., Baranwala, S., Husum, K., DeSchepper, S., Vogte, C., Andersen, N., Matthiessen, J., Andreassen, K., Jokat, W., Nam, S. & Gaina, C. 2014: Effect of early Pliocene uplift on late Pliocene cooling in the Arctic–Atlantic gateway. *Earth & Planetary Science Letters 387,* 132–144. https://doi.org/10.1016/j.epsl.2013.11.007.

Knudsen, C., Hopper, J., Bierman, P.R., Bjerager, M., Funck, T., Green, P.F., Ineson, J.R., Japsen, P., Marcussen, C., Sherlock, S.C. & Thomsen, T.B. 2017: Samples from the Lomonosov Ridge place new constraints on the geological evolution of the Arctic Ocean. *In:* Pease, V., Coakley, B. (eds.): *Circum-Arctic Lithosphere Evolution. Geological Society London Special Publication 460*, https://doi.org/10.1144/SP460.17.

Kodaira, S., Mjelde, R., Gunnarsson, K., Shiobara, H. & Shimamura, H. 1998: Structure of the Jan Mayen microcontinent and implications for its evolution. *Geophysical Journal International 132,* 383–400. https://doi.org/10.1046/j.1365-246x.1998.00444.x.

Kovacs, L.C. & Vogt, P. 1982: Depth-to-magnetic source analysis of the Arctic Ocean region. *In:* Johnson, G.L., Sweeney, J. (eds.): Structure of the Arctic. *Tectonophysics 89*, 255–294. https://doi.org/10.1016/0040-1951(82)90041-5.

Kristoffersen, Y. & Talwani, M. 1977: Extinct triple junction south of Greenland and the Tertiary motion of Greenland relative to North America. *Bulletin Geological Society America 88,* 1037–1049. https://doi.org/10.1130/0016-7606(1977)88%3C1037:ETJSOG%3E2.0.CO;2.

Kristoffersen, Y., Sorokin, M.Y., Jokat, W. & Svendsen, O. 2004: A submarine fan in the Amundsen Basin, Arctic Ocean. *Marine Geology 204,* 317–324. https://doi.org/10.1016/S0025-3227(03)00373-6

Kristoffersen, Y. & Hall, J.K. 2014: Hovercraft as a mobile science platform over sea ice in the Arctic Ocean. *Oceanography 27*(2), http://dx.doi.org/10.5670/oceanog.2014.33.

Kristoffersen, Y., Tholfsen, A., Hall, J.K. & Stein, R. 2016: Scientists Spend Arctic Winter Adrift on Sea Ice. *Eos, Transactions American Geophysical Union 97*. Published on 11 October 2016. https://doi.org/10.1029/2016EO060711

Kristoffersen, Y., Ohta, Y. & Hall, J.K. 2020: On the origin of the Yermak Plateau in the Arctic Ocean north of Svalbard. *Norwegian Journal of Geology.* https://dx.doi.org/10.17850/njg100-1-5.

Kuvaas, B. & Leitchenkov, G. 1992: Glaciomarine turbidite and current-controlled deposits in Prydz Bay, Antartica. *Marine Geology 108,* 365–381. https://doi.org/10.1016/0025-3227(92)90205-V.

Laberg, J.S., Rydningen, T.A., Forwick, M. & Husum, K. 2018: Depositional processes on the distal Scoresby Trough Mouth Fan (ODP Site 987): Implications for the Pleistocene evolution of the Scoresby Sund Sector of the Greenland Ice Sheet. *Marine Geology 402*, 51–59. https://doi.org/10.1016/j.margeo.2017.11.018.

Larsen, H.C., Saunders, A.D., Clift, P., Beget, J., Spezzaferri, S., & ODP Leg 152 Scientific Party 1994: Seven Million Years of Glaciation in Greenland. *Science 264,* 952–955. https://doi.org/10.1126/science.264.5161.952.

Lemmen, D.S. & England, J. 1992: Multiple glaciations and sea level changes, northern Ellesmere Island, high arctic Canada. *Boreas 21,* 137–152. https://doi.org/10.1111/j.1502-3885.1992.tb00021.x.

Lundin, E.R. & Doré A.G. 2005. NE Atlantic break-up: a re-examination of the Iceland mantle plume model and the Atlantic–Arctic linkage. *In:* Dore´, A. G., Vinning, B. A. (eds.): Petroleum Geology: North-West Europe and Global Perspectives—*Proceedings of the 6th Petroleum Geology Conference,* 739–754. Published by the Geological Society, London. https://doi.org/10.1144/0060739.

Lutz, R., Franke, D., Berglar, K., Heyde, I., Schreckenberger, B., Klitzke, P. & Geissler, W. 2018: Evidence for mantle exhumation since the early evolution of the slow-spreading Gakkel Ridge, Arctic Ocean. *Journal of Geodynamics 118,* 154–165. https://doi.org/10.1016/j.jog.2018.01.014.

Mair, J.A. & Forsyth, D.A. 1982: Crustal structure of the Lomonosov Ridge and the Fram and Makarov basins near the North Pole. *Journal of Geophysical Research 89,* 473–481. https://doi.org/10.1029/JB089iB01p00473.

Makris, N. & Dyer, I. 1986: Environmental correlates of pack ice noise. *Journal Acoustical Society America 79*, 1434–1440. https://doi.org/10.1121/1.393671.

Masson, D.G., Harbitz, C.B., Wynn, R.B., Pedersen, G. & Løvholt, F. 2006: Submarine landslides: processes, triggers and hazard prediction. *Philosphical Transactions Royal Society 364,* 2009–2039. https://doi.org/10.1098/rsta.2006.1810.

McCave. I. 1986: Local and global aspects of the bottom nepheloid layers in the world ocean. *Netherlands Journal of Sea Research 20,* 167–181. https://doi.org/10.1016/0077-7579(86)90040-2.

Meadows, D. & Davies, R.J. 2009: Predicting porosity reduction due to silica diagenesis using seismic reflection data. *Marine and Petroleum Geology 26,* 1543–1553. https://doi.org/10.1016/j.marpetgeo.2008.09.006.

Müller-Michaels, A., Uenzelmann-Neben, G. & Stein, R. 2013. A revised Early Miocene age for the instigation of the Eirik Drift, offshore southern Greenland: Evidence from high-resolution seismic reflection data. *Marine Geology 340*, 1–15. https://doi.org/10.1016/j.margeo.2013.04.012.

Minakov, A., Podladchikov, Y.Y. 2012. Tectonic subsidence of Lomonosov Ridge. *Geology 40*(2). https://doi.org/10.1130/G32445.1.

Minakov, A., Faleide, J.I., Glebovsky, V. Yu., & Mjelde, R. 2012: Structure and evolution of the northern Barents–Kara Sea continental margin from integrated analysis of potential fields, bathymetry and sparse seismic data. *Geophysical Journal International 188,* 79–102. https://doi.org/10.1111/j.1365-246X.2011.05258.x.

Moran, K. et al. 2006: The Cenozoic palaeoenvironment of the Arctic Ocean. *Nature 441*, 601–605. https://doi.org/10.1038/nature04800.

Myhre, A.M., Thiede,J. & Firth,J.V., et al. 1995. *Proceedings ODP,* Initial Reports 151. Ocean Drilling Program, College Station, TX.

Newton, J.L. & Sotirin, B.J. 1997: Boundary undercurrent and water mass changes in the Lincoln Sea. *Journal of Geophysical Research 102* (C2), 3393–3403. https://doi.org/10.1029/96JC03441.

Nielsen, T., De Santis, L., Dahlgren, K.I.T., Kuijpers, A., Laberg, J.S., Nygård, A., Praeg, D., & Stoker, M.S. 2005: A comparison of the NW European glaciated margin with other glaciated margins. *Marine and Petroleum Geology 22,* 1149–1183. https://doi.org/10.1016/j.marpetgeo.2004.12.007.

Nielsen, T. & Kuijpers, A. 2013: Only 5 southern Greenland shelf edge glaciations since the early Pliocene. Scientific Reports 3: 1875. https://doi.org/10.1038/srep01875.

Nobes, D.C., Murray, R., Kuramoto, S., Pisciotto, K. & Holler, P. 1992: Impact of silica diagenesis on physical property variations. *In:* K. Pisciotto, J.C. Ingle, M.T. von Breymann, J. Barron (eds.): *Proceedings of the Ocean Drilling Program, Scientific Results 127/128*. https://doi.org/10.2973/odp.proc.sr.127128.111.1992.

Normark, W.R., Piper, D.J.W. & Stow, D.A. 1983: Quaternary development of channels, levees and lobes on middle Laurentian Fan. *American Association of Petroleum Geologists Bulletin 67,* 1400–1409. https://doi.org/10.1306/03B5BA33-16D1-11D7-8645000102C1865D.

Oakey, G. & Chalmers, J.A. 2012: A new model for the Paleogene motion of Greenland relative to North America: Plate reconstructions of the Davis Strait and Nares Strait Regions between Canada and Greenland. *Journal of Geophysical Research 117,* B10401. 2012. https://doi.org/10.1029/2011JB008942.

Okulitch, A.V. & Trettin, H.P. 1991: Late Cretaceous – Early Tertiary deformation, Arctic Islands. *In:* Trettin, H.P. (ed.): Geology of the Innutian Orogen and Arctic Platform of Canada and Greenland. *Geological Survey of Canada, Geology of Canada No. 3,* Chapter 17, 469–487. https://doi.org/10.4095/133999.

Oljedirektoratet 2013: *Petroleumsressursene på norsk sokkel.* 62 pp. ISBN 978-82-7257-098-8.

O'Regan, M., King, J. W., Backman, J., Jakobsson, M., Pälike, H., Moran, K. Heil, C., Sakamoto, T., Cronin, T. M. & Jordan, R. 2008: Constraints on the Pleistocene chronology of sediments from the Lomonosov Ridge. *Paleoceanography 23*(1), PA1S19, https://doi.org/10.1029/2007PA001551.

Ostenso, N. & Wold, R.J. 1977: A seismic and gravity profile across the Arctic Ocean Basin. *Tectonophysics 37*, 1–24. https://doi.org/10.1016/0040-1951(77)90036-1.

Ottesen, D. & Dowdeswell, J. 2009: An inter-ice stream glaciated margin; submarine landforms and a geomorphic model based on marine-geophysical data from Svalbard. *Bulletin Geological Society of America 121,* 1647–1665. https://doi.org/10.1130/B26467.1.

Peakall, J., Kane, I.A., Masson, D., Keevil, G. McCaffrey, W. & Corney, R. 2012: Global (latitudional) variation in submarine channel sinuosity. *Geology 40*, 11–14. https://doi.org/10.1130/G32295.1.

Peron-Pinvindic, G., Gernigon, L., Gaina, C. & Ball, P. 2012: Insights from the Jan Mayen system in the Norwegian–Greenland sea -1. Mapping of a microcontinent. *Geophysical Journal International 191,* 385–412. https://doi.org/10.1111/j.1365-246X.2012.05639.x.

Piepjohn, K. & von Gosen, W. 2001: Polyphase deformation of the Harder Fjord Fault Zone (North Greenland), *Geolgical Magazine 138*, 407–434. https://doi.org/10.1130/G32295.1.

Piepjohn, K., von Gosen, W., Läufer, A., McClelland, W. & Estrada, S. 2013: Ellesmerian and Eurekan fault tectonics at the northern margin of Ellesmere Island (Canadian High Arctic). *Zeitschrift der Deutschen Gesellschaft für Geowissenschaften 164*, 81–105. https://doi.org/10.1127/1860-1804/2013/0007.

Piepjohn, K., von Gosen, W. & Tessensohn, F. 2016: The Eurekan deformation in the Arctic: an outline. *Journal Geological Society London*. https://doi.org/10.1144/jgs2016-081.

Planke, S., Symonds, P.A., Alvestad, E. & Skogseid, J. 2000: Seismic stratigraphy of large-volume extrusive complexes on rifted margins. *Journal Geophysical Research 105* (B8), 19,335–19,351. https://doi.org/10.1029/1999JB900005.

Posamentier, H.W. & Martinsen, O.J. 2010: The character and genesis of submarine mass-transport deposits: Insights from outcrop and 3D seismic data. *In:* R. Craig Shipp, P. Weimer, H. Posamentier (eds.): Mass-Transport Deposits in Deepwater Settings. *SEPM Special Publication* No. 95. https://doi.org/10.2110/sepmsp.096.007.

Poselov, V., Butsenko, V., Chernykh, A., Glebovsky, V., Jackson, H.R., Potter, D., Oakey, G., Shimeld, J. & Marcussen, C. 2011: The structural integrity of the Lomonosov Ridge with the North American and Siberian continental margins. *In:* Stone, D.B., Grikurov, G., Clough, J., Oakey, G., Thurston, D. (eds.): *Proceedings of the International Conference on Arctic Margins VI, Fairbanks, Alaska 2011.* Published by A.P. Karpinsky Russian Geological Research Institute, St. Petersburg.

Rebesco, M., Hernabdez-Molina, F.J., Rooij, D. & Wahlin, A. 2014: Contourites and associate sediments controlled by deep-water circulation processes: State-of-the-art and future consideration. Marine Geology 352, 111–154. https://doi.org/10.1016/j.margeo.2014.03.011

Reston, T.J. 2009. The extension discrepancy and syn-rift subsidence deficit at rifted margins. Petroleum Geoscience 15: 217–237. https://doi.org/10.1144/1354-079309-845.

Riddihough, R.P., Haines, G. & Hannaford, W. 1973: Regional magnetic anomalies over the Canadian Arctic. *Canadian Journal Earth Science 10*, 157–163. https://doi.org/10.1139/e73-018.

Riefstahl, F., Estrada, S., Geissler, W.H., Jokat, W., Stein, R., Kampf, H., Dulski, P., Naumann, R. & Spiegel, C. 2013: Provenance and characteristics of rocks from the Yermak Plateau, Arctic Ocean: Petrographic, geochemical and geochronological constraints. *Marine Geology 343*, 125–145. https://doi.org/10.1016/j.margeo.2013.06.009.

Rigor, I.G., Wallace, J.M. & Colony, R.L. 2002: Response of Sea Ice to the Arctic Oscillation, Journal of Climate 15, pp. 2648–2668. https://doi.org/10.1175/1520-0442(2002)015%3C2648:ROSITT%3E2.0.CO;2.

Roest, W.R. & Srivastava, S. P. 1989: Sea-floor spreading in the Labrador Sea: A new reconstruction. *Geology 17*, 1000–1003. https://doi.org/10.1130/0091-7613(1989)017%3C1000:SFSITL%3E2.3.CO;2.

Rudels, B., Friedrich, H. J. & Quadfasel, D. 1999: The Arctic Circumpolar Boundary Current, *Deep-Sea Research II 46,* 1023–1062. https://doi.org/10.1016/S0967-0645(99)00015-6.

Sellén, E., O'Reagan, M. & Jakobsson, M. 2010: Spatial and temporal Arctic Ocean depositional regimes: a key to the evolution of ice drift and current patterns. *Quaternary Science Reviews 29,* 3644–3664. https://doi.org/10.1016/j.quascirev.2010.06.005.

Shanmugam, S. 2017. Contourites: Physical oceanography, process sedimentology, and petroleum geology. *Petroleum Exploration Development 44*(2), 183–216. https://doi.org/10.1016/S1876-3804(17)30023-X.

Shipboard Scientific Party, 1994: Site 913. *In:* Myhre, A.M., Thiede, J.,Firth, J. (eds.): *Proceedings of the Ocean Drilling Program, Initial Reports Leg 151*. College Station, TX, 345–382.

Solheim, A., Faleide J.I., Andersen, E.S., Elverhøi, A., Forsberg, C.F., Vanneste K., Uenzelmann-Neben, G. & Channel, J.E.T. 1998: Late Cenozoic seismic stratigraphy and glacial geological development of the East Greenland and Svalbard-Barents Sea continental margins. *Quaternary Science Review 17*, 155–184. https://doi.org/10.1016/S0277-3791(97)00068-1.

Solli, K., Kuvas, B., Kristoffersen, Y., Leitchenkov, G., Guseva, J. & Gandjukin, V. 2007: Seismic morphology and distribution of inferred glaciomarine deposits along the East Antarctic continental margin, 20° E- 60° E. *Marine Geology 237*, 207–223. https://doi.org/10.1016/j.margeo.2006.12.002.

Soper, N.J. & Dawes, P.R. 1970: A section through the Peary Land fold belt. *Proceedings Geological Society of London 162,* 60–61.

Soper, N.J., Dawes, P.R. & Higgins, A.K. 1982: Late Cretaceous-Tertiary magmatic and tectonic events in north Greenland and the history of adjacent basins. *In:* Dawes, P.R. & Kerr, J.W. (eds.): *Nares Strait and the drift of Greenland: A Conflict in Plate Tectonics*. Meddelelser Grønland Geologiske Undersøkelser 8, 205–220.

Soper, N.J. & Higgins, A.K. 1991: Devonian- early Carboniferous deformation and metamorphism, north Greenland. A. Deformation. *In:* Trettin, H.P. (ed.): *Geology of the Innutian Orogen and Arctic Platform of Canada and Greenland,* Geological Survey of Canada Mineral Supply Service 3, 283–288.

Spielhagen, R.,Baumann, K.H., Erlenkeuser, H., Novaczyk, N.R., Nørgard-Pedersen, N., Vogt, C. & Weidel, D. 2004: Arctic Ocean deep-sea record of Northern Eurasian ice sheet history. *Quaternary Science Reviews 23*, 1455–1483. https://doi.org/10.1016/j.quascirev.2003.12.015

Stein, S., Cloetingh, S., Sleep, N. H. & Wortel, R. 1989: Passive margin earthquakes, stresses and rheology. *In: Earthquakes at North-Atlantic Passive Margins: Neotectonics and Postglacial Rebound.* Kluwer Academic Publishers, pp. 231–259.

Stein, R. 2019: The late Mesosoic-Cenozoic Arctic Ocean climate and sea ice history: A challenge for past and future scientific ocean drilling. *Paleocenography and Paleoclimatology 34.* https://doi.org/10.1007/978-94-009-2311-9_14.

Stow, D.A., 1981: Laurentian Fan: Morphology, sediments, processes, and growth pattern. *American Association of Petroleum Geologists Bulletin 65*, 375–391. https://doi.org/10.1306/2F9197DD-16CE-11D7-8645000102C1865D

Surlyk, F. & Hurst, J.M. 1984: The evolution of the early Paleozoic deep-water basin of North Greenland. *Bulletin Geological Society America 95*(2), 131–154. https://doi.org/10.1130/0016-7606(1984)95%3C131:TEOTEP%3E2.0.CO;2.

Talwani, M., Udintsev, G., White, S. & Shipboard Scientific Party 1976: *Initial reports of the Deep Sea Drilling Project Leg 38.* US Government Printing Office, Washington, 1256 pp. https://doi.org/10.2973/dsdp.proc.38.1976.

Tegnér, C., Storey, M., Holm, P., Thorarinsson, S., Zhao, X., Lo, C. & Knudsen, M. 2011: Magmatism and Eurekan deformation in the High Arctic Large Igneous Province: ^{40}Ar–^{39}Ar age of Kap Washington Group volcanics, North Greenland. *Earth & Planetary Science Letters 303,* 203–214. https://doi.org/10.1016/j.epsl.2010.12.047.

Tessensohn, F. & Piepjohn, K. 1998: Eocene Compressive Deformation in Arctic Canada, North Greenland and Svalbard and its Plate Tectonic Causes. *Polarforschung 68,* 121–124.

Thorarinsson, S., Holm, P., Tappe, S., Heaman, L. & Tegnér, C. 2011: Late Cretaceous–Palaeocene continental rifting in the High Arctic: U–Pb geochronology of the Kap Washington Group volcanic sequence, North Greenland. *Journal Geological Society London 168,* 1093–1106. https://doi.org/10.1144/0016-76492011-018.

Thorsteinsson, R. & Tozer, E.T. 1970: Geology of the Arctic Archipelago. In: Douglas, R.J.W. (ed.): Geology and Economic Minerals of Canada. *Geological Survey of Canada, Economic Geology Report 1,* 547–590.

Tikku, A.A. & Cande, S. 2000. On the fit of Broken Ridge and Kerguelen Plateau. *Earth & Planetary Science Letters 180,* 117-132. https://doi.org/10.1016/S0012-821X(00)00157-6.

Treshnikov, A.F., Balakshin, L.L., Belov, N.A., Demenitskaya, R.M., Dibner, V.D., Karasik, A.M., Shpaikher, A.D. & Shurgaeva, N.D. 1966: Geographical names of the main relief sections of the seafloor in the Arctic Basin. *Problemy Arktiki I Antarktiki 27*, 1-25 (Translated from Russian).

Trettin, H.P. 1987: Pearya: a composite terrane with Caledonian affinities in northern Ellesmere Island. – *Canadian Journal of Earth Science 24,* 224–245. https://doi.org/10.1139/e87-025.

Trettin, H. P. 1991: Tectonic framework. *In:* Trettin, H.P. (ed.): Geology of the Innutian Orogen and Arctic Platform of Canada and Greenland. *Geological Survey of Canada, Geology of Canada 3,* 59–66. https://doi.org/10.4095/133959.

Vanneste, K., Uenzelmann-Neben, G. & Miller, H. 1995: Seismic evidence for long term history of glaciation on central East Greenland shelf south of Scoresby Sund. *Geo-Marine Letters 15,* 63–70. https://doi.org/10.1007/BF01275408.

Voelker D. 2016: Subsidence of Oceanic Crust. *In:* Harff, J., Meschede M., Petersen S., Thiede, J. (eds.): Encyclopedia of Marine Geosciences. *Encyclopedia of Earth Sciences Series.* Springer, Dordrecht. https://doi.org/10.1007/978-94-007-6238-1_213.

Vogt, P.R., Taylor P.T., Kovacs, L.C. & Johnson, G.L. 1979: Detailed Aeromagnetic Investigation of the Arctic Basin. *Journal of Geophysical Research 84,* 1071–1089. https://doi.org/10.1029/JB084iB03p01071.

von Gosen, W. & Piepjohn, K. 1999: Evolution of the Kap Cannon Thrust Zone (north Greenland). *Tectonics 18*(6), 1004–1026. https://doi.org/10.1029/1999TC900035.

Walker, F., Schofield, N., Millett, J., Jolley, D., Hole, M. & Stewart, M. 2019: *In:* D. Chiarella, S.G. Archer, J. Howell, Jackson, C., Kombrink, H., Patruno, S. (eds.): Cross-Border Themes in Petroleum Geology II: Atlantic Margin and Barents Sea, *Geological Society London Special Publications 495.* https://doi.org/10.1144/SP495-2019-13.

Weissel, J.K. & Karner, G.D. 1989: Flexural uplift of rift flanks due to mechanical unloading of the lithosphere during extension. *Journal Geophysical Research 94* (B10), 13919–13950. https://doi.org/10.1029/JB094iB10p13919.

Wessel, P., Smith, W., Scharroo, R., Luis, J., & Wobbe, F. 2011: GMT 5: A major new release of the Generic Mapping Tool. *Abstract Fall Meeting American Geophysical Union 1.* 05.

Wilson, J.T. 1965: A new class of faults and their bearing on continental drift. *Nature 207*, 343–347. https://doi.org/10.1038/207343a0.

Wilson, M.A. & Palmer, T.J. 1992: "Hardgrounds and hardground faunas". University of Wales, Aberystwyth, *Institute of Earth Studies Publications 9,* pp. 131.

Wold, C.N. 1994: Cenozoic sediment accumulation on drifts in the northern North Atlantic. *Paleoceanography 9* (6), 917–941. https://doi.org/10.1029/94PA01438.

Wright, K.A., Davies, R.J., Jerram, D.A., Morris, J. & Fletcher, R. 2012: Applications of seismic and sequence stratigraphic concepts to a lava-fed delta system in the Faroe-Shetland Basin, UK and Faroes. *Basin Research 24,* 91–106. https://doi.org/10.1111/j.1365-2117.2011.00513.x.

Wynn, R.B. & Stow, D.A.V. 2002: Classification and characterization of deep-water sediment waves. *Marine Geology 192*, 7–22. https://doi.org/10.1016/S0025-3227(02)00547-9.

Zalan, P. 1987: Indentification of Strike-Slip Faults in Seismic Sections. *Abstract American Association Petroleum Geologist Annual Convention, Los Angeles, California, June 7–10. 1987.* https://doi.org/10.1190/1.1892142.